

University of Ljubljana
Faculty of Mathematics and Physics
Department of Physics

DIAGRAMMATIC THEORY OF STRONGLY CORRELATED ELECTRON SYSTEMS

THESIS

Kristjan Haule

Ljubljana, 2002

Univerza v Ljubljani
Fakulteta za matematiko in fiziko
Oddelek za Fiziko

DIAGRAMSKA TEORIJA SISTEMOV Z
MOČNIMI ELEKTRONSKIMI KORELACIJAMI

DISERTACIJA

Kristjan Haule

Ljubljana, 2002

URŠI

ACKNOWLEDGMENTS

I would like to gratefully acknowledge the supervision of Prof. Janez Bonča, his continued guidance, encouragement and support. I would like to express my deepest gratitude to Prof. Peter Wölfle for recommending this research topic and for his invaluable help. He is acknowledged, in particular, for sharing the wealth of knowledge and experience so freely. I am especially grateful to Prof. Peter Prelovšek and Dr. Achim Rosch for providing me with invaluable insights into the complexities of the field. I would particularly like to thank Dr. Hans Kroha for detailed discussion and encouragement in the area of auxiliary particle technique. I am grateful to Prof. Anton Ramšak and Dr. Igor Sega for numerous stimulating discussions and support. I am indebted to Tomaž Rejec for his help and suggestions over all those years. Thanks also to Primož Zihelr and all other members of the Department of Theoretical Physics, Jožef Stefan Institute for providing a stimulating environment. I am also grateful to Rose Schrempp, Dr. Ferdinand Evers, Markus Garst and all other friends from the University of Karlsruhe for their moral support and for their hospitality. Finally, I am forever indebted to my parents and Urša for their understanding, endless patience and encouragement when it was most required.

The work was supported by Slovene Ministry of Education Science and Sport and by European science foundation FERLIN. The thesis was completed under the roofs of the Department of Theoretical Physics, Jožef Stefan Institute and Institut für Theorie der Kondensierten Materie, Universität Karlsruhe.



ABSTRACT

Dynamic and static properties of the strongly correlated electrons are investigated within the paramagnetic metallic state of the t-J model. We used the Extended dynamical mean field theory, which scales the inter-site interaction term J in the same way as hopping term t , to the order $1/\sqrt{d}$. In the limit of large spatial dimensions the intersite quantum fluctuations are therefore treated on an equal footing with local ones. The lattice problem is mapped onto the effective impurity problem where the local moment is coupled to both the self-consistent fermionic and self-consistent vector-bosonic bath. A diagrammatic auxiliary-particle technique is developed to solve the self-consistent quantum impurity problem. Thermodynamics, spectral and charge transport properties are studied as a function of temperature and doping.

The Mott insulating gap of the half-filled t-J model is slowly destroyed with adding holes to the system but a remnant of the gap persists up to the overdoped regime. The non-Fermi liquid state with a large pseudogap of order J is found in the underdoped regime while a Fermi-liquid metallic state is stable for doping $\delta \gtrsim 24\%$. The Fermi-liquid characteristic energy scale ε^* is monotonically increasing with doping and is found to be of order J in the crossover region between Fermi and non-Fermi liquid state.

The results furthermore suggest that the Luttinger theorem is not satisfied for doping below 20%. The Fermi surface is hole-like and centered around (π, π) for underdoped and optimum doped case, while it is electron-like for the overdoped system. The Hall number changes sign from positive to negative slightly above the optimum doping and diverges as $1/(e_0\delta)$ close to the Mott-Hubbard transition in agreement with experiments on cuprates.

As a function of doping, the entropy shows a rather broad maximum at the hole density of 15% corresponding to optimum doping. The degeneracy temperature associated with the release of the entropy is relatively small $T_{deg} < J$. The chemical potential increases with increasing temperature in the underdoped regime while it decreases with temperature in the overdoped regime. The point, where μ is temperature independent coincides with the point of maximal entropy and characterizes optimum doping. An excellent agreement is found between the exact diagonalization and EDMFT results for all temperatures and all dopings considered.

We also developed an extension of the non-crossing approximation, used to solve the quantum impurity problem, to the case of finite U . The approximation correctly recovers the low energy scale T_K , in contrast to other simpler approximations discussed in the literature.

POVZETEK

Dinamične in statične lastnosti močno koreliranih elektronov smo obravnavali v okviru paramagnetnega kovinskega stanja modela t - J . Uporabili smo Razširjeno teorijo dinamičnega povprečnega polja, kjer je sklopitev med sosedi J skalirana enako kot skakalni člen t , namreč kot $1/\sqrt{d}$. V limiti visokih dimenzij so tako kvantne fluktuacije med sosedi obravnavane enako kot lokalne fluktuacije. Mrežni model se preslika na efektivni kvantni problem magnetne nečistoče, kjer je lokalni moment sklopljen s fermionskim in bozonskim rezervoarjem, ki morata biti določena samousklajeno. Razvili smo diagramsko metodo, s katero smo rešili kvantni problem magnetne nečistoče. Študirali smo spektralne, termodinamske in transportne lastnosti modela v odvisnosti od temperature in dopiranja.

Mottova energijska špranja polzapolnjenega modela t - J z dopiranjem počasi izginja vendar je ostanek špranje opazen vse do območja močnega dopiranja. Pseudo-energijska vrzel velikosti J je prisotna v šibko dopiranem sistemu, kjer model nima lastnosti Fermijeve tekočine. Šele pri dopiranju nad 24% postane ta kovina Fermijeva tekočina z značilno energijsko skalo ε^* , ki je v tem prehodnem območju reda J in z dopiranjem monotonno narašča.

Rezultati kažejo, da je v predstavljenem modelu Luttingerjev teorem kršen pri dopiranju pod 20%. Pri šibkem in zmernem dopiranju ima Fermijeva površina karakter vrzeli s središčem v (π, π) , v področju močnega dopiranja pa dobi elektronski značaj. Predznak Hallovega koeficienta se spremeni s pozitivnega v negativnega samo malo nad mestom optimalnega dopiranja in v bližni Mott-Hubbardovega prehoda divergira semiklasično kot $1/(e_0\delta)$, kar je v skladu z eksperimenti na kupratih.

Entropija pri konstantni temperaturi doseže maksimum pri optimalnem dopiranju $\delta \sim 0.15$. Kemični potencial narašča s temperaturo v rahlo dopiranem sistemu, medtem ko pada s temperaturo v močno dopiranem sistemu. Točka, kjer je kemični potencial skoraj neodvisen od temperature sovpada s točko maksimalne entropije in določa optimalno dopiranje. Rezultati EDMFT in rezultati točne diagonalizacije dvodimenzionalnega $t - J$ modela se kvalitativno in kvantitativno zelo dobro ujemajo.

Metodo NCA, ki se uporablja za rešitev kvantnega problema magnetne nečistoče, smo razširili za primer končne Coulombske interakcije U . Za razliko od mnogih enostavnejših približkov, ki jih lahko najdemo v literaturi, ta približek vsebuje pravilno nizkoenergijsko skalo T_K .

Contents

Kratek povzetek	i
Uvod	i
Metoda	iii
Rezultati	vii
1 Introduction	3
2 Dynamical mean-field theory	7
2.1 Derivation of DMFT effective action	8
2.2 The impurity representation	12
2.3 Local nature of DMFT	13
3 Extended dynamical mean-field theory	15
3.1 The EDMFT effective action	17
3.2 The impurity model	20
3.3 Still local theory?	21
4 Approximate solution of EDMFT	25
4.1 Susceptibility	26
4.2 The auxiliary-particle representation	27
4.3 The approximation scheme	29
4.4 Non-crossing approximation	31
4.5 Vertex corrections	36
5 EDMFT results	39
5.1 Quantum critical point and MFLT	39
5.2 Spectral Functions	41
5.3 Fermi surface	56
5.4 Thermodynamics	63
5.5 Hall coefficient	70
5.5.1 Low temperature limit	72

5.5.2	Numerical results	74
6	Anderson impurity model at finite Coulomb interaction U: generalized NCA	79
6.1	Pseudoparticle representation of the model	80
6.2	Gauge Symmetry and Projection onto the Physical Hilbert Space	81
6.3	Generating Functional	82
6.4	Results of SUNCA	86
7	Conclusions	93
A	Weiss fields	97
B	Equation of motion	99
C	Derivation of NCA equations	103
D	Friedel sum rule	109
E	Density of states	115
F	Internal and free energy	117
G	SUNCA equations	123

Kratek povzetek

Uvod

Odkritje visokotemperaturne superprevodnosti v spojinah na osnovi bakrovega oksida [1] je ponovno oživilo zanimanje za star problem močnih korelacij v trdnih snoveh. Skupna značilnost močno koreliranih sistemov je zelo močna interakcija med elektroni, ki je primerljiva ali celo presega kinetično energijo. Termodinamske in transportne lastnosti takih sistemov se lahko bistveno razlikujejo od lastnosti običajnih kovin, ki jih dokaj dobro opiše Landavova teorija Fermijeve tekočine.

Visokotemperaturna superprevodnost je skupaj z anomalnimi lastnostmi normalnega stanja bakrovih oksidov pravgotovo najbolj nenavaden primer močnih elektronskih korelacij, vendar še zdaleč ni edini. Zelo dolgo poznan in pogosto proučevan primer je Andersonov problem magnetne nečistoče, ki vodi do tako imenovanega Kondovega pojava: prevodniški elektroni se sipljejo na magnetni nečistoči in jo pod določeno značilno temperaturo popolnoma zasenčijo in zato oddaljeni elektroni ne čutijo več njenega magnetnega momenta. Pri nizki temperaturi ta nečistoča deluje kot nemagnetni sipalec, zato lahko sistem še vseeno opišemo kot Fermijevo tekočino. Vendar je lahko značilna energija te kvantne tekočine zelo drugačna od značilne energije prostih delcev. Če pa je magnetna nečistoča s polovičnim spinom sklopljena z dvema ali več prevodniškimi pasovi, jo ti pri nizki temperaturi preveč zasenčijo in zato sistem nima lastnosti Fermijeve tekočine. Ta sistem je eden najenostavnejših primerov kvantne tekočine, ki ni Fermijeva tekočina.

Napredek pri razvoju teoretičnih metod, ki bi opisale močno korelirane elektronske sisteme, je bil v zadnjih desetletjih izjemno skromen. Tudi najenostavnejši modeli, kot so Hubbardov model, Kondov mrežni model ali t-J model, so ostali nerešeni. Le v eni prostorski dimenziji imamo na voljo nekaj teoretičnih metod, s katerimi znamo točno rešiti najenostavnejši Hubbardov model. Večino trdnih snovi v naravi pripada dvo ali tri-dimenzionalnim sistemom, ki pa jih z enakimi metodami ne moremo rešiti. Pri teh sistemih je ponavadi zelo težko ugotoviti, ali je določen fizikalni pojav mogoče

opisati z obravnavanim idealiziranim modelom in ali določena teoretična napoved izhaja iz modela ali pa je samo posledica uporabljenega približka. Te težave izhajajo iz dejstva, da omenjenih sistemov ne moremo rešiti s standardno teorijo motnje in da imamo v sistemu več približno enako pomembnih fizikalnih mehanizmov, ki si ponavadi nasprotujejo. Posledica naštetih dejstev pa je, da sistema ne moremo opisati z eno samo energijsko skalo, saj tudi najenostavnejši model vsebuje več značilnih energij.

V zadnjih nekaj desetletjih je bilo predlagano mnogo približnih metod, ki so skušale zaobiti ta problem. Najenostavnejša med njimi temelji na Hartree-Fockovem približku, kjer so vse fluktuacije, tako krajevne kot časovne, zamrznjene. Z razvojem okrog Hartree-Fockove rešitve so časovne fluktuacije pozneje dodane v približku naključnih faz. Lokalne časovne fluktuacije pa pogosto nimajo perturbativnega značaja zato taka teorija ne more uspešno opisati nizkotemperaturno obnašanje sistemov z močnimi korelacijami. Druga vrsta približka temelji na razvoju po obratni vrednosti spinske degeneracije N . V limiti velikega N je spekter sestavljen samo iz koherentnega dela, nekoherentnega dela pa s to metodo ne moremo izračunati.

V Teoriji dinamičnega povprečnega polja (DMFT) so zamrznjene samo krajevne fluktuacije, medtem ko so časovne fluktuacije upoštevane točno. To je še posebej pomembno zato, ker kvantne časovne fluktuacije nimajo perturbativnega značaja in jih ni mogoče obravnavati s teorijo motnje. Hkrati je v DMFT nizkoenergijski koherentni del spektra obravnavan enakovredno z visokoenergijskim nekoherentnim delom, kar je pomembno za študij fizikalnih lastnosti pri končni temperaturi. Največja pomankljivost te teorije pa je, da nelokalno sklopitev obravnava statično, na nivoju Hartreejevega približka. Zaradi tega magnetno sklopitev ni moč opisati, kadar je sistem v paramagnetnem stanju, kadar pa je prisoten red dolgega dosega, teorija upošteva le statični del magnetne interakcije.

V razširjeni teoriji dinamičnega povprečnega polja (EDMFT)[6, 8, 7, 22] so kvantne fluktuacije med sosedi obravnavane enako kot lokalne časovne fluktuacije. EDMFT zato dinamično, in ne le statično kot DMFT, upošteva magnetno sklopitev med sosednjimi spini. To je še posebej pomembno v t-J modelu, kjer sta kinetični člen t in magnetni člen J približno enako pomembna in je zato nujno, da ju približek enakovredno upošteva. Prvi namreč skuša zasenčiti lokalne magnetne momente, medtem ko jih drugi skuša uređiti.

V tem delu bomo večino pozornosti posvetili t-J modelu v paramagnetnem kovinskem stanju v limiti visokih dimenzij. Z uporabo EDMFT bomo proučevali enodelčni spekter sistema, termodinamske in transportne lastnosti modela. Predstavljena metoda ima pomembno prednost pred mnogimi drugimi numeričnimi metodami, ker z vsega začetka obravnava neskončen sis-

tem in so zato rezultati že v termodinamski limiti. Največja slabost metode pa je, da skoraj popolnoma zamrzne krajevne fluktuacije in zato zanemari odvisnost lastne energije od gibalne količine. To pa najbrž ni bistvenega pomena za razlago anomalnih lastnosti normalnega stanja bakrovih oksidov. Tako numerični rezultati [9] kot tudi eksperimenti na kupratih [10] potrjujejo, da je le frekvenčna odvisnost bistvena za razlago anomalnih lastnosti in da bi lahko bila \mathbf{k} odvisnost zanemarljiva.

Metoda

Razširjena teorija dinamičnega povprečnega polja enakovredno obravnava kinetični člen t_{ij} in magnetni izmenjalni člen J_{ij} modela t-J. V tej teoriji sta namreč oba člena enako skalirana z dimenzijo in to kot $1/d^{|i-j|/2}$.

Ker nelokalni izmenjalni člen izhaja iz dvostopenjskega skakalnega procesa in je zato sorazmeren z $J_{ij} \propto t_{ij}^2/U$ bi pričakovali, da je reda $1/d^{|i-j|}$, če je $t_{ij} \propto 1/d^{|i-j|/2}$. V standardni teoriji dinamičnega povprečnega polja, kjer je tako skaliranje privzeto, izmenjalni člen J_{ij} postane zanemarljiv v primerjavi s skakalnim členom t_{ij} v limiti visokih dimenzij. Edini magnetni prispevek, ki v tej limiti ostane pomemben, je Hartree-jev prispevek, ki je sorazmeren z $J \langle S \rangle$ in je v standardni teoriji reda 1, ker je z koordinacijsko število sorazmerno z dimenzijo d . V paramagnetnem stanju, kjer je $\langle S \rangle = 0$ je ta najnižji red identično enak nič.

Členi višjega reda so sorazmerni $z^n J^{2n+m}$, kjer sta n in m pozitivni celi števili. Osnovna ideja razširjene teorije dinamičnega povprečnega polja je, da lahko J skaliramo tudi kot $J_{(ij)} \propto 1/d^{|i-j|/2}$, torej enako kot $t_{(ij)}$. V limiti visokih dimenzij potem prispevajo vsi členi oblike $z^n J^{2n}$. V stanju z redom dolgega dosega, kjer je $\langle S \rangle \neq 0$ in kjer zato Hartreejev člen ne odpade, moramo operator spina pred skaliranjem nadomestiti z njegovim odstopanjem od povprečja $S \rightarrow S - \langle S \rangle$. Ta člen bi bil sicer sorazmeren z $J \propto \sqrt{d}$ in bi ne imel končne limite.

V razširjeni teoriji dinamičnega povprečnega polja ostanejo prisotne tudi kvantne fluktuacije med spini na sosednjih mestih in so obravnavane enakovredno z lokalnimi kvantnimi fluktuacijami med štirimi možnimi lokalnimi stanji ($|\uparrow\rangle$, $|\downarrow\rangle$, $|\uparrow\downarrow\rangle$, $|0\rangle$).

V nadaljevanju se bomo posvetili predvsem mrežnemu t-J sistemu v paramagnetni fazi

$$H = - \sum_{\langle ij \rangle, \sigma} (t_{ij} \tilde{c}_{i\sigma}^\dagger \tilde{c}_{j\sigma} + H.c.) + \sum_{\langle ij \rangle} J_{ij} \vec{S}_i \cdot \vec{S}_j. \quad (1)$$

Tukaj so $\tilde{c}_{i\sigma}^\dagger$ ($\tilde{c}_{i\sigma}$) projecirani fermionski operatorji, ki izključujejo dvojno

zasedenost mesta. Z zgoraj predlaganim skaliranjem $t_{\langle ij \rangle} = t^*/\sqrt{2d}$ in $J_{\langle ij \rangle} = J^*/\sqrt{2d}$ postane v limiti $d \rightarrow \infty$ lastna energija lokalna, zato je Greenova funkcija mrežnega modela enaka

$$G_{\mathbf{k}}(i\omega) = \frac{1}{i\omega + \mu - \varepsilon_{\mathbf{k}} - \Sigma(i\omega)}. \quad (2)$$

Spinsko susceptibilnost lahko v isti limiti izrazimo z

$$\chi_{\mathbf{q}}(i\omega) = \frac{1}{M^{-1}(i\omega) + J_{\mathbf{q}}}, \quad (3)$$

kjer je M nereducibilna spinska kumulanta in je v tem primeru lokalna (ni odvisna od valovnega vektorja). Odvisna pa je od frekvence in mora biti določena samousklajeno.

V standardni teoriji dinamičnega povprečnega polja lahko mrežne modele vedno preslikamo na Andersonov problem magnetne nečistoče, vendar morajo biti parametri tega modela določeni samousklajeno [5]. Mrežni t-J model se v limiti visokih dimenzij in EDMFT skaliranju še zmeraj lahko preslika na efektivni kvantni problem magnetne nečistoče, vendar pa je v tem primeru nečistoča sklopljena ne le s fermionskim rezervoarjem (prevodnim pasom elektronov), ampak tudi z bozonskim rezervoarjem. Vse lokalne korelacijske funkcije je zato moč izračunati iz rešitve naslednjega modela

$$\begin{aligned} H_{imp} = & \sum_{l\sigma} \varepsilon_l c_{l\sigma}^\dagger c_{l\sigma} + V \sum_{l\sigma} \left(c_{l\sigma}^\dagger b^\dagger f_\sigma + f_\sigma^\dagger b c_{l\sigma} \right) + \\ & -\mu n_f + \sum_q w_q \vec{\Phi}_q^\dagger \vec{\Phi}_q + g \sum_q \vec{S}_f \cdot (\vec{\Phi}_q + \vec{\Phi}_{-q}^\dagger), \end{aligned} \quad (4)$$

kjer $c_{l\sigma}^\dagger(c_{l\sigma})$ pripadajo prevodnemu pasu prostih elektronov in $\vec{\Phi}_q^\dagger(\vec{\Phi}_q)$ predstavljajo rezervoar prostih vektorskih bozonov. Operator magnetne nečistoče $\tilde{c}_{o\sigma}^\dagger$ smo nadomestili s produktom pomožnega-fermionskega operatorja f_σ in pomožnega-bosonskega operatorja b tako, da velja $\tilde{c}_{o\sigma}^\dagger = f_\sigma^\dagger b$. Ker smo s tem povečali Hilbertov prostor, moramo v rešitvi izluščiti (sprojecirati) samo fizikalni podprostor, ki ustreza zahtevi, da je v sistemu v vsakem trenutku točno eden izmed pomožnih delcev. Formalno ta pogoj izrazimo z $Q = n_f + n_b = 1$.

Parametri, ki nastopajo v problemu magnetne nečistoče (4.10) morajo biti določeni samousklajeno iz naslednji dveh pogojev

$$G_{oo}^{-1}(i\omega) + \Sigma(i\omega) = i\omega + \mu - \sum_l \frac{V^2}{i\omega - \varepsilon_l} \quad (5)$$

$$\chi_{oo}^{-1}(i\omega) - M^{-1}(i\omega) = \sum_q \frac{2g^2 w_q}{(i\omega)^2 - w_q^2}. \quad (6)$$

Tukaj je G_{oo} lokalna Greenova funkcija in χ_{oo} lokalna spinska susceptibilnost mrežnega modela, ki pa sovpadata z ustreznimi količinami modela nečistoče (4.10).

Kvantni problem magnetne nečistoče (4.10) smo rešili s pomočjo diagramске metode pomožnih delcev, katere prednost je, da velja Wickov teorem in hkrati točno upošteva velik Coulombski odboj med dvema elektronoma na istem mestu. Poleg tega pa lahko s to metodo točno sprojeciramo fizikalni podprostor $Q = 1$ iz celotnega Hilbertovega prostora [26]. Začnemo lahko z veleanoničnim sistemom, kjer dovolimo poljubno zasedenost lokalnega stanja (Q poljubno celo nenegativno število) in vpeljemo pripadajoči kemijski potencial λ . Projekcijo potem izvedemo analitično z limito $\lambda \rightarrow \infty$. V tem pristopu lahko lokalno Greenovo funkcijo G_{oo} povežemo s sprojecirano veleanonično lastno energijo prevodniških elektronov $\Sigma_c^G(i\omega)$ in lokalno spinsko susceptibilnost χ_{oo} s sprojecirano veleanonično lastno energijo bozonov Σ_Φ^G

$$\begin{aligned}\chi_{oo}(i\omega) &= -\frac{1}{g^2}\Sigma_\Phi^G(i\omega) \\ G_{oo}(i\omega) &= \frac{1}{V^2}\Sigma_c^G(i\omega).\end{aligned}\tag{7}$$

Ti dve količini namreč nastopata v pogojih (5) in (6) in določata parametre Hamiltonke (4.10).

V približni rešitvi kateregakoli sistema je bistveno, da zajamemo najpomembnejše fizikalne procese in hkrati dosežemo, da ta rešitev ne krši ohranitvenih zakonov in vsotnih pravil. Najlažja pot do takega približka je preko tako imenovanega Luttinger-Ward funkcionala Φ . Lahko ga zgradimo po potencah sklopitvenih konstant V in g . Ker sta obe sklopitvi šibki, zadostuje že nekaj najnižjih členov. Hkrati se bomo omejili na najenostavnejši približek, ki zajame Kondo fiziko in vsebuje vse energijske skale problema v standardnem Andersonovem problemu magnetne nečistoče. V limiti $U \rightarrow \infty$ zadostuje že en sam diagram, ki definira tako imenovan približek NCA (prvi diagram na sliki 1). V primeru standardnega problema Andersonove nečistoče dobimo s tem približkom rezultate z napako pod 10% vse do temperature $T \sim 0.2T_K$.

V problemu, ki je definiran s Hamiltonko (4.10), moramo dodati še diagrame, ki vsebujejo vektorske bozone iz dodatnih bozonskih rezervoarjev. Ker je sklopitvena konstanta g majhna, najpomembnejši diagrami vsebujejo samo majhno število bozonskih linij. Tudi če se omejimo samo na tiste renormalizirane diagrame, ki vsebujejo eno samo bozonsko linijo, lahko še zmeraj narišemo neskončno vrsto diagramov, ki prispevajo k Luttinger-Ward funkcionalu. V paramagnetni fazi sistema pa je zaradi ohranitve spina en sam tak diagram različen od nič. Vsi diagrami razen drugega na sliki 1 vsebu-

$$\begin{aligned}
\Phi &= \text{diagram 1} + \frac{1}{2} \text{diagram 2} \\
\Sigma_f &= \text{diagram 3} + \text{diagram 4} \\
\Sigma_b &= \text{diagram 5} \\
V^2 G_{00} &= \text{diagram 6} \\
-g^2 \chi_{00} &= \text{diagram 7}
\end{aligned}$$

Figure 1: Dva diagrama najnižjega reda, ki prispevata k Luttinger-Ward funkcionalu in pripadajoče lastne energije. Prekinjena črta predstavlja pomožne-fermione, valovita pomožne-bozone, polna prevodniške elektrone in vzmet bozone iz rezervoarjev. Predstavljen približek bomo poimenovali NCA približek.

jejo vsaj eno fermionsko zanko narisano na sliki 2. Ker mora biti spin obeh pomožnih-fermionov v tej zanki enak, se lahko izmenja samo z komponenta vektorskega bozona. Ta pa vsebuje člen $(-1)^s$ in je tako pozitivna za spin \uparrow in negativna za spin \downarrow . Ker v paramagnetni fazi nobena smer spina ni privilegirana, se prispevek obeh ravno odšteje.

Najenostavnejši približek, ki pravilno opiše vse energijske skale običajnega Andersonovega problema nečistoče in vsebuje vse dodatne diagrame reda g^2 zaradi dodatnega bozonskega rezervoarja, ter ne krši ohranitvenih zakonov, je predstavljen na sliki 1. Ker je približek definiran z Luttinger-Ward funkcionalom, morajo biti lastne energije določene samousklajeno, kar je enakovredno neskončni vsoti diagramov nerenormalizirane perturbacijske teorije. Približek, definiran na sliki 1, ne vsebuje prekržanih diagramov, zato ga bomo v nadaljevanju imenovali NCA približek.

V območju močnega dopiranja, kjer ima sistem lastnosti Fermijeve tekočine in je magnetni člen J nepomemben, NCA približek velja do temperature $T \gtrsim 0.2\varepsilon^*$ [28], kjer je ε^* značilna temperatura Fermijeve tekočine in je

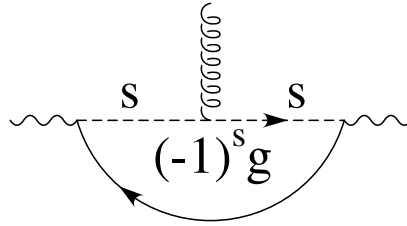


Figure 2: Fermionska zanka, katere prispevek je v paramagnetnem stanju zaradi ohranitve spina enak nič.

velikosti J pri dopiranju okoli 25%. Zaradi odsotnosti popravkov višjega reda NCA približek odpove tudi v limiti majhnega dopiranja in je zanesljiv le nad temperaturo $T \sim 0.2J$.

Rezultati

Enačbe razširjene teorije dinamičnega povprečnega polja za t-J model (5) in (6) smo rešili numerično z uporabo NCA rešitve za problem magnetne nečistoče (4.10). V duhu DMFT teorije smo uporabili gostoto stanj za dvo-dimenzionalno kvadratno mrežo, da bi izboljšali primerjavo med našimi rezultati in rezultati drugih metod, ki so bile večinoma uporabljene le za ta primer kristalne mreže.

V nadaljevanju se bomo osredotočili le na paramagnetno kovinsko stanje modela, ker kvantne fluktuacije, vsebovane v EDMFT, uničijo red dolgega dosega pri vsaki končni temperaturi v eni ali dveh dimenzijah. Hkrati nelo-kalne kvantne fluktuacije uničijo stanje Fermijeve tekočine pri šibkem in zmernem dopiranju sistema in odprejo tako imenovano energijsko pseudo-vrzel. Ta se odraža v močnem zmanjšanju vrednosti lokalne spektralne funkcije na Fermijevem nivoju in okoli njega.

V t-J modelu s polzapolnjenim pasom se zaradi močnega Coulombskega odboja med elektroni ustvari tako imenovana Mottova energijska špranja, zaradi katere ima sistem lastnosti izolatorja. Z dodajanjem vrzeli pa Mottova energijska špranja počasi izginja, vendar ostaja na Fermijevem nivoju tako imenovana pseudo-energijska vrzel, ki je opazna vse do območja močnega dopiranja $\delta \sim 0.20$. Sistem je prevodnik, vendar v tem področju majhnega in zmerne dopiranja nima lastnosti Fermijeve tekočine. Pri šibkem dopiranju je enodelčni lokalni spekter sestavljen iz širokega nekoherentnega Hubbardovega pasu in koherentnega vrha oblečene vrzeli s širino J , ki je pomaknjen za razdaljo J pod Fermijev nivo μ . Poleg tega pa se pojavi nad μ še majhen vrh z utežjo 2δ in se z dopiranjem povečuje in približuje μ , dokler se

v območju močnega dopiranja ne zlije s kvazidelčnim vrhom pod μ . Tako nastane pri dopiranju $\delta \sim 0.24$ en sam koherentni vrh širine $\sim J$, ki zadošča Friedelovemu vsotnemu pravilu. To pa pomeni, da ima sistem pri dopiranju nad $\delta \gtrsim 0.24$ lastnosti Fermijeve tekočine. To lahko razložimo z dejstvom, da postane v tem področju magnetna sklopitev nepomembna in je zato učinkovitni model magnetne nečistoče ekvivalenten standardnemu Andersonovemu modelu. Slednji pa ima zmeraj lastnosti Fermijeve tekočine z dobro določeno značilno temperaturo T_K , ki je sorazmerna širini kvazidelčnega vrha v spektralni funkciji. Od tod vidimo, da se značilna temperatura Fermijeve tekočine z dopiranjem monotonno povečuje od J do t .

EDMFT rezultati kažejo, da je v predstavljenem modelu Luttingerjev teorem kršen v območju, kjer sistem nima lastnosti Fermijeve tekočine. Kršitev je najočitnejša pri šibkem dopiranju, kjer je volumen znotraj Fermijeve površine kar dvakrat večji, kot ga napoveduje teorem. Nato pa se monotonno zmanjšuje tako, da je pri dopiranju nad $\sim 20\%$ Luttingerjev teorem zadoščen. Rezultati podpirajo skoraj togo sliko dopiranja Mottovega izolatorja, ki jo je predlagal že Hubbard: v polzapolnjenem pasu je kemični potencial med Hubbardovima pasovoma, z dopiranjem pa se ta počasi premika od zgornjega roba v notranjost spodnjega Hubbardovega pasu. Pri šibkem in zmernem dopiranju ima Fermijeva površina karakter vrzeli s središčem v (π, π) , v področju močnega dopiranja pa dobi elektronski značaj.

S spremembo značaja Fermijeve površine je tesno povezan Hallov koeficient, ki je pri nizki temperaturi pozitiven v območju majhnega dopiranja in negativen v področju močnega dopiranja. Predznak se spremeni samo malo nad mestom optimalnega dopiranja. V bližni Mott-Hubbardovega prehoda divergira semiklasično kot $1/(e_0\delta)$, kar je v skladu s semiklasično sliko dopiranja Mottovega izolatorja z neodvisnimi vrzeli in eksperimenti na kupratih. Pri šibkem dopiranju Hallov koeficient monotonno pada s temperaturo kar je pravtako v skladu z eksperimenti.

Ker je v EDMFT teoriji privzeto, da je lastna energija neodvisna od valovnega vektorja, kar je popolnoma upravičeno samo v limiti visokih dimenzij, je ta model lahko slab približek za dvodimenzionalni t-J model. Numerični rezultati [9] in eksperimenti [10] kažejo, da je v območju optimalnega dopiranja $\delta \sim 0.15$ lastna energija zares skoraj neodvisna od valovnega vektorja in so zato EDMFT rezultati smiselni tudi za dve dimenziji. Tega pa ne moremo trditi v območju zelo majhnega dopiranja, kjer bi bilo potrebno obstoječo teorijo popraviti, da bi veljala tudi za dvodimenzionalni sistem.

Termodinamske lastnosti sistema smo izračunali iz proste energije, ki se lahko izrazi s prosto energijo učinkovitega modela nečistoče, z enoelektronsko

Greenovo funkcijo in susceptibilnostjo sistema kot

$$\Omega = N\Omega_{imp} + \frac{1}{\beta} \sum_{i\omega, \mathbf{k}\sigma} \ln(G_{\mathbf{k}\sigma}(i\omega)) - \ln(G_{oo}(i\omega)) - \frac{1}{2} \frac{1}{\beta} \sum_{i\omega, \mathbf{q}\alpha} \ln(\chi_{\mathbf{q}}^{\alpha\alpha}(i\omega)) - \ln(\chi_{oo}^{\alpha\alpha}(i\omega)). \quad (8)$$

Entropija pri konstantni temperaturi doseže maksimum pri optimalnem dopiranju $\delta \sim 0.15$. Značilna temperatura degeneracije, kjer se entropija bistveno spremeni, je relativno majhna, celo manjša kot J . Specifična toplota je pri zmernem dopiranju skoraj neodvisna od temperature v širokem obsegu temperatur med $T/t^* \sim 0.05 - 0.5$. Kemični potencial narašča s temperaturo v rahlo dopiranem sistemu, medtem ko pada s temperaturo v močno dopiranem sistemu. Točka, kjer je kemični potencial skoraj neodvisen od temperature sovpada s točko maksimalne entropije in določa optimalno dopiranje. Rezultati EDMFT in rezultati točne diagonalizacije dvodimenzionalnega $t - J$ modela [9] se kvalitativno in kvantitativno zelo dobro ujemajo.

Chapter 1

Introduction

The discovery of the high-temperature superconductivity in the copper-oxide based compounds [1] has revived interest in the old problem of strong electronic correlations in condensed matter physics. The common feature of strongly correlated systems is the strength of the electron-electron interaction which is comparable to or larger than the kinetic energy. These systems can display thermodynamic and transport properties which are fundamentally different from those of the usual metallic systems which are well described by the Landau Fermi-liquid theory.

While high temperature superconductivity as well as anomalous normal state properties of the copper oxides are likely to be the most fascinating examples of strongly correlated electron systems, they are by far not the only ones. The archetype case of strong electron correlations is the Anderson impurity model displaying the Kondo effect, where conduction electrons scatter off a localized magnetic impurity and form a local singlet. The low temperature properties of the latter model can still be described by the local Fermi liquid theory, however, the characteristic energy scale can be strongly renormalized. The multi-channel Kondo problem, on the other hand, is one of the simplest examples of non-Fermi liquid behaviour due to strong electron correlations.

The theoretical progress in the field has been impeded by the extreme difficulty of dealing with even the simplest model Hamiltonians appropriate for these systems, such as the Hubbard model, Kondo lattice model or the $t - J$ model. Only in the one-dimensional case, we have a variety of theoretical tools at our disposal to study the simplest Hubbard model in a systematic manner. For two- and three-dimensional models, one is often unable to access confidently whether a given physical phenomenon is indeed captured by the idealized Hamiltonian under consideration or whether a theoretical prediction reflects a true feature of this Hamiltonian, rather than an arti-

fact of the approximation used in its solution. These difficulties originate in the nonperturbative nature of the problem, and reflects the presence of several *competing physical mechanisms* and *several energy scales* for even the simplest models.

Numerous approximation schemes have been employed during the past decades to circumvent these difficulties. The simplest mean-field methods are based on the Hartree-Fock approximation, where all fluctuations (spatial and temporal) are frozen. The fluctuations can then be treated by making random phase approximation expansion around the static and uniform solution. Local quantum fluctuations, however, are often nonperturbative in character so that such expansions do not capture them correctly. Another type of approximation is based on large N expansion [2, 3], where N is spin degeneracy. In the limit of $N \rightarrow \infty$, high energy incoherent excitations (i.e. Hubbard bands) are completely absent and must be reintroduced by expanding in $1/N$.

The Dynamical mean-field theory (DMFT) [4, 5] freezes only spatial fluctuations while it takes full account of local temporal fluctuations being usually nonperturbative in character. At the same time, DMFT treats the low energy coherent and the high energy incoherent excitations on the same footing. This is important for studying any finite temperature property of the model. One of the major drawbacks of DMFT is that it treats all nonlocal interactions on the Hartree level. In particular, the magnetic exchange interaction is therefore completely absent in the paramagnetic state while only the static part of the interaction is considered in the system with long range order.

The extended dynamical mean-field theory (EDMFT) [6, 7, 8] treats the inter-site quantum fluctuations on an equal footing with local ones. EDMFT thus captures not only the static but also the dynamic component of the magnetic exchange interaction. It is particularly important for the $t - J$ model to capture the competition between the kinetic energy term being reduced due to strong on site repulsion, and magnetic exchange interaction. The hopping term tends to quench local moments, and gives rise to Kondo effect in the limit of large dimensions, while the exchange term promotes magnetic ordering.

In this thesis, we will mostly focus on the paramagnetic metallic state of the $t - J$ model in the limit of large dimensions. By using EDMFT, we will study the single particle spectra, thermodynamic and transport properties of the model. The important advantage of EDMFT over the many other numerical methods is that the thermodynamic limit is built in from the beginning in this approach. The major drawback, on the other hand, is that the spatial fluctuations are mainly frozen, i.e., the self-energy is momentum

independent. However, this might not be crucial to explain many anomalous properties of the finite dimensional (or 2D) $t - J$ model since many numerical studies [9] and also experiments on cuprates [10] suggest that the momentum dependence of the self-energy is not crucial to explain anomalies.

The thesis is organized as follows. In chapter 2 we give an introduction to the limit of large dimensions and derive the dynamical mean-field equations for the Hubbard model. Chapter 3 introduces extended dynamical mean-field theory that avoids one of the major drawbacks of the usual large d limit. The corresponding impurity model is presented and it is shown that the theory remains local despite the introduction of the momentum dependent vertex function. Chapter 4 presents the auxiliary particle technique and the approximation scheme appropriate for the EDMFT impurity Hamiltonian. The NCA equations, which are used in subsequent chapters, are explicitly given while the vertex corrections are discussed and partly calculated. In chapter 5 we present numerical results for the $t - J$ model obtained by EDMFT and compare them to the exact diagonalization results. Section 5.1 discusses the possible reason why the momentum dependence of the self-energy might be neglected. One particle spectra and Fermi-surface of the $t - J$ model are presented in sections 5.2 and 5.3, respectively. In 5.4 we study thermodynamic properties like entropy, specific heat and compressibility and compare them to the exact diagonalization results. The transport properties are considered in section 5.5 where we particularly focus on the Hall number which is closely related to the nature of the Fermi-surface. The extension of the auxiliary particle method to the case of finite Coulomb interaction is given in chapter 6. The impurity spectral function is evaluated numerically and compared to the NRG result.

Chapter 2

Dynamical mean-field theory

This chapter introduces the Dynamical mean-field theory (DMFT), a method that was developed to investigate strongly correlated electron systems. These are systems in which strength of the electron-electron interaction is comparable to or larger than the kinetic energy therefore there seems to be no natural small parameter which allows an expansion around a solvable limit. However, Metzner and Vollhardt [4] realized that on the lattice with coordination number z (i.e. the number of the nearest neighbors) an expansion in its reciprocal value $1/z$ can be performed leading to a nontrivial limit of the model.

The most serious limitation of the DMFT is that it ignores spatial fluctuations (the wave number dependence of the self energy) and includes only magnetic fluctuations of Kondo type while it neglects Ruderman-Kittel-Kasuya-Yosida (RKKY) interaction beyond the Hartree level. The extension of the method to clusters in k space [11] and clusters in real space [12] has been proposed recently to include spatial fluctuations. Magnetic fluctuations of RKKY type can also be included in the theory [7, 6] with not much additional effort, as will be shown in the next section. On the other hand, it should be stressed that DMFT does not suffer from the finite-size effects since the thermodynamic limit is built in from the beginning in this approach.

Let us briefly mention few other approaches to lattice models of strongly correlated electron systems which have been developed over the last couple of decades. Several simple models, in particular the Hubbard model can be solved exactly in one spatial dimension using Bethe Ansatz method [13, 14]. While these solutions have given invaluable insights, the extraction of important physical information, in particular of dynamical correlation functions, is still not possible. Additionally, not many features of one-dimensional solutions survive in higher spatial dimensions. Among the first serious attacks on the strong correlation problem in more than one spatial dimension were

the original papers by Hubbard [15, 16, 17] on the Hubbard model. He introduced various expansions around the atomic limit, which are decoupled in an uncontrolled way. While these approximations capture the high-energy features of the Hubbard model correctly, they cannot be trusted to adequately describe the low energy physics of the metallic regime. Numerical approaches based on exact diagonalization of small clusters and Monte Carlo methods have lead to important insights into the complicated physics of strong correlations, but are seriously limited with the size of the clusters since the Hilbert space grows exponentially with the number of lattice sites.

The essential idea of the presented method is to replace a lattice model by a single-site quantum impurity problem embedded in an effective medium determined self-consistently [5]. The impurity model offers an intuitive picture of the local dynamics of a quantum many-body system while the self-consistency condition captures the translation invariance and coherence effects of the lattice.

The DMFT is the natural generalization of quantum many-body problems of the Weiss mean-field theory familiar from classical statistical mechanics. The term "mean-field theory" should be taken with caution however since the present approach does not assume that all fluctuations are frozen (this would lead to the Hartree-Fock approximation). Rather, it freezes spatial fluctuations but takes full account of local quantum fluctuations - of temporal fluctuations between the possible quantum states at a given lattice site. The main difference with the classical case is that the on-site quantum problem remains a many-body problem.

As in classical statistical mechanics, this dynamical mean-field theory becomes exact in the limit of large spatial dimensions $d \rightarrow \infty$, or more appropriately in the limit of large lattice coordination number z . Note that this number is already quite large for several three dimensional lattices: $z = 6$ for simple cubic lattice or $z = 12$ for a face-centered-cubic lattice. This ensures the internal consistency of the approach and establishes $1/z$ as a control parameter. However, this approach may be viewed in a broader context, as a starting point for the investigation of many finite-dimensional strongly correlated systems, in the same sense that the Weiss mean field theory is the starting point of most investigations in the classical statistical mechanics.

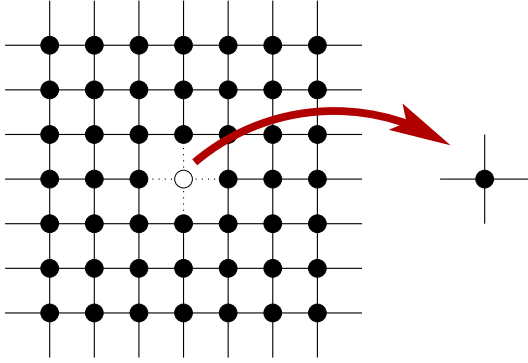
2.1 Derivation of DMFT effective action

First we will focus on maybe the simplest theoretical model capturing the competition between itinerant and strong local correlations, the single band

Hubbard model

$$H = - \sum_{ij,\sigma} t_{ij} c_{i\sigma}^\dagger c_{j\sigma} + U \sum_i n_{i\uparrow} n_{i\downarrow}. \quad (2.1)$$

The derivation presented here will be borrowed from classical statistical mechanics, where it is known under the name "cavity method". The underlying idea is to focus on a given site of the lattice, say $i = o$, and to explicitly integrate out the degrees of freedom on all other lattice sites in order to define an effective dynamics for the selected site.



It will be assumed in this section, for simplicity, that no symmetry breaking occurs and we are dealing with translational invariant paramagnetic phase.

Figure 2.1: Cavity created in the lattice by removing a single site and its adjacent bonds.

It is convenient to write partition function of (2.1) as a functional integral over Grassman variables

$$Z = \int \prod_i Dc_{i\sigma}^\dagger Dc_{i\sigma} \exp(-S) \quad (2.2)$$

$$S = \int_0^\beta d\tau \left[\sum_{i,\sigma} c_{i\sigma}^\dagger(\tau) \left(\frac{\partial}{\partial \tau} - \mu \right) c_{i\sigma}(\tau) - \sum_{ij,\sigma} t_{ij} c_{i\sigma}^\dagger(\tau) c_{j\sigma}(\tau) + \sum_i U n_{i\uparrow}(\tau) n_{i\downarrow}(\tau) \right]. \quad (2.3)$$

The action can be divided into three parts: the on-site part for the chosen site (S_0), the inter-site interaction between the site and the rest of the system (ΔS) and the lattice action in the presence of the cavity ($S^{(0)}$) (i.e. with site o and its adjacent bonds removed - see Fig. 2.1)

$$S_0 = \int_0^\beta d\tau \left[\sum_\sigma c_{o\sigma}^\dagger(\tau) \left(\frac{\partial}{\partial \tau} - \mu \right) c_{o\sigma}(\tau) + U n_{o\uparrow}(\tau) n_{o\downarrow}(\tau) \right] \quad (2.4)$$

$$\Delta S = - \int_0^\beta d\tau \left[\sum_{i,\sigma} t_{io} c_{i\sigma}^\dagger(\tau) c_{o\sigma}(\tau) + t_{oi} c_{o\sigma}^\dagger(\tau) c_{i\sigma}(\tau) \right] \quad (2.5)$$

$$S^{(0)} = \int_0^\beta d\tau \left[\sum_{i \neq 0, \sigma} c_{i\sigma}^\dagger(\tau) \left(\frac{\partial}{\partial \tau} - \mu \right) c_{i\sigma}(\tau) - \sum_{i \neq 0, j \neq 0, \sigma} t_{ij} c_{i\sigma}^\dagger(\tau) c_{j\sigma}(\tau) + \sum_{i \neq 0} U n_{i\uparrow}(\tau) n_{i\downarrow}(\tau) \right]. \quad (2.6)$$

With the definition $\Delta S = \int_0^\beta \Delta S(\tau)$ the partition function can be written as

$$\begin{aligned} Z &= \int Dc_{o\sigma}^\dagger Dc_{o\sigma} \exp(-S_0) \int \prod_{i \neq 0} Dc_{i\sigma}^\dagger Dc_{i\sigma} \exp(-S^{(0)} - \int_0^\beta \Delta S(\tau) d\tau) = \\ &= \int Dc_{o\sigma}^\dagger Dc_{o\sigma} \exp(-S_0) \int \prod_{i \neq 0} Dc_{i\sigma}^\dagger Dc_{i\sigma} \exp(-S^{(0)}) \left(1 - \int_0^\beta \Delta S(\tau) d\tau + \right. \\ &\quad \left. \frac{1}{2!} \int_0^\beta d\tau_1 \int_0^\beta d\tau_2 T_\tau \Delta S(\tau_1) \Delta S(\tau_2) + \dots \right) = \\ &= \int Dc_{o\sigma}^\dagger Dc_{o\sigma} \exp(-S_0) Z^{(0)} \left(1 - \int_0^\beta \langle \Delta S(\tau) \rangle^{(0)} d\tau + \right. \\ &\quad \left. \frac{1}{2!} \int_0^\beta d\tau_1 \int_0^\beta d\tau_2 \langle T_\tau \Delta S(\tau_1) \Delta S(\tau_2) \rangle^{(0)} + \dots \right), \quad (2.7) \end{aligned}$$

where $\langle \rangle^{(0)}$ means average over cavity action $S^{(0)}$ and T_τ is the usual imaginary time ordering operator. All the odd terms in the expansion are zero therefore the lowest order contribution reads

$$\begin{aligned} &\frac{1}{2!} \int_0^\beta d\tau_1 \int_0^\beta d\tau_2 \sum_\sigma c_{o\sigma}^\dagger(\tau_1) \sum_{ij} t_{io} t_{oj} \langle T_\tau c_{i\sigma}(\tau_1) c_{j\sigma}^\dagger(\tau_2) \rangle^{(0)} c_{o\sigma}(\tau_2) = \\ &\frac{1}{2!} \int_0^\beta d\tau_1 \int_0^\beta d\tau_2 \sum_\sigma c_{o\sigma}^\dagger(\tau_1) \sum_{ij} t_{io} t_{oj} G_{ij}^{(0)}(\tau_1 - \tau_2) c_{o\sigma}(\tau_2) \quad (2.8) \end{aligned}$$

Similarly, the n -th order term contains the $2n$ -point *unconnected* Green's function of the cavity problem with n incoming and n outgoing propagators. Due to the Linked Cluster Theorem the effective action

$$e^{-S_{eff}} / Z_{eff} = \int \prod_{i \neq 0} Dc_{i\sigma}^\dagger Dc_{i\sigma} e^{-S} / Z \quad (2.9)$$

can now be expressed with the *connected* n -point Green's function with an infinite series

$$\begin{aligned} S_{eff} &= S_0 + \sum_{n=1}^{\infty} \sum_{i_1, \dots, j_n} \int t_{i_1 o} \dots t_{o j_n} c_{o\sigma}^\dagger(\tau_{i_1}) \dots c_{o\sigma}^\dagger(\tau_{i_n}) c_{o\sigma}(\tau_{j_1}) \dots c_{o\sigma}(\tau_{j_n}) \\ &\quad \times G_{i_1 \dots j_n}^{(0)}(\tau_{i_1} \dots \tau_{i_n}, \tau_{j_1} \tau_{j_n}) + const. \quad (2.10) \end{aligned}$$

2.1. DERIVATION OF DMFT EFFECTIVE ACTION

Remarkable simplification occurs in the limit of large dimensions, namely, only the first term containing the one particle Green's function survives.

In order for the large d limit to be well defined hopping amplitude t has to be scaled as $t_{ij} = t/\sqrt{2d}$. Only in that case the kinetic and interaction energies remain of the same order of magnitude. The Fourier transform of the $\varepsilon_{\mathbf{k}}$ of t_{ij} , which for a generic vector \mathbf{k} involves $\sum_{n=1}^d \cos(k_n)$, a sum of d numbers with essentially random signs is of order \sqrt{d} . More important, this scaling ensures that the density of states has a well defined limit form, which for cubic lattice with nearest-neighbor hopping reads

$$D(\epsilon) = \frac{1}{\sqrt{2\pi z t^2}} \exp\left(-\frac{\epsilon^2}{2z t^2}\right). \quad (2.11)$$

The one particle Green's function (i.e. connected two-point function) G_{ij} is proportional to $t^{|i-j|}$ therefore it scales as $1/d^{|i-j|/2}$. Similarly two particle Green's function G_{ijkl} falls off as $1/d^{|i-j|/2} d^{|i-k|/2} d^{|i-l|/2}$. With that scaling in mind it is easy to see that higher order terms in Eq. (2.10) indeed vanish in $d \rightarrow \infty$ limit. The first term has a prefactor t^2 and one particle cavity Green's function $G_{ij}^{(0)}$ gives another t^2 , since i and j are both nearest neighbors of o and therefore are at least two lattice sites apart (in Manhattan distance). The double sum over i and j gives d^2 so the first term is of order 1. The second term has a prefactor t^4 and involves two particle cavity Green's function giving $t^{|i-j|} t^{|i-k|} t^{|i-l|}$, where all differences are at least two. When i, j, k and l are all different, there are four sums which give d^4 , but in the same time cavity Green's function is proportional to t^6 so that the net results is at least of order $1/d$. Similarly, the terms where $i = j$ (distinct from k and l with $k \neq l$) contain three sums, which give d^3 . Green's function is proportional to t^4 in that case. The net result is again of order $1/d$.

Since only the term involving the one-particle Green's function survives the large d limit, the effective action can be reduced to

$$S_{eff} = - \int_0^\beta d\tau_1 \int_0^\beta d\tau_2 c_{o\sigma}^\dagger(\tau_1) \mathcal{G}_0^{-1}(\tau_1 - \tau_2) c_{o\sigma}(\tau_2) + \int_0^\beta d\tau U n_{o\uparrow}(\tau) n_{o\downarrow}(\tau) \quad (2.12)$$

where the Weiss field \mathcal{G}_0^{-1} is

$$\mathcal{G}_0^{-1}(\tau_1 - \tau_2) = -\left(\frac{\partial}{\partial \tau_1} - \mu\right) \delta_{\tau_1 \tau_2} - \sum_{ij} t_{io} t_{oj} G_{ij}^{(0)}(\tau_1 - \tau_2). \quad (2.13)$$

The last equation relates the Weiss field (\mathcal{G}_0^{-1}) with the cavity Green's function of the Hubbard model. To obtain a closed set of equations one still needs

to express the cavity Green's function with the exact Green's function of the original lattice. In the limit of infinite dimensions this relation reads

$$G_{ij}^{(0)} = G_{ij} - \frac{G_{io}G_{oj}}{G_{oo}}. \quad (2.14)$$

The expression was derived already by Hubbard [17] in the early 70s. To understand it we need to recognize that the additional paths contributing to G_{ij} and not to $G_{ij}^{(o)}$ are those which connect sites i and j through site o . Their contribution is proportional to $G_{io}G_{oj}$, but this quantity has to be divided by G_{oo} in order to count the contribution of paths leaving and returning to the intermediate site o only once.

2.2 The impurity representation

The on-site model represented with the effective action (2.12) can not be written in a Hamiltonian form involving only the on-site (atomic) degrees of freedom since eliminated bath introduces retardation effects in the atomic problem. However, it is very convenient for practical calculations to have such a Hamiltonian formulation. It is possible only upon reintroducing auxiliary degrees of freedom describing the bath. The most popular interpretation of the action (2.12) is via Anderson impurity problem [18, 19, 20], archetype and well understood model from the research of magnetic alloys in the metallic host. The atomic orbital c_o corresponds to the impurity site while the Weiss field is mimicked with the conduction band that has to be self-consistently determined. This mapping is also important since the variety of techniques developed during the past decades can be used to solve the effective on-site problem. However, this part of the calculation is the most difficult one and there is still no reliable tool that would work in the whole temperature range.

The Anderson impurity model

$$H = \sum_{k\sigma} \left(\varepsilon_k c_{k\sigma}^\dagger c_{k\sigma} + V_k c_{k\sigma}^\dagger c_{o\sigma} + V_k^* c_{o\sigma}^\dagger c_{k\sigma} \right) - \sum_{\sigma} \mu c_{o\sigma}^\dagger c_{o\sigma} + U n_{o\uparrow} n_{o\downarrow} \quad (2.15)$$

and the corresponding action

$$S = \int_0^\beta d\tau \sum_{k\sigma} \left[c_{k\sigma}^\dagger(\tau) \left(\frac{\partial}{\partial \tau} + \varepsilon_k \right) c_{k\sigma}(\tau) + V_k c_{k\sigma}^\dagger(\tau) c_{o\sigma}(\tau) + V_k^* c_{o\sigma}^\dagger(\tau) c_{k\sigma}(\tau) \right] + S_0 \quad (2.16)$$

$$S_0 = \int_0^\beta d\tau \left[\sum_{\sigma} c_{o\sigma}^\dagger(\tau) \left(\frac{\partial}{\partial \tau} - \mu \right) c_{o\sigma}(\tau) + U n_{o\uparrow}(\tau) n_{o\downarrow}(\tau) \right] \quad (2.17)$$

is quadratic in $c_{k\sigma}^\dagger, c_{k\sigma}$ and therefore the conduction band electrons can be integrated out exactly [21] giving the action of the form

$$S = S_0 - \int_0^\beta d\tau_1 \int_0^\beta d\tau_2 \sum_\sigma c_{o\sigma}^\dagger(\tau_1) \left(\sum_k |V_k|^2 \frac{\delta_{\tau_1\tau_2}}{\frac{\partial}{\partial\tau_1} + \varepsilon_k} \right) c_{o\sigma}(\tau_2). \quad (2.18)$$

This action is equivalent to the effective action (2.12) of the Hubbard model within DMFT with the requirement

$$\begin{aligned} \mathcal{G}_0^{-1}(\tau_1 - \tau_2) &= -\left(\frac{\partial}{\partial\tau_1} - \mu\right)\delta_{\tau_1\tau_2} - G_c(\tau_1 - \tau_2) \\ G_c(\tau_1 - \tau_2) &= \sum_{k\sigma} |V_k|^2 G_{k\sigma}(\tau_1 - \tau_2) = - \sum_{k\sigma} |V_k|^2 \frac{\delta_{\tau_1\tau_2}}{\frac{\partial}{\partial\tau_1} + \varepsilon_k}. \end{aligned} \quad (2.19)$$

2.3 Local nature of DMFT

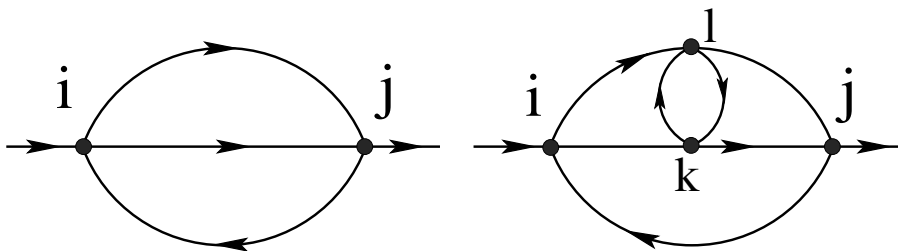


Figure 2.2: Example of diagrams contributing to the nonlocal self-energy at the third and fifth order.

In the limit of large dimensions, the lattice self-energy becomes a local quantity (i.e. \mathbf{k} independent) that can be determined from other local quantities (local Green's function and Weiss field) alone. This important fact can be shown explicitly with the diagrammatic technique within the perturbation theory in the interaction strength U . Consider a given diagram (Fig. 2.2), in which the interaction term $Un_{i\uparrow}n_{i\downarrow}$ is depicted as a four-leg vertex at site i , and in which each line stands for a full interacting fermion propagator between two sites. The crucial observation is that whenever two internal vertices (i, j) can be connected by at least two paths, they must correspond to identical sites $i = j$. This property of $d \rightarrow \infty$ limit can be shown by simple power counting. Since the hopping has been scaled by $1/\sqrt{d}$, each path made of fermion propagators connecting i to j will involve at least a factor $1/d^{|i-j|/2}$. The non-local component of the self-energy Σ_{ij} is thus proportional to $1/d^{\mathcal{P}_{ij}|i-j|/2}$ with \mathcal{P}_{ij} being the number of independent paths

joining i to j in the diagram. Fourier transformation for any generic wave vector q (not $q = 0$ or $q = (\pi, \pi, \dots)$) then brings up a factor of order $d^{|i-j|/2}$, as explained in Eq. (2.11). Since \mathcal{P}_{ij} , for any skeleton diagram, is larger than 2 the non-local component of the self-energy is at least of order $1/d$ smaller than the local one. The Luttinger Ward functional (Fig. 2.3) thus contains

$$\Phi = \begin{array}{c} \text{Hartree} \\ \text{Fock} \end{array} \begin{array}{c} \text{+} \\ \text{+} \end{array} \dots$$

Figure 2.3: First two contributions to the Luttinger-Ward functional. Only first Hartree term is important in the limit of large dimensions.

only Hartree term (site diagonal contribution) while Fock and higher order terms vanish in the $d \rightarrow \infty$ limit. Green's function of the original lattice problem therefore reads

$$G_{\mathbf{k}}(i\omega) = \frac{1}{i\omega + \mu - \varepsilon_{\mathbf{k}} - \Sigma(i\omega)} \quad . \quad (2.20)$$

With that equation in mind we can easily determine the relationship between the Weiss field, the local Green's function and self-energy. The Fourier transform of the sum in the Eq. (2.13) reduces to (see Appendix A)

$$\sum_{ij} t_{io}t_{oj} \left(G_{ij} - \frac{G_{io}G_{oj}}{G_{oo}} \right) = i\omega + \mu - \Sigma - G_{oo}^{-1} \quad (2.21)$$

and the Weiss field finally reads

$$\mathcal{G}_0^{-1} = \Sigma + G_{oo}^{-1} \quad . \quad (2.22)$$

This is the central equation of the DMFT and together with the expression for the local Green's function

$$G_{oo} = \sum_{\mathbf{k}} \frac{1}{i\omega + \mu - \varepsilon_{\mathbf{k}} - \Sigma} \quad (2.23)$$

and the solution of the Anderson impurity problem

$$G_{oo} = G_{impurity}(\mathcal{G}_0^{-1}) \quad (2.24)$$

forms a closed set of equations.

The above equations were derived for the Hubbard model in infinite dimensions. In the same way it is possible to write down the closed set of DMFT equations for many other models of strongly correlated electron systems, i.e. periodic Anderson model, Kondo lattice model...

Chapter 3

Extended dynamical mean-field theory

In the correlated electron systems, both the local and non-local interactions are important in determining the nature of the ground state and low-lying excitations. While the local quantum fluctuations of the lattice problem are completely taken into account within the DMFT, the non-local fluctuations like the RKKY interaction are mostly lost. The first are responsible for the phenomena known as the Kondo effect, that tends to quench local moments while the latter promote magnetic ordering. What happens when the two processes are about equally important is an intriguing question that remains poorly understood. In this section, we will develop a method that copes with that particular problem in the case, when the wave number dependence of the self-energy is not essential to describe the physical properties of system.

The DMFT reduces a correlated lattice problem to a self-consistent Anderson impurity problem, namely a quantum impurity coupled to a self-consistent fermionic bath. The interaction between the impurity degrees of freedom reflects the on-site interactions of the lattice problem; in this way local quantum fluctuations are retained. The self-consistent fermionic bath of the impurity problem reflects the influence, at the one-particle level, of the rest of the lattice on the selected site. All the inter-site correlations of the lattice problem, on the other hand, are neglected. In this sense, non-local quantum fluctuations are completely lost.

In the Extended dynamical mean-field theory (EDMFT) [6, 7, 8, 22] the inter-site quantum fluctuations are treated on an equal footing with local ones. The correlated lattice problem is reduced to a novel effective impurity problem, which corresponds to Anderson impurity model with an additional self-consistent bosonic baths. These bosonic baths reflect the influence, at the two-particle level, of the rest of the lattice on the impurity site (i.e. the

fluctuating magnetic fields induced by the inter-site spin-exchange interaction). Through self-consistency, they keep track of the inter-site quantum fluctuations.

Let us focus on a specific model, namely the extended Hubbard model, that becomes equivalent to the t-J model in the limit of infinite local Coulomb interaction

$$H = - \sum_{ij,\sigma} t_{ij} c_{i\sigma}^\dagger c_{j\sigma} + U \sum_i n_{i\uparrow} n_{i\downarrow} + \frac{1}{2} \sum_{ij} J_{ij} \vec{S}_i \cdot \vec{S}_j - \mu \sum_i n_i. \quad (3.1)$$

It is straightforward to extend the theory to other non-local interactions like non-local Coulomb repulsion, but since we are mainly interested in the effect of magnetic fluctuations we will neglect other terms in the Hamiltonian.

In standard DMFT, the hopping amplitude is taken to be of order $1/\sqrt{d}$ while the inter-site interaction is scaled as $1/d$, since the latter comes from the second order perturbation process proportional to t^2/U . In that case, the Hartree approximation for the inter-site interaction becomes exact and the nonlocal terms can be treated on the mean field level, i.e.,

$$J_{ij} \vec{S}_i \vec{S}_j \rightarrow 2J_{ij} S_i^z \langle S_j^z \rangle. \quad (3.2)$$

In the paramagnetic phase the latter term is exactly zero showing the equivalence between the t-J model and the infinite-U Hubbard model in the standard DMFT scaling of $d \rightarrow \infty$ limit. However, the ordered phase brings up an interesting feature, commonly known as string potential [23, 24]. Close to half-filling, the system can be described with the holes moving in the Néel background. Problem of a single hole introduced in the Néel state can be solved exactly in the $d \rightarrow \infty$ limit. In that case the local Green's function is composed of delta peaks, corresponding to the bound state of a particle in a linear or string potential. This potential is generated if the hole moves away from the initial state by m steps, destroying pairs of antiferromagnetic bonds along its path, thus enhancing the energy roughly by $mJ/2$. In the case of finite doping and finite temperature the delta peaks broaden and slightly shift, but they are still very pronounced for doping as large as 30%.

The nonphysical multipeak structure in the local spectral function can be attributed to the absence of the quantum magnetic fluctuations in this approach. Only the static (Hartree) part of the inter-site interaction is retained, while the flipping part, that would remove traces of a hole, is ignored.

In the EDMFT, an important part of nonlocal quantum fluctuations is retained. This is achieved by scaling the inter-site interaction term J in the same way as hopping term t , to the order $1/\sqrt{d}$, therefore both terms remain equally important in the limit of large d . The effective impurity problem thus

obtained is also coupled to the frequency dependent Weiss field induced by the inter-site interaction. The two-particle nature of the nonlocal interaction dictates the bosonic nature of the corresponding effective bath. As a result, the effective single-site problem can be thought of as an impurity coupled not only to a self-consistent fermionic bath but also to a self-consistent bosonic bath.

3.1 The EDMFT effective action

For simplicity, let us assume there is no long-range order (i.e. The system is in the paramagnetic state). Let us start the derivation of the EDMFT equations with the general action corresponding to the Hamiltonian (3.1)

$$S = \int_0^\beta d\tau \left[\sum_{i,\sigma} c_{i\sigma}^\dagger(\tau) \left(\frac{\partial}{\partial \tau} - \mu \right) c_{i\sigma}(\tau) - \sum_{ij,\sigma} t_{ij} c_{i\sigma}^\dagger(\tau) c_{j\sigma}(\tau) + \frac{1}{2} \sum_{ij} J_{ij} \vec{S}_i(\tau) \cdot \vec{S}_j(\tau) + \sum_i U n_{i\uparrow}(\tau) n_{i\downarrow}(\tau) \right]. \quad (3.3)$$

The action can again be divided into three parts: the on-site part is just the same like in the previous chapter Eq. (2.4), the inter-site part is superimposed with the magnetic interaction term

$$\Delta S = \int_0^\beta d\tau \left[\sum_{i,\sigma} -t_{io} c_{i\sigma}^\dagger(\tau) c_{o\sigma}(\tau) - t_{oi} c_{o\sigma}^\dagger(\tau) c_{i\sigma}(\tau) + \frac{1}{2} (J_{io} + J_{oi}) \vec{S}_i(\tau) \cdot \vec{S}_o(\tau) \right], \quad (3.4)$$

while the cavity part equals to the original action (3.3) with site o excluded from all summations. The partition function can again be expanded in the series like in Eq. (2.7). The first term linear in ΔS

$$\int_0^\beta \langle \Delta S(\tau) \rangle^{(0)} \quad (3.5)$$

vanishes, since the average of each spin $\langle \vec{S}_i(\tau) \rangle = 0$ is zero by the assumption of no long range order in the system. If the symmetry of the phase is broken like in the ferromagnets or antiferromagnets, the spin operator has to be replaced with its deviation from the average value in original Hamiltonian (3.1). The second term in the series expansion then reads

$$\begin{aligned}
 & \frac{1}{2!} \int_0^\beta d\tau_1 \int_0^\beta d\tau_2 \langle T_\tau \Delta S(\tau_1) \Delta S(\tau_2) \rangle^{(0)} = \\
 & \frac{1}{2!} \int_0^\beta d\tau_1 \int_0^\beta d\tau_2 \left\langle T_\tau \left[\sum_{i,\sigma} t_{io} c_{i\sigma}^\dagger(\tau_1) c_{o\sigma}(\tau_1) + t_{oi} c_{o\sigma}^\dagger(\tau_1) c_{i\sigma}(\tau_1) - \right. \right. \\
 & \qquad \qquad \qquad \left. \sum_i J_{oi} \vec{S}_o(\tau_1) \cdot \vec{S}_i(\tau_1) \right] \times \\
 & \qquad \qquad \qquad \left. \left[\sum_{i,\sigma} t_{io} c_{i\sigma}^\dagger(\tau_2) c_{o\sigma}(\tau_2) + t_{oi} c_{o\sigma}^\dagger(\tau_2) c_{i\sigma}(\tau_2) - \right. \right. \\
 & \qquad \qquad \qquad \left. \left. \sum_i J_{io} \vec{S}_i(\tau_2) \cdot \vec{S}_o(\tau_2) \right] \right\rangle^{(0)}. \quad (3.6)
 \end{aligned}$$

It is crucial to observe that there is no interference between the kinetic and the spin term since the average of the correlation function $\langle c_{i\sigma}(\tau_1) \vec{S}_j(\tau_2) \rangle^{(0)}$ vanishes. The leading order term in the effective action thus reads

$$\begin{aligned}
 S_{eff} = & - \int_0^\beta d\tau_1 \int_0^\beta d\tau_2 c_{o\sigma}^\dagger(\tau_1) \sum_{ij} t_{io} t_{oj} \langle T_\tau c_{i\sigma}(\tau_1) c_{j\sigma}^\dagger(\tau_2) \rangle^{(0)} c_{o\sigma}(\tau_2) - \\
 & \int_0^\beta d\tau_1 \int_0^\beta d\tau_2 \vec{S}_o(\tau_1) \frac{1}{2} \sum_{ij} J_{io} J_{oj} \langle T_\tau \vec{S}_i(\tau_1) \vec{S}_j(\tau_2) \rangle^{(0)} \vec{S}_o(\tau_2) + S_0. \quad (3.7)
 \end{aligned}$$

Within EDMFT both terms are equally important and are of order 1 in the $1/d$ expansion. The two-point Green's function and the susceptibility scale as $1/d^{|i-j|/2}$ since t and J fall off as $1/\sqrt{d}$. Furthermore i and j are neighbors of site o and are thus at least 2 lattice sites apart (in Manhattan distance) giving $1/d$ contribution. The prefactor t^2 or J^2 is proportional to $1/d$, while the double sum gives d^2 and the net results is therefore of order 1.

Further it follows from the Linked Cluster Theorem that only *connected* n -point correlation functions appear in higher order terms of the effective action. Since they have the usual dependence on $1/d$, all but the first term vanishes in the limit $d \rightarrow \infty$. For instance, next order term would involve 3-point connected correlation function $\chi_{ijk} \sim \langle S_i^z S_j^z S_k^z \rangle$ or $C_{ijk} \sim \langle S_i^z c_j^\dagger c_k \rangle$ that scale like $1/d^{|i-j|/2} d^{|i-k|/2}$. When all three variables i , j and k are different, correlation function is of order $1/d^2$ since all three sites are neighbors of o . The prefactor J^3 or Jt^2 is proportional to $1/d^{3/2}$ while sums give d^3 . The term is thus of order $1/\sqrt{d}$. If $i = j$ but distinct from k the correlation function is of order $1/d$ while sums give d^2 and the net result is again of order $1/\sqrt{d}$. Higher order terms drop even faster than $1/\sqrt{d}$. Thus, in the limit of

large d all but the first term (3.7) can be neglected and the effective action becomes

$$S_{eff} = \int_0^\beta U n_{o\uparrow}(\tau)n_{o\downarrow}(\tau) - \int_0^\beta d\tau_1 \int_0^\beta d\tau_2 c_{o\sigma}^\dagger(\tau_1)\mathcal{G}_0^{-1}(\tau_1 - \tau_2)c_{o\sigma}(\tau_2) - \frac{1}{2} \int_0^\beta d\tau_1 \int_0^\beta d\tau_2 \vec{S}_0(\tau_1)\underline{\chi}_0^{-1}(\tau_1 - \tau_2)\vec{S}_0(\tau_2) \quad (3.8)$$

where

$$\begin{aligned} \mathcal{G}_0^{-1}(\tau_1 - \tau_2) &= -\left(\frac{\partial}{\partial\tau_1} - \mu\right)\delta_{\tau_1\tau_2} + \sum_{ij} t_{io}t_{oj} \left\langle T_\tau c_{i\sigma}(\tau_1)c_{j\sigma}^\dagger(\tau_2) \right\rangle^{(0)} \\ \underline{\chi}_0^{-1}(\tau_1 - \tau_2) &= \sum_{ij} J_{io}J_{oj} \left\langle T_\tau \vec{S}_i(\tau_1)\vec{S}_j(\tau_2) \right\rangle^{(0)}. \end{aligned} \quad (3.9)$$

The Weiss fields are thus determined by the cavity Green's function $G_{ij}^{(0)}$ and cavity susceptibility $\chi_{ij}^{(0)}$

$$\begin{aligned} \mathcal{G}_0^{-1}(i\omega) &= i\omega + \mu - \sum_{ij} t_{io}t_{oj}G_{ij}^{(0)}(i\omega) \\ \chi_0^{-1}(i\omega) &= \sum_{ij} J_{io}J_{oj}\chi_{ij}^{(0)}(i\omega) \end{aligned} \quad (3.10)$$

The absence of interference between the kinetic and spin term in the Eq. (3.7) also leads to separate equations for both cavity quantities

$$\begin{aligned} G_{ij}^{(0)} &= G_{ij} - \frac{G_{io}G_{oj}}{G_{oo}} \\ \chi_{ij}^{(0)} &= \chi_{ij} - \frac{\chi_{io}\chi_{oj}}{\chi_{oo}}. \end{aligned} \quad (3.11)$$

Equations (3.8), (3.10), and (3.11) form a closed system of functional equations. The main difficulty lies in the solution of S_{eff} therefore we would like to find alternative Hamiltonian representation of the above effective action. Since S_{eff} includes retardation effects through frequency dependent Weiss fields, it is necessary to introduce auxiliary degrees of freedom describing the baths. The one-particle character of the Weiss field \mathcal{G}_0^{-1} can be represented with the fermionic bath while the two particle field χ_0^{-1} has a bosonic nature and dictates bosonic bath.

3.2 The impurity model

One of the possible choices to represent the action (3.8) in a Hamiltonian formulation is

$$\begin{aligned}
 H = & \sum_{k\sigma} \varepsilon_k c_{k\sigma}^\dagger c_{k\sigma} + V \sum_{k\sigma} (c_{k\sigma}^\dagger c_{o\sigma} + c_{o\sigma}^\dagger c_{k\sigma}) - \sum_{\sigma} \mu c_{o\sigma}^\dagger c_{o\sigma} + U n_{o\uparrow} n_{o\downarrow} + \\
 & \sum_q w_q \vec{\Phi}_q^\dagger \vec{\Phi}_q + g \sum_q \vec{S}_o \cdot (\vec{\Phi}_q + \vec{\Phi}_{-q}^\dagger), \tag{3.12}
 \end{aligned}$$

where $\vec{\Phi}_q$ corresponds to a vector-bosonic bath with the following commutation relations $[\Phi_q^\alpha, \Phi_{q'}^{\beta\dagger}] = \delta_{qq'} \delta_{\alpha\beta}$. The corresponding action

$$\begin{aligned}
 S = S_0 + \int_0^\beta d\tau \sum_{k\sigma} \left[c_{k\sigma}^\dagger(\tau) \left(\frac{\partial}{\partial\tau} + \varepsilon_k \right) c_{k\sigma}(\tau) + V c_{k\sigma}^\dagger(\tau) c_{o\sigma}(\tau) + V c_{o\sigma}^\dagger(\tau) c_{k\sigma}(\tau) \right] + \\
 \int_0^\beta d\tau \sum_q \left[\vec{\Phi}_q^\dagger(\tau) \left(\frac{\partial}{\partial\tau} + w_q \right) \vec{\Phi}_q(\tau) + g \vec{\Phi}_q(\tau) \cdot \vec{S}_o(\tau) + g \vec{S}_o(\tau) \cdot \vec{\Phi}_{-q}^\dagger(\tau) \right] \tag{3.13}
 \end{aligned}$$

is quadratic in $c_{k\sigma}$ and $\vec{\Phi}_q$, therefore both baths can be eliminated leading to

$$\begin{aligned}
 S = S_0 - \int_0^\beta d\tau_1 \int_0^\beta d\tau_2 \sum_{\sigma} c_{o\sigma}^\dagger(\tau_1) \left(\sum_k V^2 \frac{\delta_{\tau_1\tau_2}}{\frac{\partial}{\partial\tau} + \varepsilon_k} \right) c_{o\sigma}(\tau_2) - \\
 \int_0^\beta d\tau_1 \int_0^\beta d\tau_2 \vec{S}_o(\tau_1) \left(\sum_q g^2 \frac{\delta_{\tau_1\tau_2}}{\frac{\partial}{\partial\tau} + w_q} \right) \vec{S}_o(\tau_2). \tag{3.14}
 \end{aligned}$$

This action is identical to effective action (3.8) provided that the following relations hold

$$\begin{aligned}
 \mathcal{G}_0^{-1}(\tau_1 - \tau_2) &= - \left(\frac{\partial}{\partial\tau_1} - \mu \right) \delta_{\tau_1\tau_2} + \sum_k V^2 \frac{\delta_{\tau_1\tau_2}}{\frac{\partial}{\partial\tau} + \varepsilon_k} \\
 \chi_0^{-1}(\tau_1 - \tau_2) &= \sum_q g^2 \left(\frac{\delta_{\tau_1\tau_2}}{\frac{\partial}{\partial\tau} + w_q} + \frac{\delta_{\tau_1\tau_2}}{-\frac{\partial}{\partial\tau} + w_q} \right) \tag{3.15}
 \end{aligned}$$

or equivalently

$$\begin{aligned}
 \mathcal{G}_0^{-1}(i\omega) &= i\omega + \mu - \sum_k V^2 G_k(i\omega) \\
 \chi_0^{-1}(i\omega) &= - \sum_q g^2 G_{\Phi_q}(i\omega). \tag{3.16}
 \end{aligned}$$

The density of states of the fermionic and bosonic baths, coupled to the impurity, is just proportional to the imaginary part of the retarded Weiss fields $\mathcal{G}_0^{-1}(\omega + i\delta)$ and $\chi_0^{-1}(\omega + i\delta)$, respectively. They are not known a priori but must be found by solving the self-consistent problem.

3.3 Still local theory?

Within the EDMFT, the lattice problem (3.1) is mapped onto an effective impurity problem (3.12) with the self-consistency condition (3.16). Furthermore, the lattice Green's function is determined by the on-site self-energy alone. At the same time, the spin susceptibility is determined by the local on-site effective cumulant alone, or equivalently, the on-site part of the vertex function irreducible in terms of both the particle hole bubble and the single J_{ij} line. This is a consequence of the limit $d \rightarrow \infty$ and EDMFT scaling. This important statement will be shown now explicitly within the perturbation theory in the on-site interaction U and magnetic interaction J .

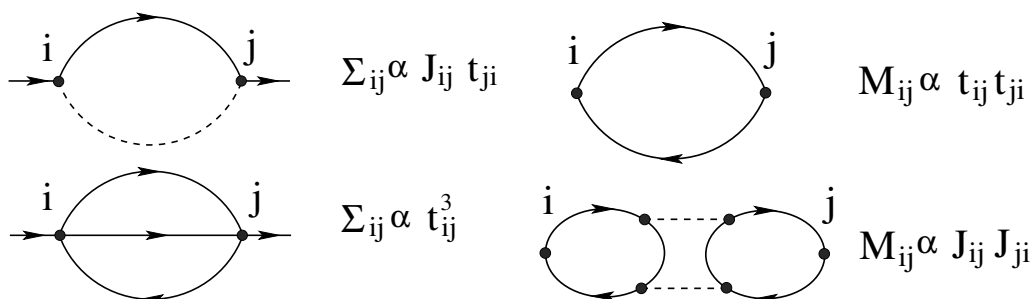


Figure 3.1: left: Example of diagrams contributing to the self-energy in second and third order. They are proportional to $1/\sqrt{d}$ and $1/d$ respectively. right: First two non-local diagrams contributing to the irreducible spin cumulant. They are also of the order $1/\sqrt{d}$.

Consider first the self-energy $\Sigma_{\langle ij \rangle}$. The Hartree contribution from $J_{\langle ij \rangle}$ vanishes since $\langle S_i \rangle = 0$, while Fock and high-order contributions can be written in a skeleton expansion. As illustrated in Fig. 3.1, any skeleton expansion diagram for the self-energy contains at least an inter-site interaction path (dotted line) and a fermion propagator from site i to site j (full line). Both are at least of order $1/\sqrt{d}$, therefore $\Sigma_{\langle ij \rangle}$ falls off at least as $1/d$. More generally, $\Sigma_{ij} \sim 1/d^{|i-j|}$, where $|i-j|$ is the the distance between sites in Manhattan metric. This implies that for any generic wave vector q the non-local self-energy is at least of order $1/\sqrt{d}$ and therefore in the large d limit $\Sigma(\mathbf{q}, \omega)$ is momentum independent and equal to the on-site part $\Sigma_{ii}(\omega)$. Similarly, any non-local diagram for irreducible spin cumulant (i.e. diagram for nonlocal spin susceptibility irreducible in terms of cutting single intersite interaction line J) contains at least two inter-site lines and therefore also falls of as $1/d^{|i-j|}$. Following the same lines of argument, one can show that irreducible spin cumulant is also \mathbf{q} independent in the large d limit $M(\mathbf{q}, \omega) = M_{ii}(\omega)$. The lattice Green's function and spin susceptibility

therefore read

$$\begin{aligned} G_{\mathbf{k}}(i\omega) &= \frac{1}{i\omega + \mu - \varepsilon_{\mathbf{k}} - \Sigma(i\omega)} \\ \chi_{\mathbf{q}}(i\omega) &= \frac{1}{M^{-1}(i\omega) + J_{\mathbf{q}}}. \end{aligned} \quad (3.17)$$

Now, we are ready to determine relationship between the fermionic (bosonic) Weiss field and local self-energy (irreducible spin cumulant). Fourier transforming sums (3.10) and taking into account the form of the lattice Green's function as well as the spin susceptibility (3.17) we get (see Appendix A)

$$\begin{aligned} \sum_{ij} t_{io}t_{oj} \left(G_{ij} - \frac{G_{io}G_{oj}}{G_{oo}} \right) &= i\omega + \mu - \Sigma - G_{oo}^{-1} \\ \sum_{ij} J_{io}J_{oj}\chi_{ij}^{(0)} &= M^{-1} - \chi_{oo}^{-1}. \end{aligned} \quad (3.18)$$

Weiss fields therefore reduce to

$$\begin{aligned} \mathcal{G}_0^{-1} &= \Sigma + G_{oo}^{-1} \\ \chi_0^{-1} &= M^{-1} - \chi_{oo}^{-1}. \end{aligned} \quad (3.19)$$

These are the basic equations of the EDMFT and together with the Eq. (3.17) and solution of the impurity problem (3.12) form a closed set of equations.

Weiss field $\mathcal{G}_0^{-1}(\tau - \tau')$ plays a role of an effective field and is equal to the amplitude for a fermion to be created on an isolated site at time τ (coming from the external fermionic bath) and being destroyed at time τ' (going back to the bath). On the other hand, $\chi_0^{-1}(\tau - \tau')$ is equal to the amplitude for the local spin to be flipped at time τ (emitting a boson) and flipped back again at time τ' (absorbing a boson). Weiss fields are just auxiliary quantities that can be eliminated from all the equations. Instead, we can also eliminate lattice self-energy and irreducible spin cumulant and keep Weiss fields. They can be calculated at the end from the Eq. (3.19). Let us insert the form of the self-energy and cumulant in Eq. (3.17)

$$\begin{aligned} G_{\mathbf{k}} &= \frac{1}{i\omega + \mu - \varepsilon_{\mathbf{k}} - \mathcal{G}_0^{-1} + G_{oo}^{-1}} \\ \chi_{\mathbf{q}} &= \frac{1}{\chi_{oo}^{-1} + \chi_0^{-1} + J_{\mathbf{q}}} \end{aligned} \quad (3.20)$$

Summing over all q we finally get

$$G_{oo} = \sum_{\mathbf{k}} \frac{1}{i\omega + \mu - \varepsilon_{\mathbf{k}} - \mathcal{G}_0^{-1} + G_{oo}^{-1}} \quad (3.21)$$

$$\chi_{oo} = \sum_{\mathbf{q}} \frac{1}{\chi_{oo}^{-1} + \chi_0^{-1} + J_{\mathbf{q}}}. \quad (3.22)$$

Once the local Green's function G_{oo} and the local susceptibility χ_{oo} is obtained from solution of the impurity problem (3.12), Weiss fields can be determined from the above equations. These Weiss fields then uniquely determine the solution of the impurity problem, particularly local susceptibility and local Green's function

$$\begin{aligned} G_{oo} &= G_{impurity}(\mathcal{G}_0^{-1}, \chi_0^{-1}) \\ \chi_{oo} &= \chi_{impurity}(\mathcal{G}_0^{-1}, \chi_0^{-1}). \end{aligned} \quad (3.23)$$

The equations indeed close. In practice, the main difficulty lies in the solution of the impurity problem (3.12). Even without bosonic bath, the Anderson impurity model is a difficult quantum many-body problem. The Bethe ansatz solution can not be directly used since it does not provide dynamical quantities. Numerical renormalization group suffers from convergence problems, while other approaches are less reliable and limited to certain set of parameters or temperatures. When bosons are added to the model, the problem becomes even more intractable due to enlarged Hilbert space. In the next section a diagrammatic method will be used to approximately solve the impurity problem (3.12).

The generalization of the method to a state with long-range commensurate spatial ordering is straightforward. It requires replacement of spin operators in the original Hamiltonian with their deviation from the average value before taking the limit of large dimensions. This ensures that the divergent Hartree term proportional to zJ is absent. Since z is large but finite for any physical system, and the Hartree term is local, it can be added back and put into the local part of the action S_0 . It plays the role of a staggered magnetic field and has the same form in the impurity model as well as in the original lattice model.

In the context of the long range Coulomb interaction, the EDMFT equations were independently derived by two groups H. Kajuter and G. Kotliar [8] and also by Q. Si and J.L. Smith [6]. Q. Si *et al.* extended the theory to spin models in the form that was presented here. They also showed that the theory is conserving despite the fact that self-energy is local, but the two particle vertex function is momentum dependent and therefore the true Luttinger-Ward functional does not exist. It does exist before taking the infinite d limit, the momentum dependent diagrams are then of leading order for the two particle vertex function while they are subleading in the context of self-energy. In spite of this, the approach is conserving since it

obeys alternative set of conserving criteria, originally proposed by Baym and Kadanoff [25].

Chapter 4

Approximate solution of EDMFT

As explained in the previous section, lattice models of correlated fermions can be mapped, in the limit of large coordination number, onto a single impurity model which has to satisfy a self-consistency condition. This condition specifies, for a given lattice, the relation between the Weiss functions (entering the impurity model effective action) and the local Green's function and local susceptibility. In this approximation, the lattice is entirely described with its density of states, since this is the only lattice quantity that enters the self-consistency condition.

In practice, this coupled problem is solved in the iterative manner: the local Green's function and local susceptibility are obtained by solving the impurity problem given particular Weiss fields (in the first step a guess for the Weiss fields is used). Then the calculated Green's function and susceptibility are used as an input into the self-consistency condition to produce new Weiss functions. The process is iterated until a converged solution is reached.

The most difficult step in the iterative procedure is the repeated solution of the impurity model, for an essentially arbitrary fermionic and bosonic baths. Even though spatial degrees of freedom have been eliminated, the impurity model remains a true many-body problem. In contrast to the solution of the impurity problem, the implementation of the self-consistency condition is relatively straightforward. Even though no rigorous proof exists concerning the convergence of the iterative process, practice has shown that it is usually not difficult to reach self-consistent solution. Convergence is usually attained after a few iterations.

In this chapter we will show how to build a conserving approximation for the impurity problem (3.12) and how to calculate local quantities (local susceptibility and local Green's function) within a particular approximation.

4.1 Susceptibility

Local susceptibility can be defined as a derivative of the magnetization at the chosen site o with respect to the applied magnetic field at that particular site $\partial m_o / \partial h_o$. In the original Hubbard model (3.1), the magnetic field couples through the term $h_o S_o^z$. This term is local and changes only the on-site action S_o which is the same for the lattice as well as for the impurity model. Therefore, the impurity model is also supplemented by the term $h_o S_o^z$. The applied magnetic field does not couple to the fermionic bath but only to the impurity spin. Since there is no interference between magnetic and hopping term in (3.8), the fermionic bath is not altered in linear order with the applied magnetic field. On the other hand, bosonic bath is changed through the self-consistency condition in linear order and therefore the bosonic non-interacting part (w_q) of the impurity Hamiltonian (3.12) is changed. The average magnetization at the impurity site is

$$\langle S_o^z(t) \rangle = \text{Tr}(\rho_0 S_o^z) - i \int_{-\infty}^t \text{Tr}(\rho_0 [S_o^z(t), \Delta H(t')]), \quad (4.1)$$

where $\Delta H = h_o S_o^z$ and $\rho_0 = \exp(-\beta H) / Z$ with H being impurity Hamiltonian (3.12) without coupling to the magnetic field. Even though the first term is zero, its derivative with respect to the applied magnetic field can be nonzero, since parameters of the Hamiltonian (w_q) are altered, when magnetic field is applied. The magnetic susceptibility is thus superimposed with the term $\beta \langle \partial H / \partial h_o S_o^z \rangle$ which involves $\langle \Phi_q^\dagger \Phi_q S_o^z \rangle$. This average is zero in the paramagnetic phase and therefore the susceptibility is not changed through the disturbance of the bosonic bath and takes its usual form

$$\chi_{oo}^{\alpha\beta}(\tau - \tau') = \langle S_o^\alpha(\tau) S_o^\beta(\tau') \rangle. \quad (4.2)$$

Note that in the molecular mean-field approximation the additional term does not vanish and the susceptibility has to be calculated from the following equation

$$\chi_{ij} = \beta [\langle S_j^z S_i^z \rangle - \langle S_j^z \rangle \langle S_i^z \rangle] + \beta \left[\left\langle \frac{\partial H}{\partial h_j} S_i^z \right\rangle - \left\langle \frac{\partial H}{\partial h_j} \right\rangle \langle S_i^z \rangle \right] \quad (4.3)$$

The local magnetic field, applied at a chosen site, polarizes neighbors of the selected site. These polarized neighbors then also affect the magnetization at the selected site and therefore the local susceptibility is not just $1/4\beta$ but contains also the nonlocal part, proportional to the derivative of the Hamiltonian with respect to the applied field

$$\partial H / \partial h_j = \sum_{kl} J_{kl} \frac{\partial \langle S_k^z \rangle}{\partial h_j} S_l^z = - \sum_{kl} J_{kl} \chi_{kj} S_l^z. \quad (4.4)$$

In the absence of spontaneous magnetization, the intersite susceptibility in the molecular mean-field approximation thus reads

$$\chi_{ij} = \beta \langle S_i^z S_j^z \rangle - \beta \sum_{kl} J_{kl} \chi_{kj} \langle S_l^z S_i^z \rangle = \frac{1}{4} \beta (\delta_{ij} - \sum_k J_{ik} \chi_{kj}) \quad (4.5)$$

or equivalently $\chi_{\mathbf{q}} = 1/(4T + J_{\mathbf{q}})$. The second term in Eq. (4.5) describes the influence of the polarized media to the selected site. Note that it is time independent (i.e. static) since all quantum fluctuations are absent in the molecular mean-field approximation. Within EDMFT the local quantum fluctuations are fully taken into account and are mediated through the bosonic bath that is coupled to the local impurity spin.

4.2 The auxiliary-particle representation

The common feature of any strongly correlated electronic system is a strong Coulomb repulsion U between electrons at the same lattice site. For simplicity, U is usually taken to be larger than any other scale in the system. In many physical systems of interest, this is not justified and one needs to work with large but finite Coulomb repulsion U . We will address that issue in chapter 6. Here, we will focus on the t-J model, which becomes equivalent to the model described by the Hamiltonian (3.1) only in the limit of infinite U . Any perturbation in the interaction strength U is not sensible in this case. Rather an alternative approach is needed, where large U term can be exactly taken into account. An elegant way is the method of auxiliary particles, where additional degrees of freedom are introduced with pseudo-bosons and pseudo-fermions [26]. Any impurity state is represented with one auxiliary particle - either boson or fermion. The powerful machinery of quantum field theory can be used to solve the problem, provided that the projection onto the physical subspace can be performed in a satisfactory way.

For a single impurity problem of spin 1/2, two pseudo-bosons (i.e. empty and doubly occupied site) and two pseudo-fermions (singly occupied site) are needed

$$\begin{aligned} |0\rangle &= b^\dagger |vac\rangle \\ |\sigma\rangle &= f_\sigma^\dagger |vac\rangle \\ |2\rangle &= a^\dagger |vac\rangle. \end{aligned} \quad (4.6)$$

The physical electron operator is expressed by

$$c_{\sigma\sigma}^\dagger |0\rangle = (f_\sigma^\dagger b + \sigma a f_{-\sigma}) |vac\rangle \quad (4.7)$$

and the number operator becomes

$$Q \equiv n_b + n_a + n_{f\uparrow} + n_{f\downarrow} = 1. \quad (4.8)$$

The problem is solved within the grand canonical ensemble where Q can take any value, and the projection onto $Q = 1$ subspace is performed at the end. It is important to note that the number operator is time independent (i.e. it commutes with the Hamiltonian) and can take only integer values.

The coupling between the local degrees of freedom and bosonic bath is particularly simple since the impurity spin, in the physical $Q = 1$ subspace, is equal to the pseudo-fermion spin

$$S_o |Q = 1\rangle = S_f |Q = 1\rangle. \quad (4.9)$$

In terms of auxiliary particles the Hamiltonian (3.12) takes the form

$$\begin{aligned} H = & \sum_{k\sigma} \varepsilon_k c_{k\sigma}^\dagger c_{k\sigma} + V \sum_{k\sigma} \left(c_{k\sigma}^\dagger b^\dagger f_\sigma + f_\sigma^\dagger b c_{k\sigma} + \sigma c_{k\sigma}^\dagger f_{-\sigma}^\dagger a + \sigma a^\dagger f_{-\sigma} c_{k\sigma} \right) + \\ & U n_a - \mu(n_{f\uparrow} + n_{f\downarrow} + 2n_a) + \sum_q w_q \vec{\Phi}_q^\dagger \vec{\Phi}_q + g \sum_q \vec{S}_f \cdot (\vec{\Phi}_q + \vec{\Phi}_{-q}^\dagger) \end{aligned} \quad (4.10)$$

The local Coulomb interaction term is now represented with a "heavy" boson state and $U - 2\mu$ plays the role of the on-site energy for that particle. The corresponding excited states are located at very high energies in the limit of large U and can be ignored in that case. In the $t - J$ model U is infinite, therefore all terms that include "heavy" boson can be omitted.

The projection onto the physical subspace can be performed exactly in a diagrammatic approach, as shown first by Abrikosov [27]. The grand canonical probability distribution function is defined by

$$\varrho_G = e^{-\beta(H+\lambda Q)} / Z_G \quad (4.11)$$

and the physical ($Q = 1$) expectation value of any operator A can be obtained by the limit of infinite λ

$$\langle A \rangle = \lim_{\lambda \rightarrow \infty} \frac{\langle QA \rangle_G}{\langle Q \rangle_G}. \quad (4.12)$$

Within a conserving approximation, derived from a Luttinger-Ward functional Φ , the diagrams contributing to the local magnetic susceptibility (4.2) can be easily determined. For the system described by the Hamiltonian (4.10) an exact relation between the *grand canonical* boson self-energy and local susceptibility exists (see Appendix B)

$$\chi_{oo}(i\omega) = -\frac{1}{g^2} \Sigma_\Phi(i\omega). \quad (4.13)$$

This implies that only diagrams, obtained by cutting a single vector boson line in the Luttinger-Ward functional, contribute to the local spin susceptibility. In the same way one can derive the relation between the local physical electron Green's function and *grand canonical* conduction electron self-energy

$$G_{oo}(i\omega) = \frac{1}{V^2} \Sigma_c(i\omega) \quad (4.14)$$

4.3 The approximation scheme

The choice of diagrams for a certain approximation should be dictated by the dominant physical processes in the system. At the same time, the approximation should obey sum-rules and conservation laws. The simplest way to build such approximation is to define corresponding Luttinger-Ward functional Φ and derive other quantities (self-energies and irreducible vertices) from it, instead of choosing diagrams for each quantity separately. This ensures that the approximation is conserving.

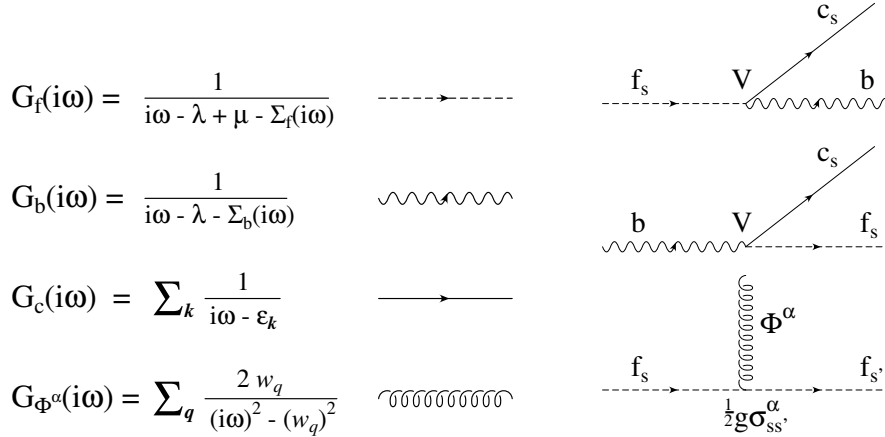


Figure 4.1: Fully renormalized Green's functions and bare vertices corresponding to the Hamiltonian (4.10)

The Luttinger-Ward functional Φ consists of all vacuum skeleton diagrams built out of fully renormalized Green's functions (G_f , G_b , G_c , G_Φ) and bare vertices V and g (see Fig. 4.1). The self-energies (Σ_f , Σ_b , Σ_c , Σ_Φ) are obtained by taking the functional derivative of Φ with respect to the corresponding Green's function (cutting the Green's function line in each diagram in all possible ways).

The Luttinger-Ward functional Φ may be built in powers of coupling constants V and g , since both can be considered small. In addition, we

$$\begin{aligned}
 \Phi = & \text{I} + \frac{1}{2} \text{II} + \frac{1}{2} \text{III} + \frac{1}{4} \text{IV} + \frac{1}{2} \text{V} + \\
 & \frac{1}{2} \text{VI} + \text{VII} + \text{VIII} + \frac{1}{2} \text{IX} + \frac{1}{6} \text{X} + \dots
 \end{aligned}$$

Figure 4.2: A few lowest order diagrams contributing to the Luttinger-Ward functional for the EDMFT impurity problem (4.10).

will limit our analysis to the simplest approximation that captures Kondo as well as mixed valence physics and recovers correct Kondo scale in the usual Anderson model. In the limit $U \rightarrow \infty$ one single diagram is enough (first diagram in Fig. 4.2) to get reliable results for temperatures above $\approx 0.2 T_K$. This method has been extensively tested in the case of DMFT [28] and it was shown to be reliable in the whole parameter range except for $T \ll T_K$, where T_K can be determined as the width of the quasiparticle peak in the local spectral function. It was also stressed by many authors, that NCA breaks down at that point, since it slightly underestimates the value of the self-energy close to the chemical potential, which is small in the Fermi liquid case and approaches zero as T^2 . Hence, at that point NCA produces non-physical results (negative self-energy and spectral function). In the single impurity problem, NCA also gives a few percent too high Abrikosov-Suhl resonance, but in that case the limitation is not so serious, since imaginary part of the impurity self-energy goes to a constant ($\Gamma/\sin^2(\pi n_d/2)$), rather than to zero at zero temperature and few percent smaller self-energy results in a few percent higher Kondo peak.

Now we need to add diagrams that involve bosons from a vector bosonic bath. For that purpose, one needs to consider the diagrams of bare perturbation theory instead of only skeleton ones. Then one needs to add bosons in all possible ways between various pseudo-fermions in any diagram. A conserving approximation is then constructed by replacing the bare propagators with fully dressed ones and by keeping only the skeleton diagrams. The number of possible diagrams blows up very rapidly since there is no restriction on the way how those bosons can be connected to fermions or how they can cross. However, the vertex g can be considered as a small quantity and leading order diagrams, at least at sufficiently high temperatures, will involve only small number of these vertices.

There are still infinite number of skeleton diagrams involving a single

boson line, however, in the symmetry-unbroken phase only a single diagram (diagram number II in Fig. 4.2) gives a nonzero contribution. All the rest involve a fermionic loop composed of pseudo-fermion and conduction electron propagator and one outgoing Φ^z boson line. The lowest order diagram of that type is the diagram number III in Fig. 4.2. Consider the upper-left fermionic loop in that diagram. The whole loop has a definite spin (it is not changed inside the loop), therefore the boson from the bath cannot flip the spin. Thus only the z component of the vector bosons can be exchanged Φ^z , which involves the vertex $g(-1)^s$. Since both values of spin are equally probable, the net contribution is zero. From the same reason also the diagrams VII and VIII do not contribute in the paramagnetic state. Thus only limited number of skeleton diagrams involving two vector bosons survive. First few of them are diagrams number IV, V and VI in Fig. 4.2.

4.4 Non-crossing approximation

$$\begin{aligned}
 \Phi &= \text{[Diagram 1]} + \frac{1}{2} \text{[Diagram 2]} \\
 \Sigma_f &= \text{[Diagram 3]} + \text{[Diagram 4]} \\
 \Sigma_b &= \text{[Diagram 5]} \\
 G_{00} &= \text{[Diagram 6]} \\
 \chi_{00} &= \text{[Diagram 7]}
 \end{aligned}$$

Figure 4.3: The two lowest order contributions to the Luttinger-Ward functional and corresponding self-energies. We will call the approximation "Non-crossing approximation" (NCA) since only diagrams with no line-crossings are taken into account.

It is natural to start the analysis of the model in the lowest possible order, including just the first two diagrams in the Fig. 4.2 (see Fig. 4.3).

To consider the magnitude of the coupling vertices V and g , we need to examine the smallness of the density of local conduction states near the chemical potential multiplied by V^2 as well as the density of bosonic states

multiplied by g^2

$$A_c(\varepsilon) = V^2 \sum_k \delta(\varepsilon - \varepsilon_k). \quad (4.15)$$

$$D_\Phi(\varepsilon) = g^2 \sum_q [\delta(\varepsilon - w_q) - \delta(\varepsilon + w_q)] \quad (4.16)$$

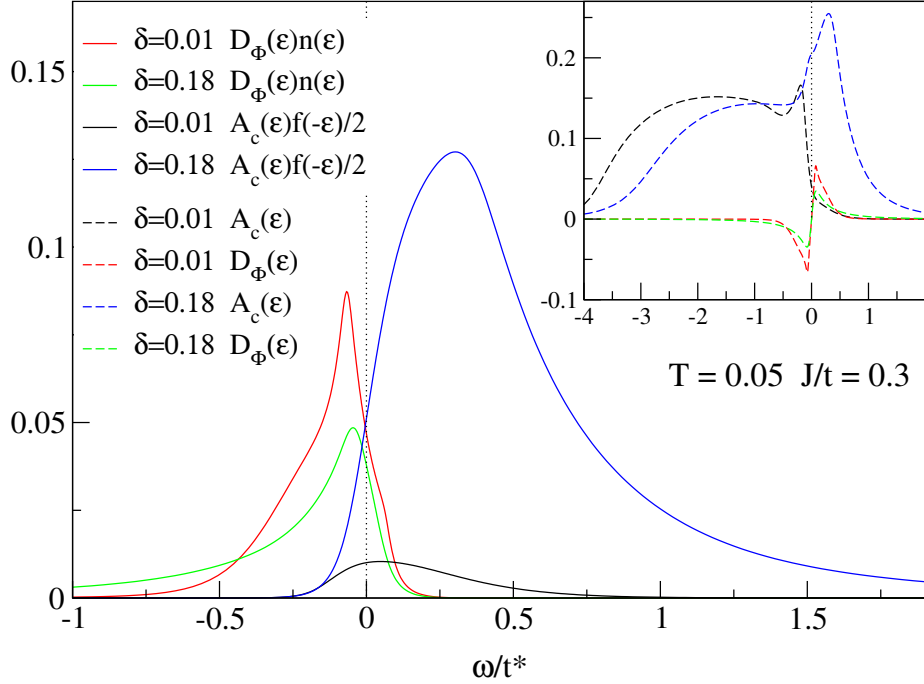


Figure 4.4: The main part shows the unoccupied part of the fermionic bath as well as the occupied part of the bosonic bath density of states corresponding to the NCA solution of the t-J model in the EDMFT. The inset shows the full fermionic and bosonic bath density of states.

Both vertices g and V are strong functions of doping. The solution shows, what could be also guessed by the physical intuition, that g dominates in the underdoped regime while V is the only important bare vertex in the overdoped regime (see Fig. 4.4). The reason is that V comes from the kinetic energy term which is obviously small near half-filling due to small amount of holes in the system but dominates in the overdoped regime. On the other hand, g originates from the intersite magnetic interaction therefore loses its strength with doping. The solution of the NCA equations also shows that g can be considered to be small for all doping concentrations and that maximum value of V (in the overdoped regime) is larger than maximum

value of g (in the underdoped regime) as long as J is smaller than t , which is usually taken to be around $J/t = 0.3$ for the t - J model.

Since NCA neglects all crossing diagrams, it is most reliable only when one of the vertices is much more important than the other. This is true for small doping $\delta \lesssim 0.1$ as well as for large doping $\delta \gtrsim 0.2$. Unfortunately, the NCA solution is less reliable in the optimally doped regime where the Kondo like interaction, or the kinetic part is equally important than the magnetic intersite interaction. The crossing terms between both processes (for example the diagram number V or VI in Fig. 4.2) should also be considered in this case. However, for high enough temperature vertex corrections can still be neglected even in this region and NCA should again be applicable.

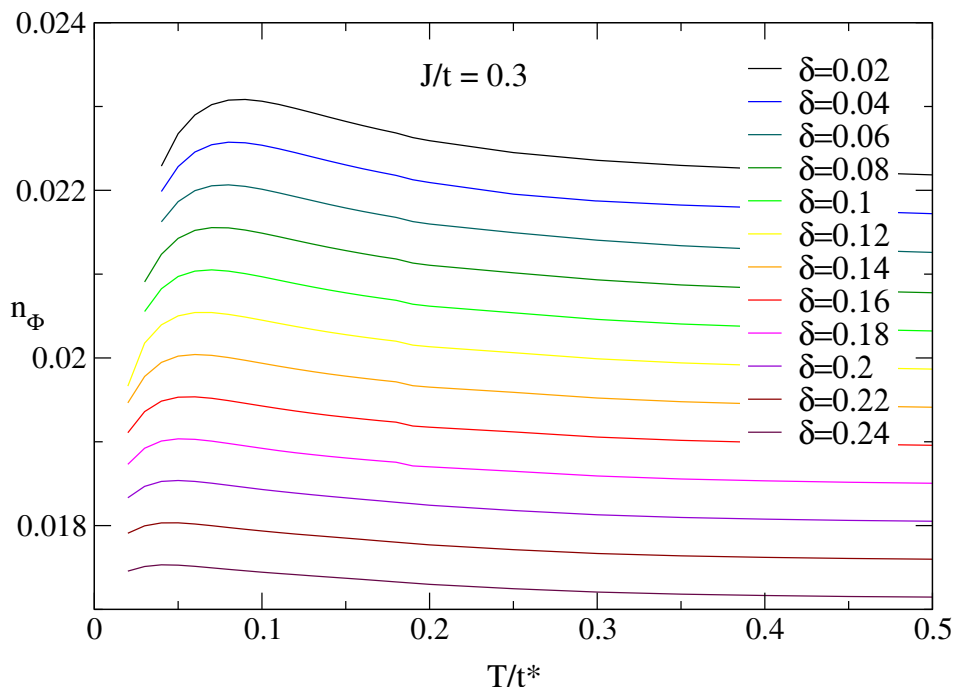


Figure 4.5: The occupation of the bosonic bath as defined in Eq. 4.17.

As shown in Fig. 4.4, the second vertex g , that couples the impurity spin with the bosonic bath, can be taken to be small for any doping as long as J/t is small quantity (0.3 in our case). The bosonic density of states never exceeds 0.1 and is nonzero only in a very narrow frequency range ($\approx \sqrt{z}J$) therefore the occupation of the bosonic bath, defined as

$$n_{\Phi} = \int n(\varepsilon)D_{\Phi}(\varepsilon)d\varepsilon \quad (4.17)$$

is always very small, never much above 2% (see Fig. 4.5).

For these reasons, we will mainly focus on the solution of the simple NCA equations (Fig. 4.3), that give qualitatively and also quantitatively reliable results at sufficiently high temperatures. This will be shown in the next chapter with comparison to the exact diagonalization results of the two dimensional t-J model.

After analytic continuation to real frequencies and projection onto the physical subspace, the NCA equations (see Appendix C) for paramagnetic phase explicitly read

$$\begin{aligned} \Sigma_f(\omega + i\delta) = & \int f(-\varepsilon)A_c(\varepsilon)G_b(\omega - \varepsilon + i\delta)d\varepsilon + \\ & \frac{3}{4} \int n(\varepsilon)D_\Phi(\varepsilon)G_f(\varepsilon + \omega + i\delta)d\varepsilon \end{aligned} \quad (4.18)$$

$$\Sigma_b(\omega + i\delta) = 2 \int f(\varepsilon)A_c(\varepsilon)G_f(\omega + \varepsilon + i\delta)d\varepsilon \quad (4.19)$$

$$\text{Im } G_{oo}(\omega + i\delta) = -\frac{\pi}{f(-\omega)} \int e^{-\beta\varepsilon} A_f(\varepsilon + \omega)A_b(\varepsilon)d\varepsilon \quad (4.20)$$

$$\text{Im } \chi_{oo}(\omega + i\delta) = \frac{\pi}{2n(\omega)} \int e^{-\beta\varepsilon} A_f(\varepsilon - \omega)A_f(\varepsilon)d\varepsilon. \quad (4.21)$$

The t-J lattice problem is then entirely determined in combination with the following EDMFT equations

$$A_c = \frac{1}{\pi} \text{Im } \mathcal{G}_0^{-1} \quad (4.22)$$

$$D_\Phi = \frac{1}{\pi} \text{Im } \chi_0^{-1} \quad (4.23)$$

$$G_{oo} = \sum_{\mathbf{k}} \frac{1}{\omega + \mu - \varepsilon_{\mathbf{k}} - \mathcal{G}_0^{-1} + G_{oo}^{-1}} \quad (4.24)$$

$$\chi_{oo} = \sum_{\mathbf{q}} \frac{1}{\chi_{oo}^{-1} + \chi_0^{-1} + J_{\mathbf{q}}}. \quad (4.25)$$

Another possibility to test the approximation is to compare it with the high temperature expansion results. For simplicity, we will focus only on the zero doping case of the t-J model. For high enough temperatures, the average value of the magnetization can be calculated with a straightforward expansion in powers of $1/T$

$$\langle S_i^z \rangle = \frac{1}{Z} \left\{ -\beta \text{Tr} (e^{-\beta H_0} \Delta H S_i^z) + \frac{\beta^2}{2!} \text{Tr}([\Delta H, H_0] S_i^z) - \right.$$

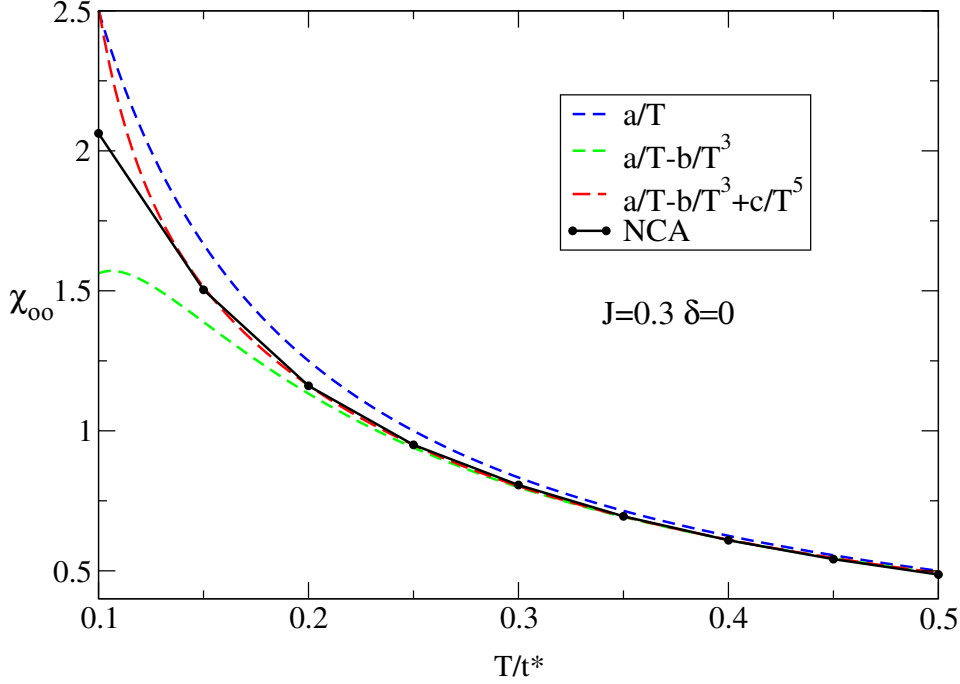


Figure 4.6: The local spin susceptibility calculated with the NCA and EDMFT compared with the high-temperature expansion.

$$\frac{\beta^3}{3!} \left(2\text{Tr}(H_0 [\Delta H, H_0] S_i^z) + \text{Tr}([\Delta H, H_0] H_0 S_i^z) \right) + \dots \} \quad (4.26)$$

$$Z = \left\{ \text{Tr}(e^{-\beta H_0}) + \frac{\beta^2}{2!} \text{Tr}([\Delta H, H_0]) - \frac{\beta^3}{3!} \left(2\text{Tr}(H_0 [\Delta H, H_0]) + \text{Tr}([\Delta H, H_0] H_0) \right) + \dots \right\}, \quad (4.27)$$

where $\Delta H = \sum_i h_i S_i^z$. Keeping only the terms that survive $d \rightarrow \infty$ one obtains for the local susceptibility

$$\chi_{oo} = \frac{1}{4T} - \frac{zJ^2}{96T^3} + \frac{(zJ^2)^2}{1920T^5} \frac{D_4}{z^2} + \dots, \quad (4.28)$$

where D_4 is fourth moment of the lattice non-interacting density of states $\int \varepsilon^4 D(\varepsilon) d\varepsilon$. As can be seen from the Fig. 4.6 the overall agreement between above expression and NCA solution is very good. Note however that the discrepancy at $T = 0.1t^*$ comes from the fact that formula 4.28 is truncated at the third order and the error is of order $\mathcal{O}(1/T^7)$. Finally, it should be mentioned that for any finite dimensional system other terms, which are not of order zJ^2 , appear in the expansion (4.28) as well. The lowest order term that vanishes in the $d \rightarrow \infty$ limit is equal to $zJ^3/(384T^4)$.

4.5 Vertex corrections

At low enough temperature, one may expect that the vertex correction diverge and can not be ignored anymore. As will be shown later, NCA always breaks down at a certain low temperature. The causality problem occurs because NCA slightly underestimates the value of the self-energy at the chemical potential, which rapidly approaches zero with lowering temperature if the system is Fermi liquid. This also happens at large doping in EDMFT, when J becomes unimportant and the $t - J$ model becomes similar to $U = \infty$ Hubbard model. At small doping, on the other hand, self energy is relatively large near the chemical potential even at low temperatures. However, the imaginary part of the inverse of the irreducible effective spin cumulant M^{-1} (defined in Eq. 3.19) goes to zero at zero temperature and NCA again underestimates its value. This comes from the fact that the local spin susceptibility, calculated with NCA, is few percent too high. Again, this problem is not so serious, if the irreducible cumulant does not go to zero at any point except zero, but at small doping and small temperatures it eventually becomes zero at nonzero frequency.

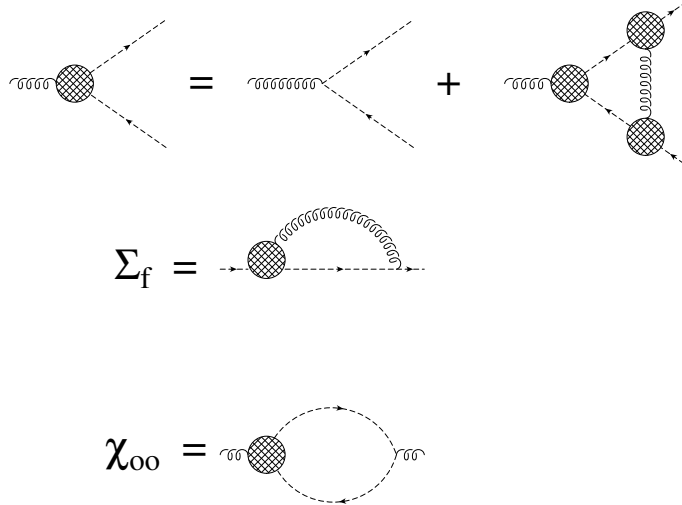


Figure 4.7: The dressed interaction between localized pseudo-fermions and vector bosonic bath. The corresponding cotributions to the self-energies are also shown.

The causality problem can be avoided by including the proper vertex corrections. If they diverge, an infinite resummation of skeleton diagrams is needed. As shown in Fig. 4.7, the interaction between the pseudo-fermion and bosons from the bath can be dressed properly. It is easy to check that this approximation is conserving and adds an infinite number of diagrams to

the Luttinger-Ward functional Φ . Among first few, the diagrams number IV and IX drawn in Fig. 4.2 are included, while number X is still missing. It is also important that the approximation counts each topologically different diagram only once, thus no double counting is present.

The drawback of the approximation is that the Bethe-Salpeter equation is highly nonlinear in the vertex (i.e. cubic) therefore it can not be simply transformed into the system of linear equations. The problem might be circumvented by linearizing the equation in iterative process and replacing the unknown vertex by the old one (vertex from the previous step) at the two locations on the right hand side of the Bethe-Salpeter equation, thus changing the kernel.

For completeness, let us write the self-consistent equations explicitly. The Bethe-Salpeter equation for the vertex function with incoming pseudo-fermion frequency ω' and outgoing ω reads

$$B(\omega, \omega') = 1 - \frac{1}{4} \int d\xi \left\{ D_{\Phi}(\xi) n(\xi) B(\omega, \omega + \xi) B(\omega + \xi, \omega' + \xi) \times \right. \\ \left. B(\omega' + \xi, \omega') G_f(\omega + \xi) G_f(\omega' + \xi) \right\}. \quad (4.29)$$

The pseudo-fermion self-energy contribution is

$$\Sigma_f(\omega) = \frac{3}{2} \int d\xi D_{\Phi}(\xi) n(\xi) G_f(\omega + \xi) B(\omega + \xi, \omega). \quad (4.30)$$

And finally, the local magnetic susceptibility involves all four vertices, either retarded or advanced in any of the two vertex frequencies

$$\text{Im } \chi_{oo}^{zz}(\omega + i\delta) = \frac{1}{2} \int \frac{d\xi}{2\pi i} e^{-\beta\xi} \left\{ G_f(\xi + \omega) \left[G_f(\xi + i\delta) B(\xi + \omega, \xi + i\delta) - \right. \right. \\ \left. \left. G_f(\xi - i\delta) B(\xi + \omega, \xi - i\delta) \right] + \right. \\ \left. G_f(\xi - \omega) \left[G_f(\xi + i\delta) B(\xi + i\delta, \xi - \omega) - \right. \right. \\ \left. \left. G_f(\xi - i\delta) B(\xi - i\delta, \xi - \omega) \right] \right\}. \quad (4.31)$$

The solution of these coupled nonlinear integral equations hasn't been yet obtained numerically but we expect the approximation to improve the results at sufficiently low temperatures and small doping, where NCA breaks down due to the somewhat higher local magnetic susceptibility.

Chapter 5

EDMFT results

5.1 Quantum critical point and MFLT

Strongly correlated electron systems like heavy fermions or high- T_c superconductors have very rich phase diagram with many different low temperature phases. In heavy fermion materials [29], a low temperature ordered phase exists whose transition temperature goes to zero upon doping or applying external pressure. The point, where the transition temperature is zero (i.e. the end point of the ordered state), is called the quantum critical point [30, 31, 32, 33]. The behavior of the system close to the quantum critical point is very different from the behavior in the vicinity of the classical phase transition.

The immediate vicinity of the phase transition is characterized by vanishing characteristic energy scale ω_c , which is proportional to the inverse of the characteristic time scale $\omega_c = 1/\tau$. Due to the critical slowing down, the time scale diverges as $\tau \sim \xi^\kappa$. The correlation length itself diverges with the characteristic exponent μ $\xi = |T - T_c|^{-\nu}$, therefore the energy scale goes to zero as $\omega_c = |T - T_c|^{\nu\kappa}$.

In the vicinity of the classical phase transition, the characteristic energy scale gets much smaller than the critical temperature $\omega_c \ll T_c \neq 0$. Since the temperature is high compared to the characteristic energy scale, the transition is governed by the classical statistical physics (i.e. the thermal occupation of bosonic modes is large and hence classical). Statistics plays the major role and dynamics can be adequately described just by time-dependent Landau-Ginzburg type of equations.

In the vicinity of the quantum critical point, the characteristic energy scale is larger than temperature therefore quantum mechanical nature of the dynamical fluctuations becomes important, more important than statistics.

At the quantum critical point, the dynamics must be determined from the quantum-mechanical equations of motion. The general scaling behavior near a $T = 0$ transition can be discussed with the formalism of dynamical scaling [34, 35, 36]. The correlation length is diverging when doping is approaching critical doping as $\xi \sim |\delta - \delta_c|^{-\nu}$. The critical slowing down is characterized by the diverging time scale $\xi_\tau = \tau = \xi^\kappa$. In quantum statistical calculations the time-wise direction becomes like an additional dimension, so that ξ_τ plays the role of a correlation length in this direction. Therefore, the effective dimension of the problem is larger than space dimension and is $d + \kappa$. The critical exponent κ is usually larger than one, so that even in the two dimensional case the effective dimension is larger than three.

If the effective dimension is above upper critical dimension, the space fluctuations can be ignored and the mean-field description of the long-range fluctuations is sufficient. In this case, the momentum dependence of the self-energy is not crucial, rather the frequency dependence plays essential role [37]. The local theory that correctly describes quantum (i.e. temporal) fluctuations and freezes spatial fluctuations should be applicable here. The EDMFT takes a full account of both local quantum fluctuations present in most generic models of strong electronic correlations, namely, the Kondo type fluctuations as well as short range magnetic fluctuations. It should be noted, that the proximity to the quantum critical point is characterized by the anomalous T dependence in the physical quantities in the whole region above the ordered state up to some high-energy cut-off (for example J or t) and also for doping larger than critical doping and temperature larger than some characteristic temperature, below which the quantum fluctuations prevail and the system becomes Fermi liquid.

Although the question concerning the origin of the behavior of high temperature superconductors is not settled yet, there are some indications that much of their behavior might be governed by the proximity to a quantum critical point [37] located at the optimum doping and $T = 0$. It is not yet known whether this point is the end point of a continuous transition line because underdoped samples do not show any broken symmetry (either translational or spin rotational) below a certain critical temperature. However, a sharp change in transport and thermodynamic properties is indeed observed in that region below a certain continuous line in $\delta - T$ diagram. This state has a d-wave pseudogap in the density of states and is called the pseudogap state.

This line of reasoning led to a phenomenological marginal Fermi liquid theory (MFLT)[10, 38] describing normal state properties of cuprates for temperatures above the d-wave pseudogap state in the underdoped samples, in the whole temperature range in the optimally doped samples and for temperatures above Fermi liquid state in slightly overdoped samples. Since the

spatial correlations play no role in determining the frequency dependence of the self-energy the k dependence can be neglected or equivalently the effective dimension of the problem is infinite ($1/\kappa = 0$). The self-energy in MFLT was postulated to be

$$\Sigma(k, \omega) = g^2 \left(\omega \ln\left(\frac{x}{\omega_c}\right) - i\frac{\pi}{2}x \right) \quad (5.1)$$

valid for $x \ll \omega_c$ and $v_F|q - k_F| \gg \omega_c$ and where x is $\max(T, |\omega|)$, ω_c is an upper cut-off and g is a constant.

The major point in MFLT theory is that the dynamically generated low energy excitations of a many body states are such that single particle scattering rate is proportional to x rather than to x^2 as in Landau Fermi liquids. As a consequence, the quasi-particle renormalization amplitude Z scales to zero at zero temperature and zero frequency

$$Z = \left(1 - \lambda \ln\left(\frac{x}{\omega_c}\right) \right)^{-1}. \quad (5.2)$$

Hence, there are no well defined quasi-particles and the single particle occupation number has no discontinuity at the Fermi surface, but its derivative does. So the Fermi surface remains a well-defined concept both in energy and momentum space. It can also be shown that the above choice for the self-energy (5.1) leads to a finite compressibility. Note however, that compressibility for two dimensional models of strong electron correlations (Hubbard, t-J) diverges at low temperature close to the Mott-Hubbard transition [39].

Many normal state properties of cuprates can be very well explained with the phenomenological MFLT, especially linear resistivity and spectral properties at optimum doping [37].

As we will show in the next section, many results of EDMFT are indeed consistent with the MFLT scenario. However, our present method for solving impurity problem (NCA) is most limited in the optimally doped regime, where Kondo physics and magnetic interaction are about equally important. In this region, one Feynman bubble for each process is naturally not enough and one needs to include vertex corrections of type presented in Fig. 4.2. On the other hand, MFLT most successfully describes samples in the optimally doped region what makes the comparison somewhat harder.

5.2 Spectral Functions

In the following sections, we will present numerical results of the EDMFT applied to the t-J model. The corresponding impurity problem is solved with

the NCA method discussed in Section 4 and Appendix C. In order to obtain a meaningful limit for fermion models of large dimensions the lattice density of states must be bounded. In the hypercubic lattices, the short wavelength cut-off associated with the kinetic or intersite interaction term is $\varepsilon = zt$ or $\varepsilon = zJ$ respectively, where z is the coordination number (i.e. the number of nearest neighbors). In the case of infinite z and DMFT scaling $t = t^*/\sqrt{z}$ the density of states is unbounded since the tails extend up to $\sqrt{z}t^*$. This leads to the infinite antiferromagnetic transition temperature, which is also proportional to the coordination number $T_c \propto zJ$ and therefore scales as $T_c \propto \sqrt{z}J^*$. It is therefore essential to work with a physical density of states which is always bounded. In order to compare our results with the exact diagonalization results of the two dimensional t-J model we will use 2D density of states.

The t-J model is characterized by near-neighbor hopping $t = t^*/\sqrt{z}$ and intersite magnetic interaction $J = J^*/\sqrt{z}$. We choose $t^* = 1$ to establish the unit of energy and if not otherwise mentioned $J/t = J^*/t^*$ is chosen to be 0.3. The coordination number z is 4 in the two dimensional square lattice and therefore $t = 1/2$ and $J = 0.15$ in above chosen units. We will work within the paramagnetic metallic state of the model since the long range order in two dimensions is possible only at zero temperature. It is important that quantum fluctuations contained in EDMFT destroy long range order at any nonzero temperature for one or two dimensional systems so that EDMFT satisfies Mermin-Wagner theorem. The reason is that the density of states has a finite jump at the short wavelength cut-off and therefore the real part of the Hilbert transform diverges at that point, or equivalently the phase space is too small to allow solution of Eq. (3.22). Close to the ordering wave vector \mathbf{Q} this equation takes the form

$$\chi_{oo}(\omega = 0) = \frac{2}{zJ} \int \frac{\tilde{q}^{d-1} d\tilde{q}}{1/\tilde{\xi}^2 + \tilde{q}^2}, \quad (5.3)$$

where $\tilde{\mathbf{q}} = \mathbf{q} - \mathbf{Q}$ and

$$\tilde{\xi}^2 = \frac{1}{2} zJ \chi(Q, \omega = 0). \quad (5.4)$$

The dynamic correlation length $\tilde{\xi}$ is diverging close to the phase transition therefore the right hand side of the Eq. (5.3) also diverges for $d \leq 2$. Since the local susceptibility χ_{oo} does not diverge at any nonzero temperature the EDMFT does not allow long range order in one or two dimensions at any nonzero temperature.

The EDMFT includes dynamical nonlocal quantum magnetic fluctuations beyond the Hartree level. These nonlocal fluctuations suppress long-range

order found in the DMFT solution with mean field treatment of magnetic interaction [24]. In addition, nonlocal fluctuations destroy Fermi liquid metallic state at small doping and open a pseudogap, which is characterized by enormous reduction of the density of states at the Fermi level and around it. This gap is remnant of the Mott gap at half filling and develops due to the short range antiferromagnetic correlations present in the underdoped phase. The associated energy scale is of order J therefore the gap is clearly seen at temperatures reached with our present NCA method $T \sim J/5$. The so-called large pseudogap was found numerically in the t-J model [9, 40, 41] and also experimentally in the normal state of cuprate superconductor (LSCO) [42, 43].

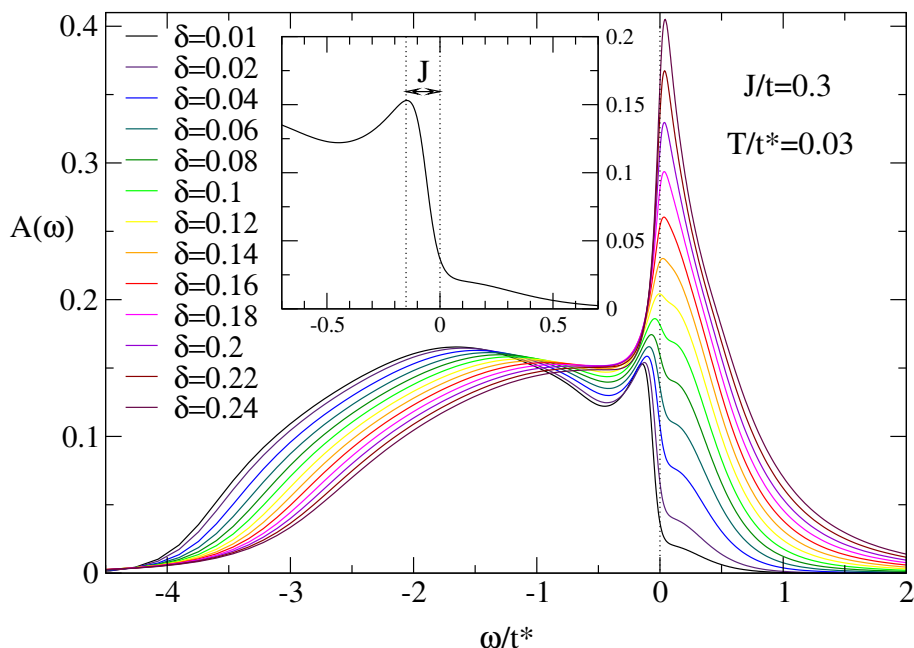


Figure 5.1: The local spectral function plotted versus frequency for $T=0.03$ and $J=0.15$ for various doping concentrations δ . The chemical potential is located at $\omega = 0$ marked with a dotted vertical line. The inset magnify the structure at $\omega = 0$ for the smallest doping shown.

At half-filling ($\delta = 0$) t-J model is antiferromagnetic Mott insulator with infinitely large Mott gap. However, the transition to the ordered state occurs only at $T = 0$ in the 2D system in accordance with the Mermin-Wagner theorem. The Mott insulating gap is slowly destroyed with adding holes to the system as shown in Fig. 5.1 but a remnant of the gap persists up to the overdoped regime. The effect of doping is that the chemical potential gradually cuts deeper and deeper into the Hubbard band, forming a hole-

like Fermi surface centered around (π, π) at the top of the lower-Hubbard band. The spectral weight is transferred from the incoherent Hubbard band to the quasiparticle peak which is substantially increased with doping. This quasiparticle peak, corresponding to the dressed holes in the paramagnet with short but strong antiferromagnetic correlations, is located approximately J below the chemical potential at zero doping and is slowly approaching the chemical potential with increasing doping. The small shoulder above the chemical potential, seen in the local density of states, is also enlarged and finally merges with the quasiparticle peak in the overdoped regime ($\delta \sim 0.2$). As we will show below, the Fermi liquid state is developed for doping above $\delta \sim 0.24$ when corresponding Kondo temperature exceeds the strength of the magnetic interaction J .

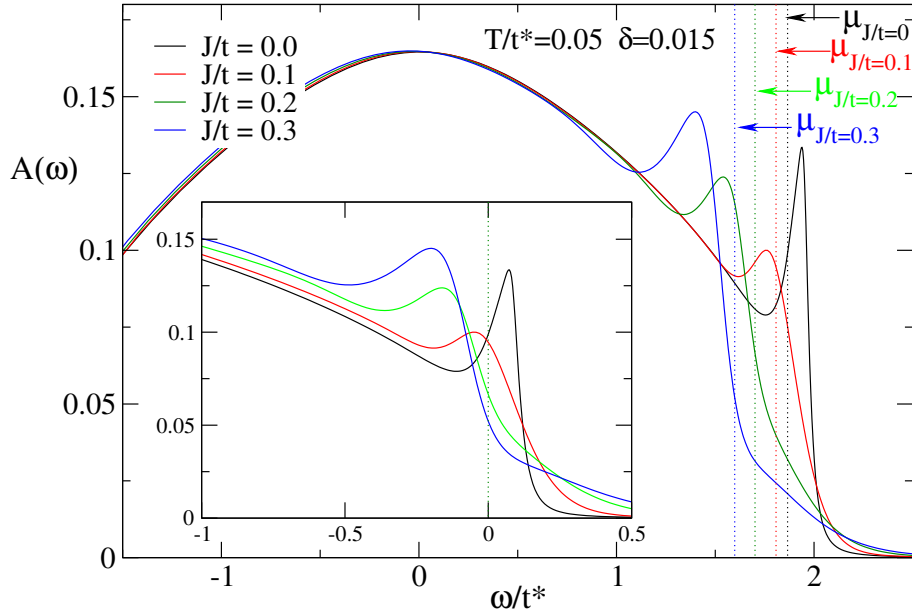


Figure 5.2: The local spectral function for four different $J/t = 0, 0.1, 0.2$ and 0.3 . The evolution of pseudogap and destruction of Fermi liquid quasi-particle peak seen at $J = 0$ is clearly visible. Vertical lines mark chemical potentials for various J/t . The inset shows the same spectral functions at constant chemical potential set to zero.

The local density of states confirms the destruction of the Fermi liquid quasiparticle peak by short-range antiferromagnetic correlations. With increasing J , the pseudogap is increased and the spectral weight of the Fermi liquid quasiparticle seen at $J = 0$ is transferred deeper and deeper below the chemical potential into the so called Hubbard sideband of width approximately $\sim J$. The correlation length for $J/t = 0.3$ is only about 4 lattice spacings (see Fig. 5.3) confirming the short-range nature of the fluctuations

that prevent the formation of many-body singlet state of Fermi liquid nature. Because of strong antiferromagnetic correlations that introduce pseudo-

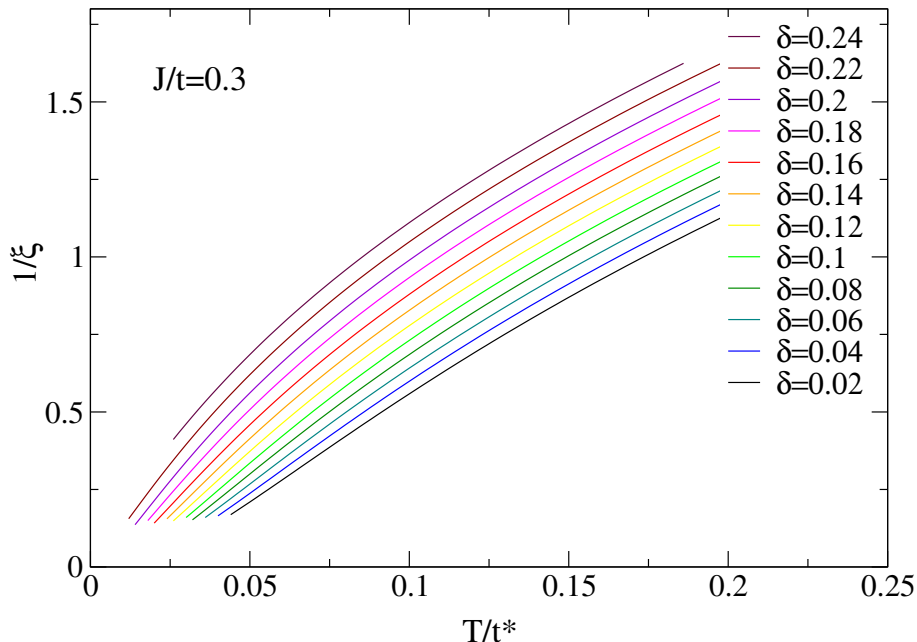


Figure 5.3: The inverse of dynamic correlation length for the t-J model calculated within EDMFT+ NCA as a function of temperature for various doping concentrations. The correlation length is calculated from the magnetic susceptibility as $\xi = \sqrt{\frac{1}{2}zJ\chi_{(\pi,\pi)}(0)}$ (see Eq. 5.4).

gap into paramagnetic metal, there is no adiabatic continuity between the noninteracting and interacting eigenstates and the system is not Fermi liquid.

If $J = 0$, the model is called t-model and is equivalent to the infinite U Hubbard model. The latter can be mapped onto the usual Anderson impurity model in the limit of large dimensions and therefore the metallic state without broken symmetry is always Fermi liquid [5] below the characteristic temperature ε^* , which is just the Kondo temperature of the corresponding Anderson impurity model. As we know from the Kondo physics, a narrow quasiparticle resonance appears at the Fermi energy in the single-particle spectrum for temperature around and below ε^* (see Fig. 5.2). This characteristic temperature is monotonically decreasing with decreasing doping and eventually, at half filling, becomes zero since charge excitations are not allowed anymore. At temperatures much larger than ε^* , the electrons behave as nearly independent localized spins and the local spin response has Curie-like behavior. As the temperature is lowered below the small energy scale ε^* , the electrons start to couple strongly and the Fermi liquid metallic state

emerges. The physics of the t -model gets complicated by various phases with broken symmetry and long-range order. Indeed, as Nagaoka showed in a milestone paper [44], a single hole in the infinite- U Hubbard model on any finite bipartite cluster with periodic boundary conditions, for any dimension $d \geq 2$ has a fully polarized ferromagnetic ground state, i.e., the ground state has maximum spin S . Numerical calculations support the idea that ferromagnetic ground-state survives even at finite hole densities but small enough doping [45].

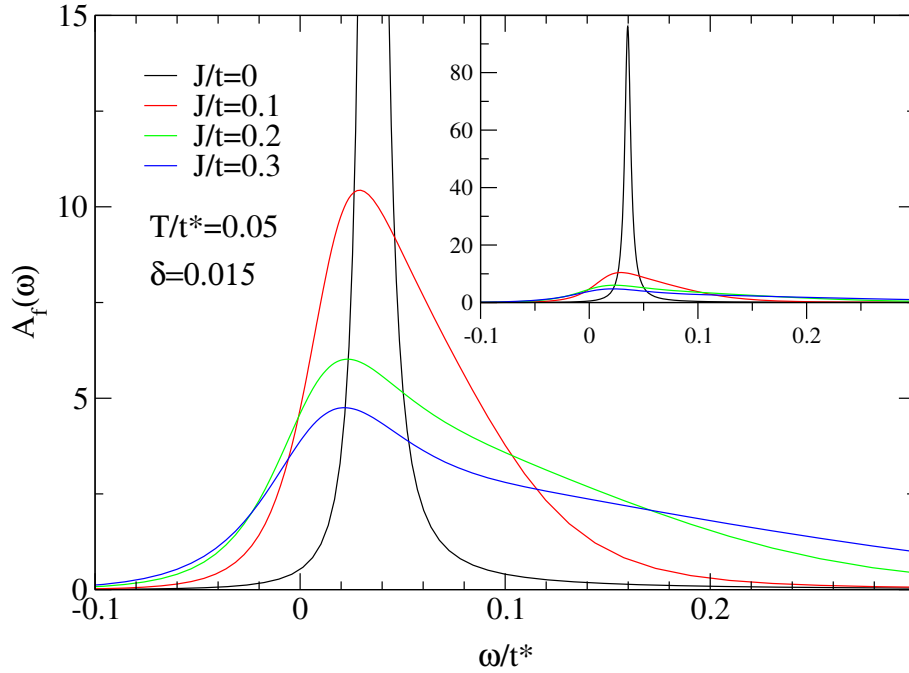


Figure 5.4: The pseudo-fermion spectral function as a function of frequency for four different values of J . The inset shows the blowup of the peak in the case of $J = 0$.

The pseudo-fermion spectral function shown in Fig. 5.4 illustrates how intersite interaction J changes the localized nature of electrons. The temperature in Fig. 5.4 is somewhat higher than the small energy scale ε^* below which the Fermi liquid regime applies for $J = 0$, therefore the system is caricatured as a collection of weakly coupled magnetic moments. Thus, the local pseudo-fermion spectral function is extremely sharply peaked. In our calculations, the frequency scale is chosen such that the pseudo-particle spectral functions are peaked at zero frequency when the temperature goes to zero. At $T = 0$ and $J = 0$, they diverge for $\omega < \varepsilon^*$ with a characteristic exponent α_f or α_b , which is a function of doping only and is a signal of formation of the Fermi liquid singlet ground state. However, if the temperature is above ε^* ,

the pseudo-fermion spectral function is still very sharply peaked, signaling the localized nature of magnetic moments, but the peak is shifted to positive frequency for a small amount $\sim T$ (because of the orthogonality catastrophe it has to be above zero).

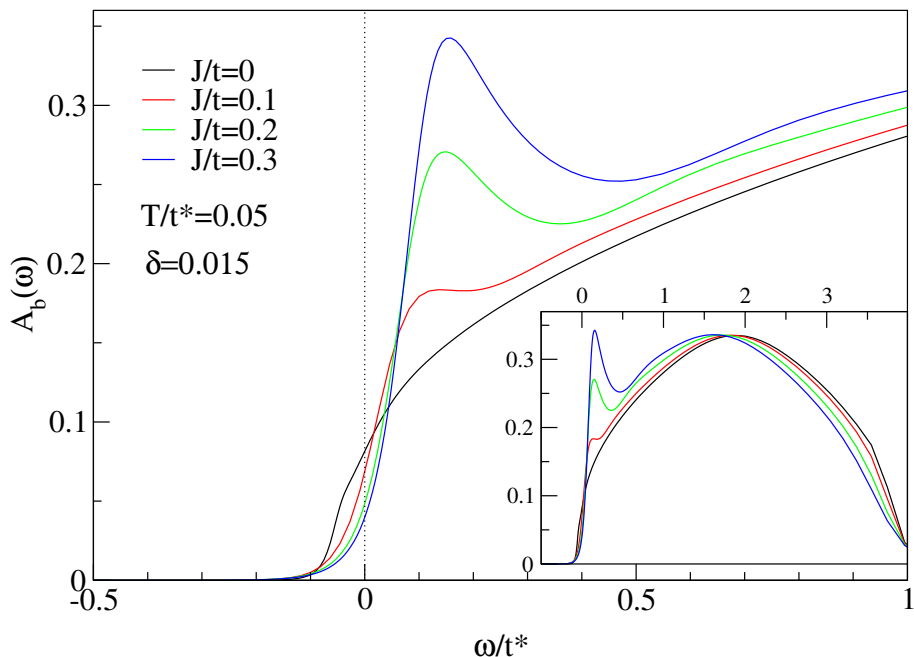


Figure 5.5: Pseudo-boson spectral function as a function of frequency for four different values of J . The inset shows the same spectral-functions on a larger scale so that the Hubbard band is clearly visible.

As shown in Fig. 5.4, the nonzero J enables fermions to exchange energy and therefore the pseudo-fermion spectral function is substantially broadened. The width of the peak becomes approximately J and the small energy scale, that was manifested in the local spectral function A_{oo} as a sharp quasi-particle resonance at the chemical potential (Abrikosov-Suhl peak), disappears. The Fermi liquid state is thus destroyed. However, if the characteristic temperature ε^* is larger than J , the shape of the peak in the pseudo-fermion spectral function is determined by ε^* and not by J , therefore the latter is irrelevant. As we will show later, this is the case for the overdoped t - J model ($\delta > 24\%$), where Fermi liquid metallic state is recovered.

The pseudo-boson spectral function is shown in Fig. 5.5 for the same parameters as pseudo-fermion spectral function in Fig. 5.4. In the case of $J = 0$ and for temperature smaller than the characteristic Fermi liquid temperature ε^* , a very sharp peak develops at zero frequency in the the pseudo-boson spectral function. However, if the temperature is larger than ε^* (like in the

Fig. 5.5) only the broad Hubbard band remains.

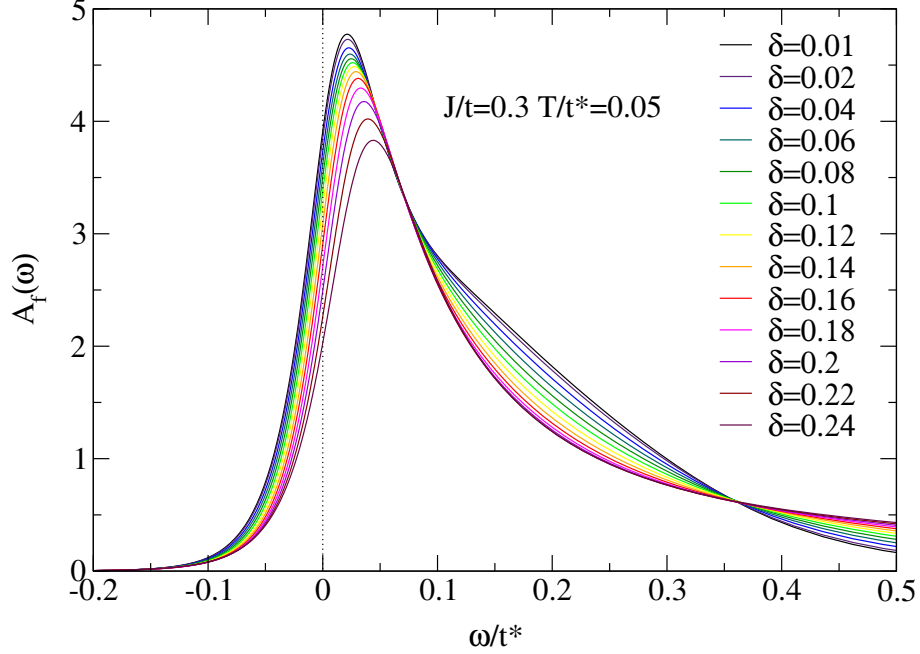


Figure 5.6: Pseudo-fermion spectral function plotted vs frequency for various doping concentrations. The relevant energy scale is of order J in the whole doping range.

When J is turned on, a pseudogap develops around zero frequency and a broad quasiparticle peak emerges above it. Thus, the hole excitations are gapped around the threshold frequency causing pseudogap also in the local physical spectral function A_{oo} . This is because A_{oo} is a convolution of pseudo-boson (sometimes called holon) and pseudo-fermion (spinon) spectral function (see Eq. 4.20). The size of the pseudogap as well as the width of the quasiparticle peak is approximately J . This peak corresponds to a dressed hole moving in the paramagnetic medium and is also reflected in the quasiparticle peak of the local physical spectral function A_{oo} that occurs below the chemical potential.

We can see from Fig. 5.6 that the pseudo-fermion spectral function is only weakly doping dependent and the width of the peak is approximately J for essentially all doping concentrations shown. This comes from the fact that the relevant energy scale in the underdoped case is J and is not strongly doping dependent, while it changes to ε^* in the overdoped case. As we will show later on (see Fig. 5.8), Kondo temperature (ε^*) is just around J for the largest doping ($\delta = 0.24$) shown in Fig. 5.6 and therefore the relevant energy scale is almost a constant in this range of doping concentrations. Note

however, that the temperature dependence of the spectral function is very strong for any doping.

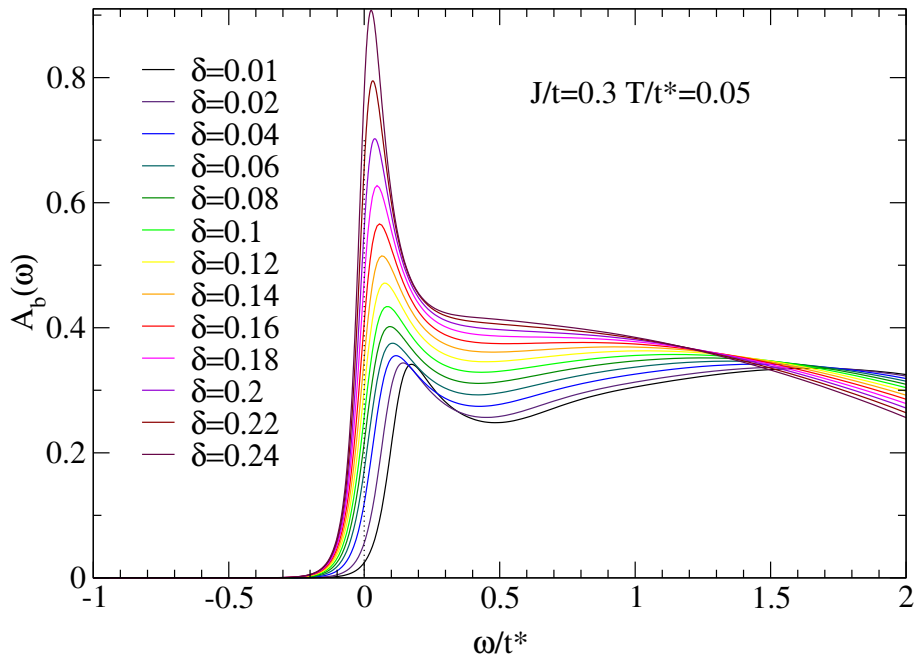


Figure 5.7: Pseudo-boson spectral function plotted vs frequency for various doping concentrations. The pseudogap, dominating close to the Mott-Hubbard transition, gradually evolves to a sharp peak signaling the development of the Fermi liquid state in the overdoped regime.

The pseudo-boson spectral function, on the other hand, is strongly doping dependent (see Fig. 5.7). The pseudogap seen at small doping is slowly disappearing and the spectral weight is transferred from the Hubbard band to the quasiparticle peak. For the largest doping shown, the characteristic Fermi liquid temperature or Kondo temperature is already larger than J and therefore the peak in the pseudo-boson spectral function is proportional to $A_b \sim \omega^{-\alpha_b}$ between $\omega \sim T_K$ and $\omega \sim T$.

For sufficiently large doping, t-J model is expected to be Fermi liquid since the strength of the magnetic intersite interaction must become small when the number of electrons per-site is small. The question is, where is the crossover between Fermi and non Fermi liquid state. We argue, that the Fermi liquid metallic state is stable when corresponding Kondo temperature exceeds the strength of the magnetic interaction J . For $J/t = 0.3$, this happens around $\delta \sim 0.24$ close to the so called mixed-valence regime of the Anderson impurity model.

Because the role of J becomes unimportant in the overdoped regime

the EDMFT impurity model (3.12) gets close to the Anderson impurity model (2.15) arising in the DMFT study of the infinite U Hubbard model. At this point, the Anderson impurity model already enters the so-called mixed-valence regime where charge fluctuations become important and the Abrikosov-Suhl resonance merges with the incoherent Hubbard band. The energy of the local level E_d of the impurity model, which has opposite sign but the same magnitude than the chemical potential μ of the lattice model, approaches the Fermi level. The distance between the E_d and μ gets small compared to the width of the Hubbard band. In this crossover region between Fermi and non-Fermi liquid, the doping of the system is already close to 30% so that the occupation of the impurity level of the Anderson model is around 70% therefore the impurity system cannot be mapped onto the usual Kondo impurity model anymore. The strong Kondo limit with small energy scale T_K is thus never observed in the t-J model. To show that, we need to find the correct expression for the Kondo temperature which for the infinite-U Anderson impurity model takes the form

$$T_K = \sqrt{D\Gamma} \exp\left(\frac{\pi E_d}{2\Gamma}\right), \quad (5.5)$$

where D is high energy band cut-off, E_d is the energy of the local impurity orbit and $\Gamma = \pi V^2 \mathcal{N}(0)$ denotes the effective hybridization or the broadening of the local level. For the case of the t-J model, the high-energy cut-off is just the width of the lattice density of states t^* and the energy of the local orbit is the chemical potential $E_d = -\mu$. This can be most easily seen from the mapping of the lattice effective action (3.8) onto the impurity problem (3.12). The chemical potential μ is positive at low doping, and hence the energy of the local orbit E_d negative. The effective hybridization Γ may be expressed in terms of the improper impurity self-energy Λ as

$$\Gamma = -\text{Im} \Lambda(0), \quad (5.6)$$

where Λ is the exact self-energy of the noninteracting impurity problem (i.e. without Coulomb interaction U and magnetic interaction J). The latter can be expressed by the fermionic Weiss field \mathcal{G}_0^{-1} as

$$\Lambda(\omega) = \omega + \mu - \mathcal{G}_0^{-1}(\omega) \quad (5.7)$$

since the density of states of the auxiliary conduction band is

$$A_c(\omega) = -\frac{1}{\pi} \text{Im} \Lambda(\omega). \quad (5.8)$$

Finally, the Kondo temperature becomes

$$T_K = \sqrt{t^* \Gamma} \exp\left(-\frac{\pi\mu}{2\Gamma}\right), \quad (5.9)$$

where the effective hybridization is

$$\Gamma = -\text{Im} \Lambda(0) = \pi A_c(0) = \text{Im} \mathcal{G}_0^{-1}(0). \quad (5.10)$$

There are two difficulties in using the above formula. One is that the parameters like Γ and μ are changing with temperature because they are determined self-consistently and therefore the Kondo temperature itself is not a constant for a fixed t , J and δ . We may however expect that when the temperature is below the smallest energy scale in the system those parameters do not change anymore. The second problem is that conduction electron band is described just by two numbers in the above formula: the band cut-off D and the effective value of the density of states at the chemical potential Γ . This is quite accurate approximation in the usual impurity problem where the improper self energy Λ is very slowly varying function of frequency close to the chemical potential and can be replaced by a constant up to the band cut-off. In the DMFT problem, however, this quantity is self-consistently determined and is composed of incoherent and coherent part. The latter is a strong function of frequency around the chemical potential which makes the formula (5.9) less reliable. Nevertheless, it gives a good estimate of the low-energy scale below which the many-body singlet ground state might be formed. We stress, however, that this scale was found only in the overdoped regime and that it does not have any physical meaning in the underdoped or optimally doped regime.

Fig. 5.8 shows that the effective hybridization Γ is monotonically increasing with increasing doping. This is due to the increase of the value of the local spectral function at the chemical potential. On the other hand, the chemical potential is always decreasing with doping and therefore Kondo temperature is monotonically increasing function of doping. More importantly, Kondo temperature exceeds J just above $\delta \sim 0.2$ therefore we expect that the Fermi liquid ground state is formed in the overdoped regime. In order to show that, we will compare the value of the local physical spectral function at the chemical potential $A_{oo}(\omega = 0)$ with the prediction of the Friedel sum rule. As shown in Appendix D, $A_{oo}(\omega = 0)$ is uniquely determined by the effective hybridization Γ and by the change in number of electrons due to the introduction of the impurity

$$A_{oo}(0) = \frac{\sin^2\left(\frac{\pi}{2}(n - n_c)\right)}{\pi\Gamma}, \quad (5.11)$$

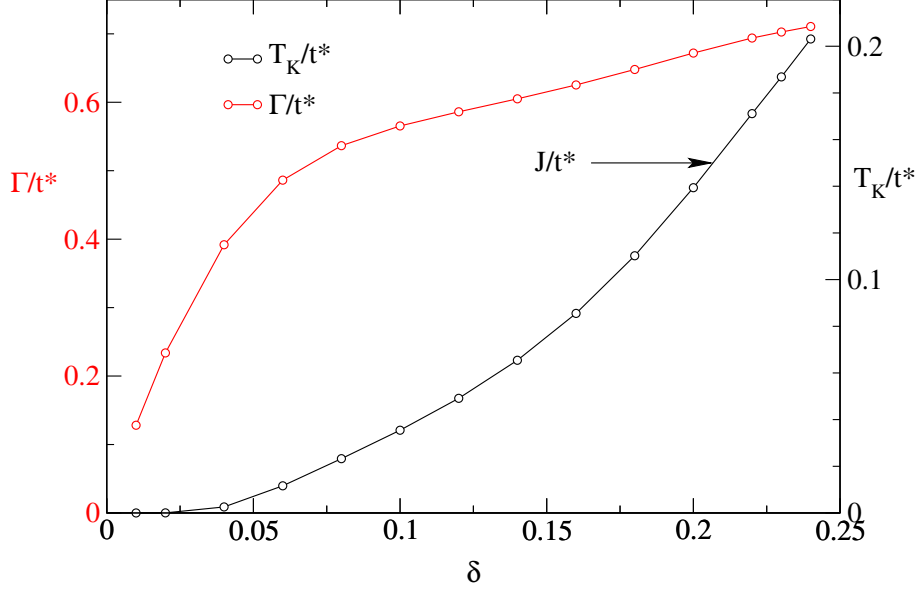


Figure 5.8: The effective hybridization Γ and the Kondo temperature for the t-J model in the EDMFT calculated at $T/t^* = 0.05$.

where $n = 1 - \delta$ and

$$n_c = -2 \operatorname{Im} \int_{-\infty}^0 \frac{d\xi}{\pi} G_{oo}(\xi) \frac{\partial \Lambda}{\partial \xi}. \quad (5.12)$$

To prove this sum rule, we need to assume that the exact solution can be obtained by perturbing the system of non-interacting electrons (i.e. the system with $U = 0$ and $J = 0$) or equivalently, that the one-to-one correspondence exists between the one-particle excitation of the interacting problem and those of the non-interacting problem.

Fig. 5.9 shows the value of the local spectral function at the chemical potential $A_{oo}(\omega = 0)$ as a function of temperature. The value predicted by the Friedel sum rule is indicated in the left by the line with two arrows. The uncertainty comes from the fact that Γ and n_c are changing with temperature and are determined from the self-consistent solution. Therefore, the zero temperature limit can not be obtained by our approach and must be found by extrapolation. Nevertheless, it is clear from Fig. 5.9 that the Friedel sum rule can be obeyed for doping $\delta \gtrsim 0.23$ while it is completely off in the optimally doped regime, since the sum rule predicts increase of the $A_{oo}(0)$ with decreasing doping while the value actually decreases with doping.

It is also instructive to study the imaginary part of the self-energy at the chemical potential vs temperature. If the low temperature phase of the system has a Fermi liquid characteristics, the scattering rate near the Fermi en-

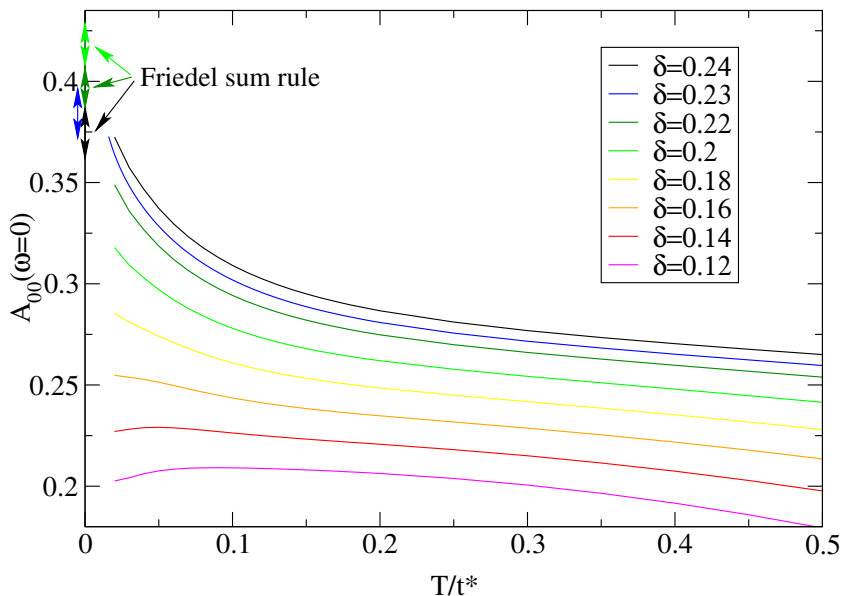


Figure 5.9: The value of the local spectral function at the chemical potential vs temperature for various doping concentrations. The value predicted by the Friedel sum-rule is marked on the right with the line with arrows.

ergy vanishes faster than the energy of the quasiparticles so that the lifetime is large and the quasiparticles are well defined. Likewise, at the Fermi energy $\text{Im} \Sigma$ varies with temperature as T^2 . The breakdown of the Fermi liquid theory occurs, when the scattering rate at the Fermi energy is proportional to T and ω so that no well-defined quasiparticle exists. If the self-energy is also momentum independent, then the metal is termed marginal Fermi liquid [37].

In Fig. 5.10 we present results for the imaginary part of the self-energy at the chemical potential vs temperature. For low doping ($\delta \lesssim 0.1$) $\text{Im} \Sigma$ is a monotonically increasing function of doping and may be extrapolated linearly to the origin. In the heavy overdoped regime, on the other hand, the quadratic low temperature part is most likely. However, the simple NCA method breaks down when the temperatures is much smaller than the characteristic Fermi liquid scale ε^* , therefore the parabolic part cannot be obtained in this simplified approach. Optimally doped regime is characterized by very large scattering rate in the whole temperature range. Despite the fact that the downturn of $\text{Im} \Sigma$ at the lowest temperature reached is not very pronounced, we believe that $\text{Im} \Sigma$ vanishes linearly with temperature but with very large prefactor. We note however, that our present method for solving impurity problem (NCA) is most limited in the optimally doped regime, where Kondo physics and magnetic interaction are about equally im-

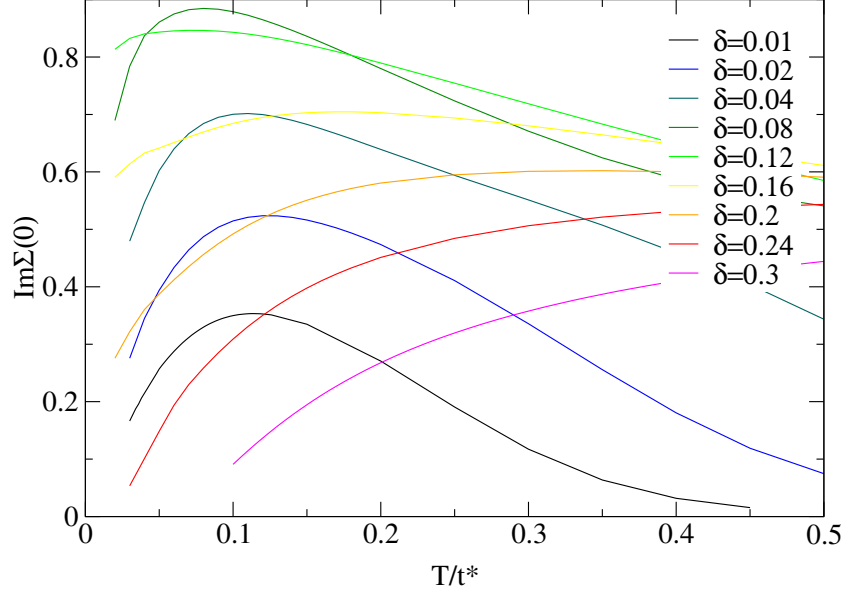


Figure 5.10: The imaginary part of the self-energy at the chemical potential plotted vs temperature for various doping concentrations.

portant. Since we have described each process with a bubble and we have not yet included crossing diagrams (i.e. vertex corrections of type presented in Fig. 4.2), the approximation might be less reliable at very low temperatures and optimum doping.

Another quantity that distinguishes Fermi liquids from non Fermi liquids is the quasiparticle renormalization amplitude Z defined by

$$Z = \left(1 - \frac{\partial \text{Re} \Sigma}{\partial \omega} \right)_{\omega=0}^{-1}. \quad (5.13)$$

It measures the overlap of the ground state wave function of the system of interacting $N \pm 1$ electrons with the wave function of N interacting particles and a bare electron. The Landau Fermi liquids are characterized by finite renormalization amplitude at $T = 0$ while in the marginal Fermi liquid case, Z scales to zero logarithmically with temperature (see Eq. (5.2)).

Fig. 5.11 displays the variation of Z with temperature and clearly shows that even though Z is relatively large for temperature $T \sim J$ it scales to zero at $T = 0$ and small or moderate doping. For the largest doping shown $\delta = 0.24$, renormalization factor does not vanish and approaches the value $Z \sim 0.12$. In this case, the system is Fermi liquid and the characteristic energy scale ε^* is determined from the cut-off energy t^* and renormalization amplitude Z by $\varepsilon^* \sim Z t^* = 0.12 t^* = 0.8J$. This is consistent with the upper observation that the Kondo temperature is of order J for doping $\delta \sim 0.24$.

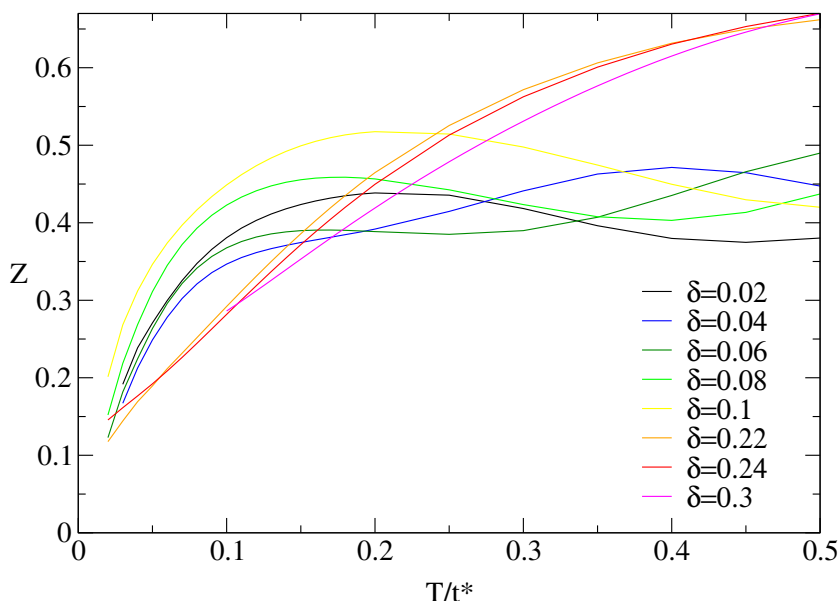


Figure 5.11: Quasiparticle renormalization amplitude Z plotted vs temperature for various doping concentrations. Nonzero Z at $T = 0$ is obtained only in the overdoped regime signaling the formation of the Fermi liquid state below the temperature Zt^* .

Finally, in Figs. 5.12 and 5.13 we would like to give an impression of the variation of the one particle spectra with temperature for an underdoped and overdoped system, respectively. At very high temperatures ($T \gtrsim J$) and small doping, only a broad incoherent Hubbard band is observed, with the chemical potential located at the top edge of the band. For temperatures lower than J , spectral weight is transferred from the region above the chemical potential to the broad quasiparticle peak located below μ . The density of states at the chemical potential is reduced with temperature and a pseudogap opens. A coherent peak above the chemical potential, corresponding to a Fermi liquid quasiparticle, does not appear in the system at low and optimum doping.

The spectral function of overdoped system, on the other hand, shows a typical Fermi liquid characteristics. The coherent part of spectra appears above the chemical potential, the peak is narrowed and increased with lowering the temperature. The incoherent Hubbard band is almost merged with the quasiparticle peak therefore the spectra shown in Fig. 5.13 resembles mixed-valence spectra of Anderson impurity model with Kondo temperature of order J .

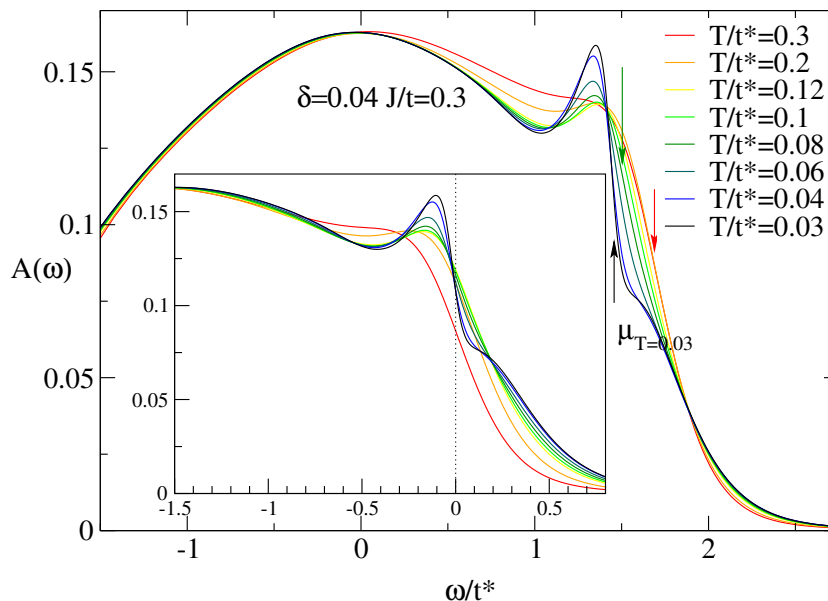


Figure 5.12: Local spectral function for doping $\delta = 0.04$ and various temperatures. In the main part, the chemical potential is marked with vertical lines with arrows. The inset shows the same spectra at fixed chemical potential located at zero frequency.

5.3 Fermi surface

An additional result from microscopic theory is the so-called Luttinger theorem, which states that the volume enclosed by the Fermi surface does not change due to interactions [46, 47, 48]. Luttinger's original proof in 1960 was based on the perturbation theory [46]. The mathematics behind the theorem is that with the assumption of Fermi liquid theory, the number of poles in the interacting Green's function below the chemical potential is the same as that for the non-interacting Green's function. Recall that latter is just the number of particles in the system (see Appendix D). Recently, the theorem was proven also by nonperturbative method for the case of Kondo lattice model [49] in arbitrary dimension. The latter approach can be extended to other lattice models, including the Hubbard and t-J model. However, it should be stressed that Luttinger theorem can be proven with the latter nonperturbative method only if a system is a Fermi liquid. The perturbative [50] and nonperturbative [51] proofs for the Luttinger theorem were given also for the one dimensional counterpart of the Fermi liquid, namely the Tomonaga-Luttinger-liquid.

However, strongly correlated systems with no definite quasiparticles do not need to satisfy the Luttinger theorem. Indeed, it is an exiting open question whether the volume of the Fermi surface is consistent with the Luttinger

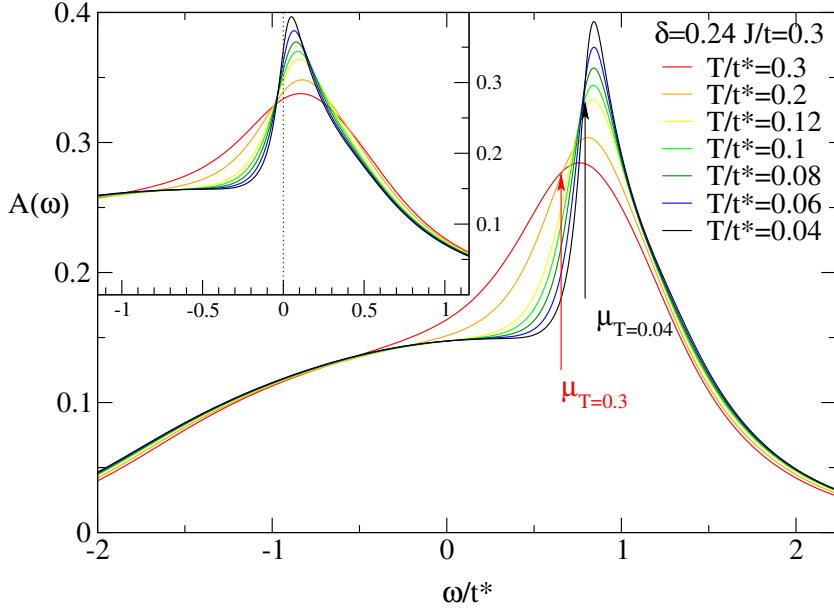


Figure 5.13: Local spectral function for doping $\delta = 0.24$ and various temperatures. In the main part, the chemical potential is marked with vertical lines with arrows. The inset shows the same spectra at fixed chemical potential located at zero frequency.

theorem in the non-Fermi liquid phases of these models or not. Using exact-diagonalization techniques Stephan *et al.* [53] argued that t-J model satisfies Luttinger theorem for dopings above $\sim 10\%$. They performed calculations on clusters of 16 to 20 lattice sites with 2 or more holes introduced in the system. On the other hand, several groups have recently reported a breakdown of the theorem in Hubbard or t-J model [54, 55, 52, 56, 57, 58, 59, 60, 61, 62, 63]. In the paper of Putikka *et al.* [54] the high temperature series for the moment distribution function $n_{\mathbf{k}}$ of the 2D t-J model was calculated to twelfth order in the inverse temperature and then extrapolated to $T = 0.2J$, which is also the temperature we can reach with the EDMFT and NCA. They concentrate on particular doping of 20% and found a slightly larger Fermi surface than predicted by the Luttinger theorem. As shown in Fig. 5.15, our calculation supports the result of Putikka *et al.*, however this doping is already very close to the Fermi liquid region therefore the volume of the Fermi surface could be only slightly larger. Schmalian *et al.* calculated Fermi surface for the Hubbard model using fluctuation exchange approximation and also got larger volume of the Fermi surface than Luttinger theorem predicts. The discrepancy was larger for smaller doping and become negligible just around 20%. Maier *et al.* [55] also obtained Fermi surface for the Hubbard model using dynamical cluster approximation and found the crossover from the Fermi

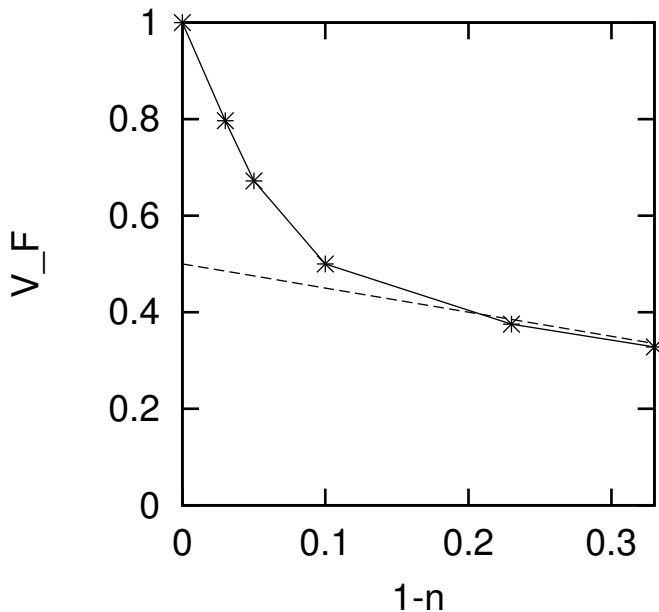


Figure 5.14: The lower bound for the Fermi surface volume as estimated from the single particle spectral functions obtained with the quantum Monte Carlo on 8×8 lattice. The dashed line gives the value predicted by the Luttinger theorem (from Ref. [52]).

liquid to non Fermi liquid state again around 20% with larger Fermi surface below this doping. Eder *et al.* [52] used quantum Monte Carlo method to study Hubbard model on 8×8 square lattice. They found surprisingly similar results than we obtained with EDMFT. In contrast to the results of Maier *et al.* or Schmalian *et al.*, they concluded that the volume of the Fermi surface monotonically drops from 1 (i.e. occupying the whole Brillouin zone) at zero doping to the non-interacting value at 20% doping. In Fig. 5.14, we reproduce their result for the lower bound of the volume of the Fermi surface. They however stressed, that the actual volume can be larger (but not smaller) than shown in the figure.

Many different criteria were used by various authors to determine Fermi surface. The problem is that the zero temperature limit is usually inaccessible with numerical methods or the size of the system is too small for the thermodynamic limit to be reached. As we have already discussed before, our NCA method is limited to temperatures above $T \gtrsim 0.03t^*$ and zero temperature is inaccessible. However, we believe that EDMFT is not limited in that sense. If an improved method for solving the impurity problem (3.12) is used, $T = 0$ could be reached. Nevertheless, the temperature $T = 0.03t^* = 0.2J$ is already quite small and we might expect that $T = 0$ limit can be smoothly approached if an appropriate criteria for the estimation of the Fermi sur-

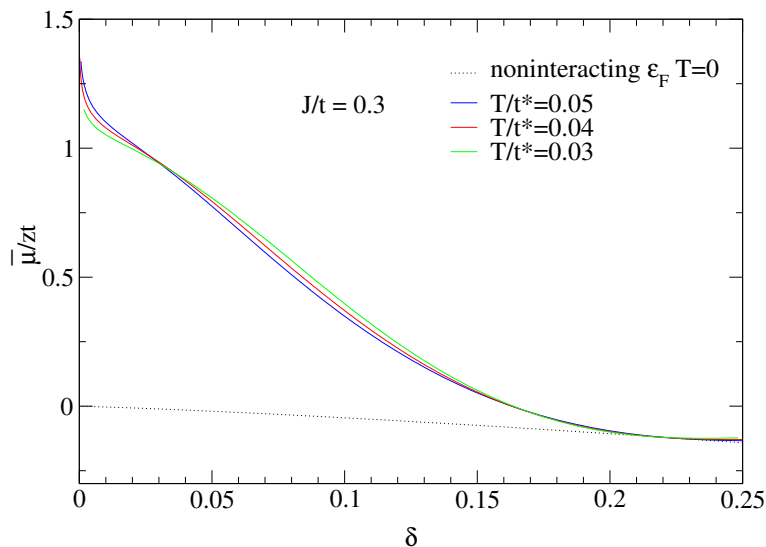


Figure 5.15: Effective chemical potential vs doping for $J/t = 0.3$. The dotted line marks the non-interacting chemical potential at zero temperature, which should coincide with the effective chemical potential according to the Luttinger theorem.

face is chosen. For comparison, we mention the lowest temperature reached by some other methods that also estimated the Fermi surface: Maier *et al.* $T = 0.066t^*$, Putikka *et al.* $T = 0.04t^*$, Eder *et al.* $T = 0.05t^*$.

In the case of the local theory, the effective chemical potential $\bar{\mu}$ can be defined, which determines the position of the Fermi surface

$$\bar{\mu} = \mu - \text{Re} \Sigma(\omega = 0). \quad (5.14)$$

The spectral function diverges at the Fermi surface defined by $\varepsilon_{\mathbf{k}} = \bar{\mu}$ since the Green's function at the chemical potential is

$$G_{\mathbf{k}}(\omega = 0) = \frac{1}{\bar{\mu} - \varepsilon_{\mathbf{k}} - i \text{Im} \Sigma(0)}. \quad (5.15)$$

The Luttinger theorem then states that $\bar{\mu}$ is equal to the noninteracting chemical potential μ_0 corresponding to the same filling. In the case of fully filled band ($n = 2$) and half-filled ($n = 1$), μ_0 is equal to zt and 0 , respectively.

Fig. 5.15 shows the effective chemical potential $\bar{\mu}$ versus doping as obtained by our method. The most important conclusion is that the Luttinger theorem is not satisfied for doping below 20%. The deviation from the Luttinger volume is quite pronounced at low doping and seems to support a simple rigid picture of doping the Mott insulator as proposed already by Hubbard: at half filling, the chemical potential is between the Hubbard bands

and the effect of doping is that the chemical potential gradually cuts into the top of the lower Hubbard band. The Fermi surface is hole-like and centered around (π, π) for underdoped and optimally doped case, while it is electron-like for the overdoped case. The same conclusion have been reached by a quantum Monte Carlo simulation for the Hubbard model by Eder *et al.* [52] as shown in the Fig. 5.14. The results of Putikka *et al.* [54] are also in agreement with our findings. However, it should be noted that all the calculations were performed for the paramagnetic phase with no broken symmetry. Thus, the true antiferromagnetic state with long range order was not allowed at any finite temperature, which is true only for strictly two dimensional systems without any inter-layer couplings.

It should be noted, that the change of the Fermi surface from hole-like to electron-like is closely related to the change in the sign of the Hall coefficient from positive to negative occurring for doping slightly above the optimum doping. We will turn to a closer examination of that issue in chapter 5.5.

Fig. 5.16 shows the spectral function at the chemical potential in upper quadrant of the first Brillouin zone $A(\mathbf{k}, \omega = 0)$ for doping concentrations 4%, 10%, 16% and 23%. The peak structure of the spectral function is characterized by yellow region in the plot and the white line marks the non-interacting Fermi surface. For the largest doping shown, the quasiparticle peak is very narrow and coincides with the non-interacting electron-like Fermi surface. This is due to the small scattering rate and long lifetime of the quasiparticles in the Fermi liquid state. The yellow region in the Fig. 5.16 is substantially increased in the optimally doped system, especially around $(\pi, 0)$, because the quasiparticle peak becomes broader. This is due to the large self-energy at the chemical potential or equivalently large scattering rate and short lifetime of quasiparticles compared to their energy. This is also closely related to the large pseudogap originating from the antiferromagnetic correlations as pointed out by Ino *et al.* [64]. As doping further decreases, the quasiparticle peak remains very broad and continues to move towards the edge of the Brillouin zone (π, π) . The transport properties are still governed by hole-like excitations.

The spectral function $A(\mathbf{k}, \omega)$ is shown also in Fig. 5.17 with frequency on the vertical axes and wave vectors \mathbf{k} on horizontal axes. The quasiparticle peak is again very narrow for 23% doping and much more broad in optimally or underdoped region. It should be noted that the quasiparticle band is very flat around $(\pi, 0)$ for optimally doped 16% system. The reason is that the renormalization factor $Z = (1 - \partial\Sigma'/\partial\omega)^{-1}$ is very small (it goes to zero at zero temperature) and therefore the quasiparticle energy $E_{\mathbf{k}}$ vanishes faster

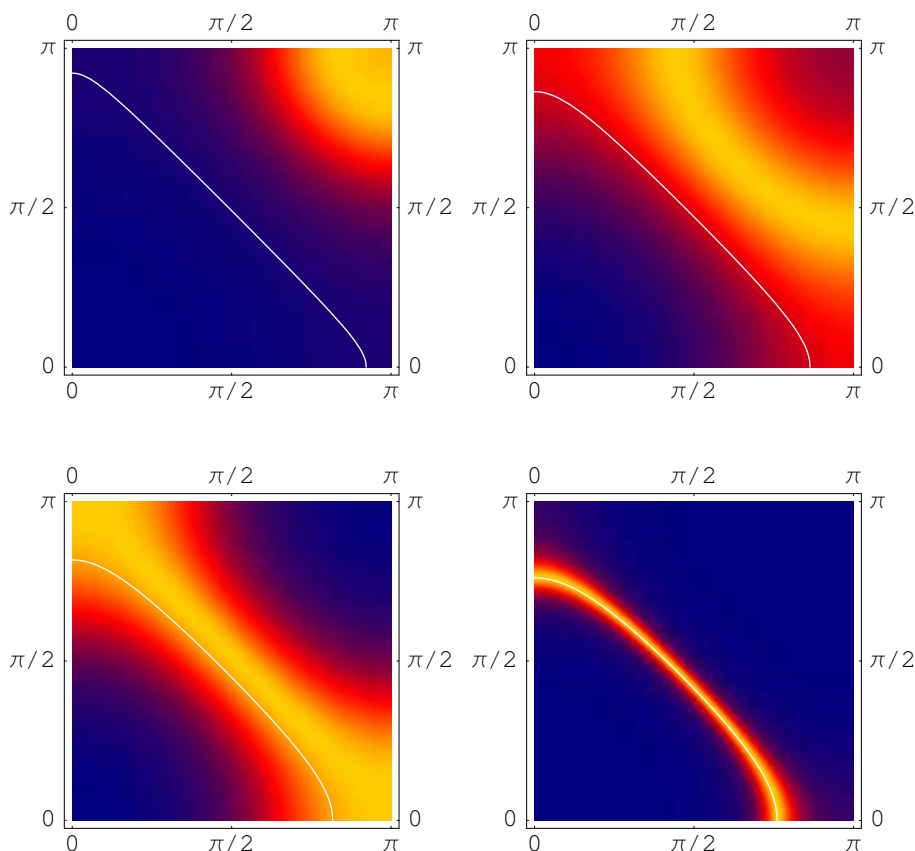


Figure 5.16: Constant energy scan of the single particle spectral function $A(\mathbf{k}, \omega = 0)$ in the right upper quadrant of the first Brillouin zone for temperature $T/t^* = 0.03$. The left upper panel corresponds to 4% doping, the right upper to 10%, left lower to 15% and right upper to 10%, left lower to 23% doping. The dark (light) represents regions with low (high) electron concentration.

than quadratically. It is the solution of the equation

$$E_{\mathbf{k}} + \mu - \varepsilon_{\mathbf{k}} - \Sigma'(E_{\mathbf{k}}) = 0 \quad (5.16)$$

and for small $E_{\mathbf{k}}$ can be expressed as

$$E_{\mathbf{k}} = Z(\varepsilon_{\mathbf{k}} - \bar{\mu}) + \dots, \quad (5.17)$$

where $\bar{\mu}$ is the effective chemical potential. At optimum doping, the effective chemical potential is close to zero and therefore the Fermi surface is around $(\pi, 0)$, where $\varepsilon_{\mathbf{k}}$ vanishes quadratically. Since Z goes to zero, the quadratic part of $E_{\mathbf{k}}$ actually vanishes and the band becomes very flat.

Finally, let us compare our results to some recent experiments made on cuprates [64, 42]. Using angle-resolved photoemission spectra, it was shown

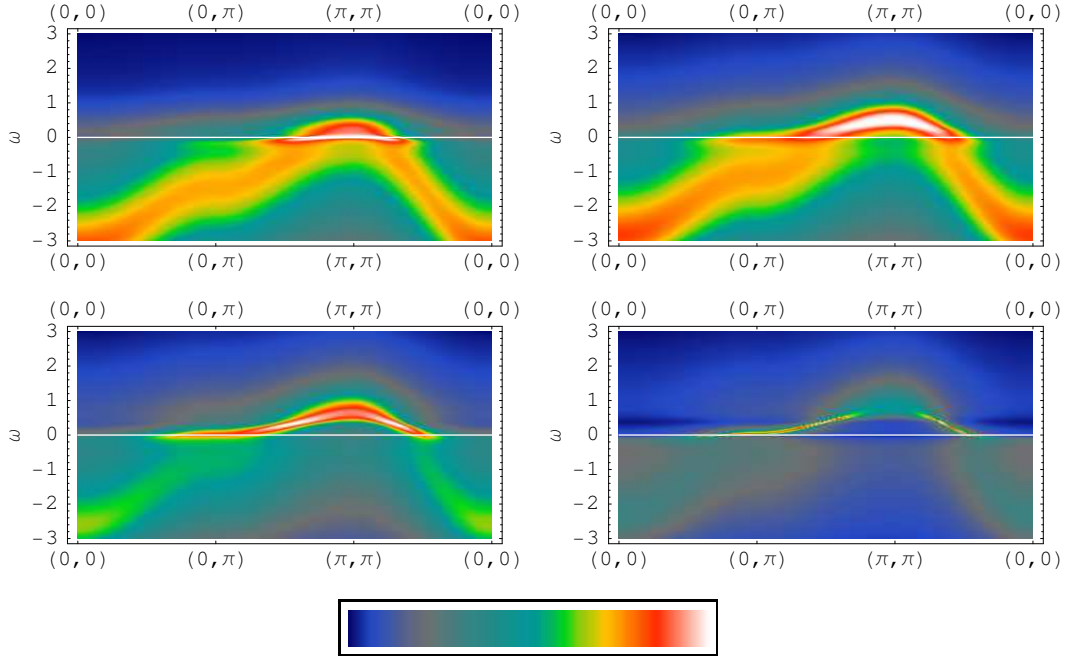


Figure 5.17: Angle-resolved single particle spectral function $A(\vec{k}, \omega)$ for various doping concentrations with frequency on vertical axes and k on horizontal axis. The left upper panel corresponds to 4% doping, the right upper to 10%, left lower to 15% and right lower to 23% doping. Temperature is $T/t^* = 0.03$. The legend is displayed below.

that the Fermi surface of LSCO is hole-like and centered at (π, π) in underdoped $\delta = 0.1$ and optimally doped $\delta = 0.15$ samples, while it is electron-like and centered at $(0, 0)$ in heavy overdoped $\delta = 0.3$ ones. The quasiparticle peak, which is indeed very broad, crosses Fermi energy around $(0.2\pi, \pi)$ for 15% doping. This is quite consistent with the Fig. 5.16. However, the experiment also shows partial truncation of Fermi surface around $(\pi/2, \pi/2)$, as no quasiparticle peak was identified in going from (π, π) to $(0, 0)$. This kind of phenomena can not be explained within a local theory like ours, since it comes from the \mathbf{k} dependent self-energy. However, the hole-like part of the Fermi surface around $(\pi, 0)$ that mainly determines the physical properties, is correctly described in EDMFT.

For heavily overdoped samples of LSCO (30%), the quasiparticle peak is much more pronounced and consistent with the Fermi liquid picture. This is naturally consistent with EDMFT result since the spin moments are completely quenched at $T = 0$ for such large doping.

For only slightly doped sample, the experimental picture is more complicated because of commensurate and incommensurate orderings. The antiferromagnetic state is reflected in the small pockets or "Fermi arc" around

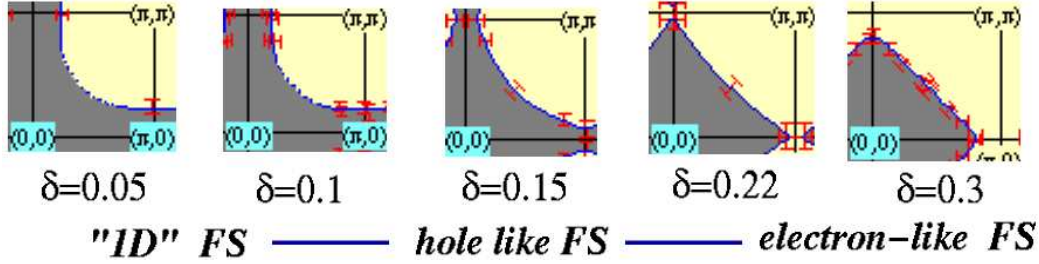


Figure 5.18: Fermi surface of LSCO as determined from ARPES data for various doping concentrations. (from Ref. [64]). Observed Fermi surface crossings are denoted by thick error bars and the dotted curve is tentatively drawn so that the area enclosed by the Fermi surface is consistent with the Luttinger theorem.

$(\pi/2, \pi/2)$ sometimes observed, while the stripe phases yield one dimensional Fermi surface consisting of vertical and horizontal lines. The commensurate and incommensurate orderings are not considered in our present method and therefore this part of experimental results cannot be explained within present approach.

5.4 Thermodynamics

Within a local theory like DMFT, free-energy of the lattice system can be expressed by the impurity free-energy and local electron self-energy alone [65]. The EDMFT includes also bosonic fields that mimic the nonlocal magnetic interaction and participate to the free energy of the system [66]. In this case, the thermodynamic potential can be written in terms of the impurity free-energy, electron self-energy and spin susceptibility as

$$\Omega/N = \Omega_{imp} + \frac{1}{\beta} \sum_{\omega, \sigma} \left\{ \sum_{\mathbf{k}} \ln(G_{\mathbf{k}}(i\omega)) - \ln(G_{oo}(i\omega)) \right\} e^{i\omega 0^+} - \frac{1}{2} \frac{1}{\beta} \sum_{\omega, \alpha} \left\{ \sum_{\mathbf{q}} \ln(\chi_{\mathbf{q}}^{\alpha\alpha}(i\omega)) - \ln(\chi_{oo}^{\alpha\alpha}(i\omega)) \right\} e^{i\omega 0^+}. \quad (5.18)$$

Here, Ω_{imp} is the local free-energy contribution of the effective impurity problem. A detailed derivation of above formula is worked out in Appendix F. Expressing the summation over momentum as an energy integration and performing the analytic continuation to real frequencies, we obtain

$$\Omega/N = \Omega_{imp} + \frac{2}{\pi} \text{Im} \int d\omega f(\omega) \int d\varepsilon D(\varepsilon) \ln[G_{oo}(\omega)(\omega + \mu - \Sigma(\omega) - \varepsilon)] + \frac{3}{2\pi} \text{Im} \int d\omega n(\omega) \int d\varepsilon D(\varepsilon) \ln[\chi_{oo}(\omega)(\chi_{oo}^{-1}(\omega) + \chi_0^{-1}(\omega) - \frac{J}{t}\varepsilon)]. \quad (5.19)$$

Although, in principle the knowledge of Ω provides everything one needs, it is helpful to have an independent expression for the internal energy E as well. In particular, the specific heat can be obtained by a single differentiation of $E(T)$ instead of double differentiation of $\Omega(T)$. The internal energy is quite generally expressed by (see Appendix F)

$$E = \frac{1}{2} \frac{1}{\beta} \sum_{\mathbf{k}, \sigma, \nu \omega} (\varepsilon_{\mathbf{k}} + \mu + \nu \omega) G_{\mathbf{k}}(\nu \omega) e^{\nu \omega 0^+}. \quad (5.20)$$

In the case of local self-energy, the expression (5.20) can be further simplified to avoid the momentum summation

$$E = -\frac{2}{\pi} \text{Im} \int d\omega f(\omega) G_{oo}(\omega) [\omega + \mu - \Sigma(\omega)/2]. \quad (5.21)$$

The entropy per-site and doping is then determined from the derivatives of the free-energy

$$S = -\frac{1}{N} \left(\frac{\partial \Omega}{\partial T} \right)_{\mu}$$

$$n = 1 - \delta = -\frac{1}{N} \left(\frac{\partial \Omega}{\partial \mu} \right)_{T}. \quad (5.22)$$

The doping can also be obtained directly from the local Green's function as

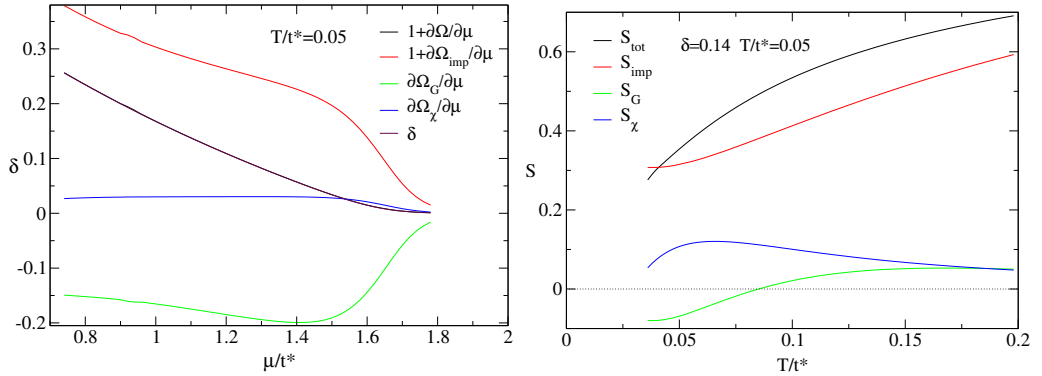


Figure 5.19: left: The derivative of the thermodynamic potential with respect to chemical potential $1 + (\partial\Omega/\partial\mu)_T/N$ is compared to the doping. The contributions from three different parts of the thermodynamic potential: impurity, electron Green's function (second term in Eq. 5.18) and spin susceptibility part (last term in Eq. 5.18) are shown separately. right: Entropy per site for optimally doped system. The three parts are again shown separately.

$$n/2 = G_{oo}(\tau = 0^-) \quad (5.23)$$

and have to give the same answer since the EDMFT as well as NCA are conserving approximations. This is checked in Fig. 5.19 where the two curves completely match.

Now we turn to the closer examination of some thermodynamic quantities like the specific heat, entropy and chemical potential. A detailed comparison will be presented between EDMFT+ NCA results and exact diagonalization results that are taken from Ref. [9] and correspond to the 2D lattice with 20 sites. The agreement is quite remarkable considering the difference between the two methods and their limitations: EDMFT ignores the wave number dependence of the self-energy and spin cumulant being justified only in the limit of large dimensions while exact diagonalization suffers from the finite size effects. Since we did not find any small energy scale within the t-J model, the small system may already capture the most important physics. On the other hand, the apparent agreement between the two methods may indicate, that the \mathbf{k} dependence of the self-energy is not crucial for the explanation of unusual properties of the two dimensional t-J model.

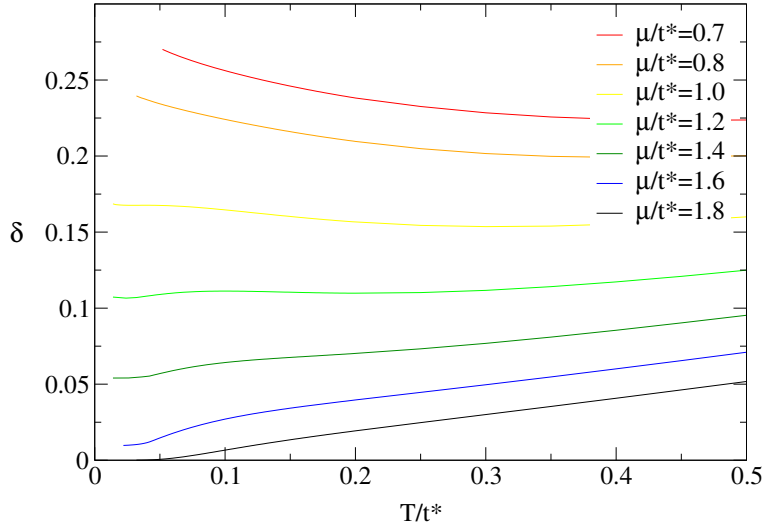


Figure 5.20: The doping δ as a function of temperature for various chemical potentials μ as obtained by EDMFT+ NCA.

The doping δ as a function of temperature is displayed in Fig. 5.20 for various chemical potentials. The most important feature is that doping is increasing with increasing temperature in the underdoped case and decreasing with increasing temperature in the overdoped regime. The latter can be understood in the Fermi liquid picture, where doping should vary as

$$\delta = \delta(T = 0) - \frac{(\pi k_B T)^2}{6} \mathcal{N}'(\bar{\mu}) \quad (5.24)$$

where $\mathcal{N}'(\bar{\mu})$ is the bare lattice density of states at the effective chemical potential. The quadratic behavior is likely to hold for the smallest chemical potential shown ($\mu = 0.7$ and $\mu = 0.8$) which corresponds to overdoped case. However, the NCA method does not work much below the corresponding characteristic energy scale ε^* and therefore the parabolic behavior is not seen in the Fig. 5.20.

The second important feature shown in Fig. 5.20 is that the doping is almost temperature independent for fixed chemical potential around optimum doping $\delta^* \sim 0.15$ and $\mu \sim 1$. This is also the point where the slope of the curves in the $\delta-T$ diagram is changed and can be related to the change of the Fermi surface from hole-like to the electron-like. As shown in Fig. 5.15, the effective chemical potential $\bar{\mu}$ indeed changes sign just around 17% doping.

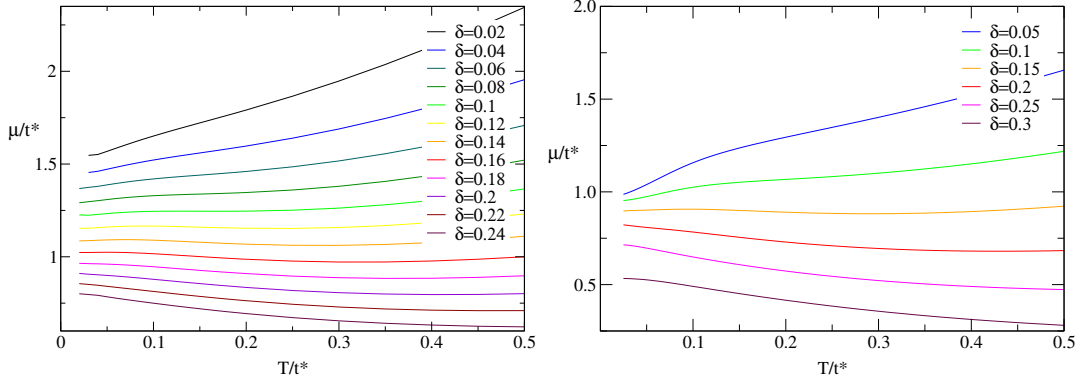


Figure 5.21: Chemical potential μ as a function of temperature for various doping concentrations δ . Left panel shows EDMFT+ NCA results while the right panel corresponds to the exact diagonalization results for the system with 20 sites (from Ref. [9]).

Next, we compare the chemical potential at fixed doping as a function of temperature with the exact diagonalization (ED) results. The left panel of Fig. 5.21 shows the EDMFT+ NCA results while the right displays corresponding ED results. Note that the flatness of the curves in the optimally doped regime is common to both approaches as well as the positive and negative slopes in the underdoped and overdoped regimes, respectively.

Finally, the doping as a function of chemical potential obtained by EDMFT+ NCA (ED) is shown in the left (right) panel of Fig. 5.22. In this case, the optimum doping is characterized by the crossing of curves at different temperatures and is again common to both approaches.

The compressibility is another quantity that can be easily deduced from

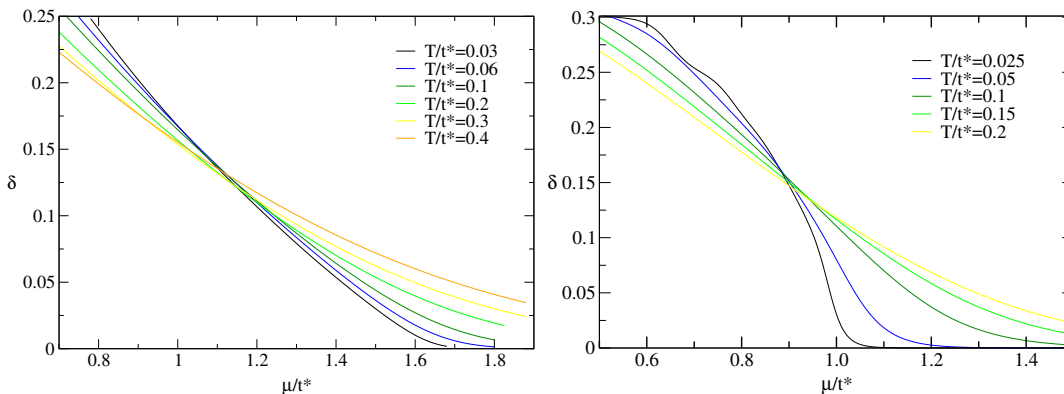


Figure 5.22: Doping δ as a function of chemical potential μ for various temperatures. Left panel again displays EDMFT+ NCA results while the right panel shows exact diagonalization results for the system with 20 sites (from Ref. [9]).

Fig. 5.22 as

$$\kappa = -\frac{1}{(1-\delta)^2} \frac{\partial \delta}{\partial \mu}. \quad (5.25)$$

It seems that within EDMFT compressibility is not diverging at least not in the temperature range where NCA is applicable. However, the compressibility should diverge close to the Mott-Hubbard transition at $T = 0$ in two-dimensional t-J model as predicted by Imada *et al.* [39]. Since the ultimate zero temperature limit is not accessible within our NCA method, we cannot completely exclude the possibility that this eventually might happen in EDMFT, but it seems more likely that the wave number dependence of the self-energy is important to explain this anomaly. We thus suspect that this feature of the Mott-Hubbard transition is not captured within EDMFT.

Now we turn to the behavior of entropy as a function of doping (Fig. 5.23) and temperature (Fig. 5.24) in the paramagnetic metallic state of the t-J model. If spin symmetry is broken, the entropy coming from the spins is reduced essentially to zero. Even without long range order, the growth of short-ranged spin correlations progressively reduces the entropy with decreasing temperature or decreasing doping. When holes are added to the Mott-Hubbard insulator, an additional entropy due to charge degrees of freedom is introduced. Thus, the entropy increases with doping due to both processes: reduction of the magnetic order and introduction of charge carriers (see Fig. (5.23)). This is true as long as magnetic correlations are important, more important than Kondo physics. However, in the overdoped case where Kondo (actually mixed valence) physics prevails, the entropy starts to decrease with doping. This is due to monotonic increase of the Kondo temperature with doping, below which the entropy is significantly reduced.

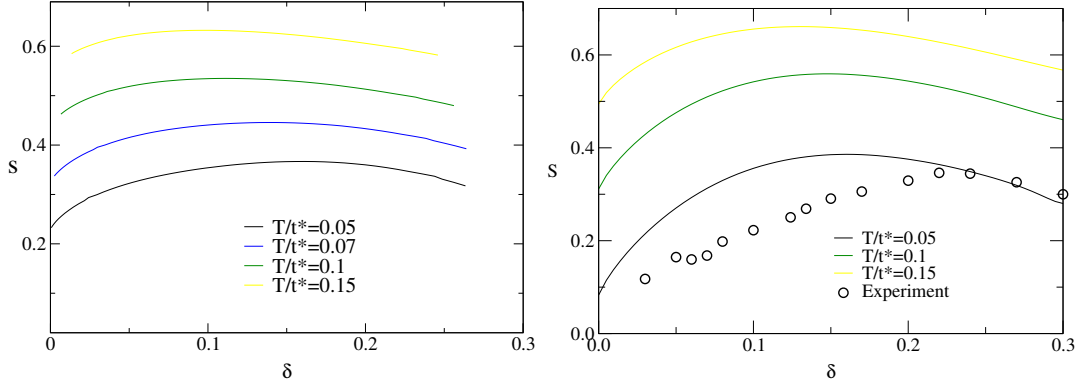


Figure 5.23: Entropy per site S as a function of doping δ at various temperatures. Left (right) panel displays EDMFT+NCA (ED) results. For comparison, the experimental result [67] for LSCO is shown in the right panel for temperature $T/t^* \sim 0.035$ corresponding to $\sim 320K$.

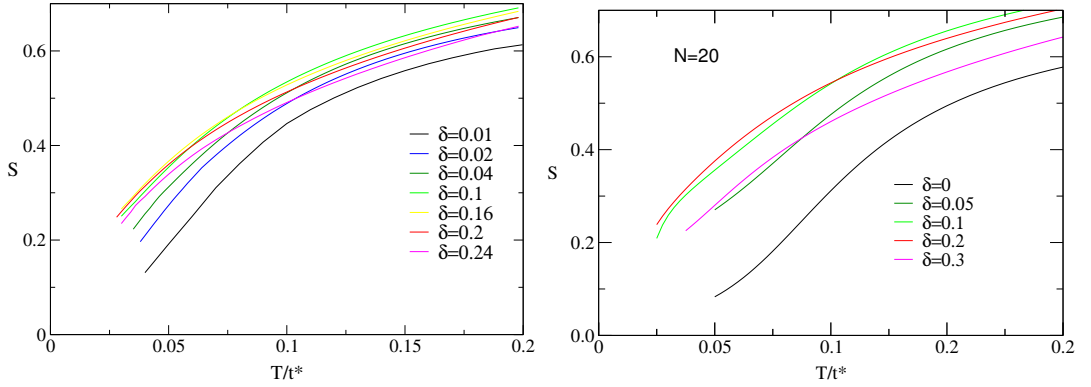


Figure 5.24: Entropy S as a function of temperature at various doping concentrations δ . Left (right) panel displays EDMFT+NCA (ED) results.

In order to better understand the role of magnetic exchange interaction J on the entropy, this behavior should be contrasted with the t -model properties in the limit of large dimensions, which is always Fermi liquid if commensurate and incommensurate ordering is ignored. As is known from the DMFT study of infinite- U Hubbard model [5], the characteristic Kondo temperature is monotonically increasing with doping and approaches zero close to the Mott-Hubbard transition (effective mass is diverging). The entropy of the t -model is essentially released above this characteristic Fermi liquid temperature so that slightly doped Mott-insulator has entropy equal to $\ln 2$ down to almost zero temperature. The effect of doping the t -model is that the characteristic temperature, above which the entropy is activated, is increased while the linear T dependence below this scale is preserved.

On the contrary, the entropy of the undoped t - J model insulating phase goes as T^2 with the characteristic scale J because the 2^N states are split below the temperature of order J (see Fig. 5.24). The effect of doping is that the spin correlations are gradually reduced and the entropy is rapidly enhanced. More importantly, the low temperature dependence changes from T^2 to T with doping. However, the difference between the t - J model and t -model disappears in the heavily overdoped phase where J becomes unimportant and additional doping reduces entropy of both models.

The entropy thus increases with doping in the underdoped regime while it decreases in the overdoped case. As shown in Fig. 5.23, a broad maximum develops in-between, which slightly shifts with temperature. At the lowest temperature shown $T = 0.05$, the maximum is just around $\sim 15\%$ doping. This maximum is also related to the flatness of the $\mu(T)$ curves in Fig. 5.21 or the crossing point of $\delta(\mu)$ curves in Fig. 5.22. Namely, from mixed derivatives of $\mathcal{F}(T, \delta)$, which is Legendre transform of the thermodynamic potential $\Omega(T, \mu)$, it follows

$$\left(\frac{\partial S}{\partial \delta}\right)_T = \left(\frac{\partial \mu}{\partial T}\right)_\delta. \quad (5.26)$$

The special point, where the derivatives (5.26) are zero, is sometimes called marginal doping δ^* , being almost temperature independent. It is ultimately related to the large degeneracy of low-lying many body states leading to the marginal Fermi liquid properties.

Besides the correct qualitative features of entropy, it is also important that its magnitude is close to the experimentally observed values in cuprates. In Fig. 5.23, the results for LSCO [67] are compared with the $t - J$ model calculations.

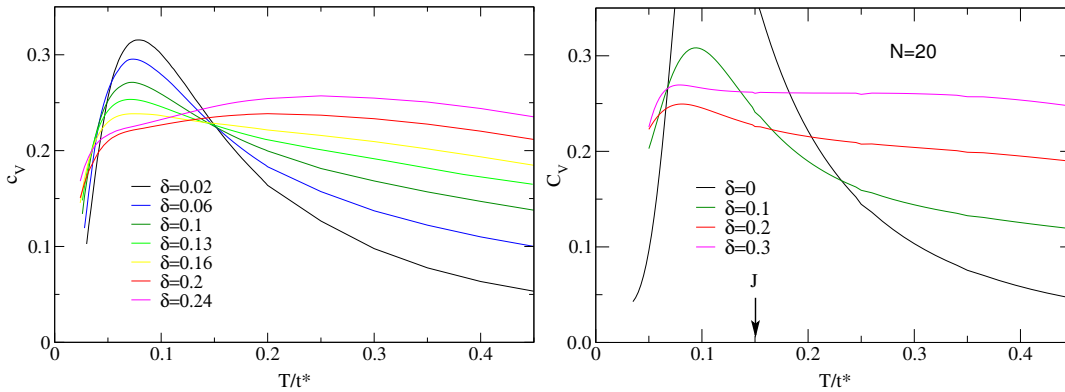


Figure 5.25: The specific heat c_v as a function of temperature for various doping concentrations. Right panel corresponds to ED results for 20 sites system while the left one shows EDMFT+NCA results.

The specific heat as a function of temperature is displayed in Fig. 5.25. The left panel again shows the EDMFT results while the right one is obtained by the exact diagonalization. For small doping, both methods show a maximum at $T = 2/3J$ and possible quadratic low temperature part consistent with the magnon excitations dominating in this regime [68]. The maximum is suppressed with doping and gradually moves to lower temperature. This is because the short range magnetic correlations are destroyed at lower temperature when the Mott insulator is doped. The maximum eventually disappears in the overdoped phase and the linear low temperature part evolves, which is consistent with the Kondo temperature of order J . The maximum of specific heat at small doping, as obtained by our method, is much less pronounced than ED results suggest. This might be due to the fact, that the correlation length gets large close to half-filling and exceeds the size of the small system studied by ED method. The antiferromagnetic correlations are then overestimated in latter approach. On the other hand, the wave-vector independent self-energy might be in question here, since the growth of the antiferromagnetic correlations might require substantial change in the shape of the Fermi surface which can be described only by strongly \mathbf{k} -dependent self-energy.

5.5 Hall coefficient

In this section, we investigate the impact of magnetic field on the charge transport properties of the t-J model within EDMFT. This issue was addressed by many authors [69, 70, 71] in the context of Hubbard model and DMFT. While the DMFT still captures many properties of real three-dimensional transition-metal oxides, it fails to describe cuprate superconductors equally well, mainly because it does not properly take into account magnetic correlations. This drawback of the method is circumvented in EDMFT with including short range magnetic fluctuations. In addition, another non-trivial simplification of both approaches is that the transport properties are described solely by the single-particle spectrum [72, 73, 5]. This comes from the fact that the self-energy is momentum independent and therefore the \mathbf{k} dependence of the dressed current vertex function $\Gamma^\alpha(\mathbf{k}, \mathbf{k})$ can be ignored. The non-local part of both quantities is of the same order in $1/d$ expansion and therefore vanishes in the limit of large dimensions. This observation was first made by Khurana [73] with the power counting argument. A more detailed proof follows from the Ward identity

$$\Omega \Gamma_{\mathbf{k}+\mathbf{q}, \mathbf{k}}^0(\omega + \Omega, \omega) + \mathbf{\Delta}(\mathbf{q}) \cdot \mathbf{\Gamma}_{\mathbf{k}+\mathbf{q}, \mathbf{k}}(\omega + \Omega, \omega) = G_{\mathbf{k}+\mathbf{q}}^{-1}(\omega + \Omega) - G_{\mathbf{k}}^{-1}(\omega) \quad (5.27)$$

where Γ^0 and $\mathbf{\Gamma}$ denote the density and current vertex functions respectively and $\Delta^\alpha(\mathbf{q}) = 2 \sin(q_\alpha/2)$ on the hypercubic lattice. This identity follows from the equation of continuity $\nabla \cdot \mathbf{J} - \partial\rho/\partial t$ and was first shown by Ward [74].

Since EDMFT self-energy is independent of momentum, and the density vertex is even in \mathbf{q} , expanding Eq. (5.27) to first order in \mathbf{q} , we get

$$\mathbf{\Gamma}_{\mathbf{k},\mathbf{k}}(\omega + \Omega, \omega) = -\frac{\partial \varepsilon_{\mathbf{k}}}{\partial \mathbf{k}}. \quad (5.28)$$

Thus, the current vertex function is unrenormalized for $q = 0$ and only the elementary particle-hole bubble contributes to optical conductivity in this case. Note that the conclusion is false for any finite q because Eq. (5.27) can not be simply decoupled into density and current part for $q \neq 0$.

Hence, the paramagnetic contribution to the optical conductivity for $\mathbf{q} = 0$ can be expressed as

$$\sigma_{xx}(i\omega) = \frac{e^2}{\omega} \frac{1}{\beta} \sum_{\mathbf{k}\sigma, \omega'} (v_{\mathbf{k}}^x)^2 G_{\mathbf{k}}(i\omega') G_{\mathbf{k}}(i\omega' + i\omega), \quad (5.29)$$

where $v_{\mathbf{k}}^x = 2t \sin k_x$ is the bare vertex. Since the Green's function depends on \mathbf{k} only through $\varepsilon_{\mathbf{k}}$, the sum over momenta in 5.29 can be further simplified, by expressing it as an energy integration

$$\text{Re } \sigma_{xx}(\omega + i\delta) = 2\pi e^2 \int d\varepsilon \Phi_{xx}(\varepsilon) \int d\omega' \frac{f(\omega') - f(\omega' + \omega)}{\omega} A(\varepsilon, \omega') A(\varepsilon, \omega' + \omega) \quad (5.30)$$

where the corresponding density of states reads

$$\Phi_{xx}(\varepsilon) = \sum_{\mathbf{k}} (v_{\mathbf{k}}^x)^2 \delta(\varepsilon - \varepsilon_{\mathbf{k}}). \quad (5.31)$$

Finally, the zero frequency conductivity takes a very simple form

$$\sigma_{xx} = 2\pi e^2 \int d\varepsilon \Phi_{xx}(\varepsilon) \int d\omega \left(-\frac{\partial f}{\partial \omega} \right) A(\varepsilon, \omega)^2. \quad (5.32)$$

Similarly, one can show that all vertex corrections of the conductivity tensor vanish in the limit of large spatial dimensions [75, 76, 77], and therefore the off-diagonal component σ_{xy} is given by

$$\sigma_{xy} = \frac{4\pi^2 e^3}{3} H \int d\varepsilon \Phi_{xy}(\varepsilon) \int d\omega \left(-\frac{\partial f}{\partial \omega} \right) A(\varepsilon, \omega)^3, \quad (5.33)$$

where another density of states is introduced, that can be expressed in terms of the bare band structure by

$$\Phi_{xy}(\varepsilon) = \sum_{\mathbf{k}} \det(\mathbf{k}) \delta(\varepsilon - \varepsilon_{\mathbf{k}})$$

$$\det(\mathbf{k}) = \begin{vmatrix} \epsilon_k^{xx} & \epsilon_k^{xy} \\ \epsilon_k^{yx} & \epsilon_k^{yy} \end{vmatrix} \quad \epsilon_k^\alpha = \frac{\partial \varepsilon_{\mathbf{k}}}{\partial k_\alpha} \quad \epsilon_k^{\alpha\beta} = \frac{\partial^2 \varepsilon_{\mathbf{k}}}{\partial k_\alpha \partial k_\beta} \quad (5.34)$$

For two and infinite dimensional hypercubic lattices, both densities Φ_{xx} and Φ_{xy} can be expressed by elementary functions given explicitly in Appendix E.

Finally, the Hall coefficient is given by

$$R_H = \frac{\sigma_{xy}}{\sigma_{xx}^2 H}, \quad (5.35)$$

where we have assumed a symmetry between x and y direction (i.e. $\sigma_{xx} = \sigma_{yy}$ and $\sigma_{xy} = \sigma_{yx}$).

5.5.1 Low temperature limit

Most relevant low temperature limit is usually hard to reach by simple numerical methods like NCA. It is therefore important to find simple expressions relating various physical quantities like Hall number or conductivity with more fundamental quantities like self-energy and band structure of the system.

In a local theory, the momentum dependence of the lattice Green's function comes only through $\varepsilon_{\mathbf{k}}$ therefore the spectral function is a simple Lorentz curve with respect to band energy $\varepsilon_{\mathbf{k}}$. Thus, the integral over this energy variable (i.e. the momentum sum) can be performed exactly

$$A(\varepsilon, \omega) = -\frac{1}{\pi} \frac{\Sigma''(\omega)}{(\omega + \bar{\mu} - \varepsilon)^2 + (\Sigma''(\omega))^2} \quad (5.36)$$

$$\int d\varepsilon A(\varepsilon, \omega) = 1 \quad (5.37)$$

$$\int d\varepsilon A(\varepsilon, \omega)^2 = \frac{1}{2\pi |\Sigma''(\omega)|} \quad (5.38)$$

$$\int d\varepsilon A(\varepsilon, \omega)^3 = \frac{3}{8\pi^2 |\Sigma''(\omega)|^2} \quad (5.39)$$

At low temperatures, the derivative of the Fermi function can be approximated by a delta function in Eq. (5.32). In addition, the imaginary part

of the self-energy at zero frequency is small, therefore the spectral function $A(\varepsilon, 0)$ is sharply peaked at the effective chemical potential $\varepsilon = \bar{\mu}$ and hence the energy integral can be evaluated analytically. The conductivity at low temperature is finally given by

$$\sigma_{xx} \approx 2\pi e^2 \int d\varepsilon \Phi_{xx}(\varepsilon) A(\varepsilon, 0)^2 \approx e^2 \frac{\Phi_{xx}(\bar{\mu})}{|\Sigma''(0)|}. \quad (5.40)$$

The effective chemical potential is only weakly temperature dependent therefore the resistance at constant doping is proportional to $|\Sigma''(0)|$

$$\rho \approx \frac{1}{e^2} \frac{|\Sigma''(0)|}{\Phi_{xx}(\bar{\mu})}. \quad (5.41)$$

In the case of Fermi liquid and Marginal Fermi liquid, this gives $\rho \propto T^2$ and $\rho \propto T$, respectively.

Similarly, the off-diagonal component of the conductivity can be approximated by

$$\sigma_{xy} \approx \frac{4\pi^2 e^3}{3} H \int d\varepsilon \Phi_{xy}(\varepsilon) A(\varepsilon, 0)^3 \approx \frac{1}{2} e^3 H \frac{\Phi_{xy}(\bar{\mu})}{|\Sigma''(0)|^2}. \quad (5.42)$$

Finally, the Hall number becomes

$$R_H \approx \frac{1}{2e} \frac{\Phi_{xy}(\bar{\mu})}{(\Phi_{xx}(\bar{\mu}))^2}. \quad (5.43)$$

Hence, the Hall number does not depend on the imaginary part of the self-energy but only on the effective chemical potential $\bar{\mu}$ and band structure of the lattice. For the hypercubic lattices, $\Phi_{xx}(\varepsilon)$ is even and $\Phi_{xy}(\varepsilon)$ is odd function of frequency ε . Furthermore, $\Phi_{xy}(\varepsilon)$ is negative for positive ε and vice-versa. Since the effective chemical potential $\bar{\mu}$ is positive for doping less than $\sim 17\%$ and because $e = -e_0$, the Hall number is positive in the underdoped and optimally doped region. However, in the overdoped regime Fermi surface becomes electron-like and $\bar{\mu}$ changes sign causing the Hall number to become negative. For doping above $\sim 20\%$, $\bar{\mu}$ gets unrenormalized and equals to the noninteracting value μ_0 , therefore the Hall number becomes identical to the free fermion value R_H^0 .

We now consider the two dimensional square lattice, where all densities $D(\varepsilon)$, $\Phi_{xx}(\varepsilon)$ and $\Phi_{xy}(\varepsilon)$ are elementary functions (see Appendix E). Close to the Mott-Hubbard transition, $\bar{\mu}$ approaches the upper edge of the lower Hubbard band (see Fig. 5.15), where the expansion of Φ_{xx} and Φ_{xy} is possible

and equals

$$\Phi_{xx}^{\varepsilon \rightarrow 4t}(\varepsilon) \approx \frac{1}{2\pi}(4t - \varepsilon) \quad (5.44)$$

$$\Phi_{xy}^{\varepsilon \rightarrow 4t}(\varepsilon) \approx -2t\Phi_{xx}^{\varepsilon \rightarrow 4t}(\varepsilon). \quad (5.45)$$

The Hall number can therefore be approximated by

$$R_H^{\delta \rightarrow 0} \approx -\frac{1}{e} \frac{2\pi t}{(4t - \bar{\mu})}. \quad (5.46)$$

It obviously diverges when doping goes to zero and if we assume, that the effective chemical potential approaches the value $4t$ linearly, i.e., $\bar{\mu} = 4t(1 - C\delta)$, then

$$R_H^{\delta \rightarrow 0} \approx -\frac{\pi}{2C} \frac{1}{e\delta}. \quad (5.47)$$

It has been proven [78], that a single charge carrier introduced by doping Mott-Hubbard insulator gives rise to $R_H = 1/(e_0\delta)$ under the following two conditions: optical response needs to have a pseudogap (i.e. $\sigma_{xx}(\omega \rightarrow 0) \rightarrow 0$) and quadratic dispersion for a mobile hole (i.e. $\epsilon_{q \rightarrow 0} \propto q^2$) is required.

These two conditions are certainly fulfilled in the case of EDMFT for the t-J model, therefore we expect the constant C to be approximately given by $C \approx \pi/2$. As seen in Fig. 5.15, the $\bar{\mu}(\delta)$ curve is indeed very flat around $\delta \sim 0$ consistent with the small C of order 1.

Finally, we can insert the effective chemical potential $\bar{\mu} \approx 4t(1 - \pi/2\delta)$ in Eq. (5.44) and simplify the expression for the conductivity (5.40) close to the Mott-Hubbard transition and low temperature as

$$\sigma^{\delta \rightarrow 0} \approx e^2 \frac{t\delta}{|\Sigma''(0)|}. \quad (5.48)$$

5.5.2 Numerical results

The behavior of Hall coefficient at intermediate temperatures and various doping concentrations is shown in Figs. 5.26 and (5.27). We know from previous section that Hall number should diverge as $1/\delta$ close to the Mott-Hubbard transition if the system has a gap in optical response. This important nontrivial limit is indeed captured in the present method as can be seen in Fig. 5.26.

It is remarkable that even the prefactor comes out correctly so that $R_H \delta$ approaches 1 when temperature and doping go to zero. By further doping the system, the Hall number is decreasing with increasing doping for temperatures less than $\sim J/2$ and increasing above that temperature. It changes sign

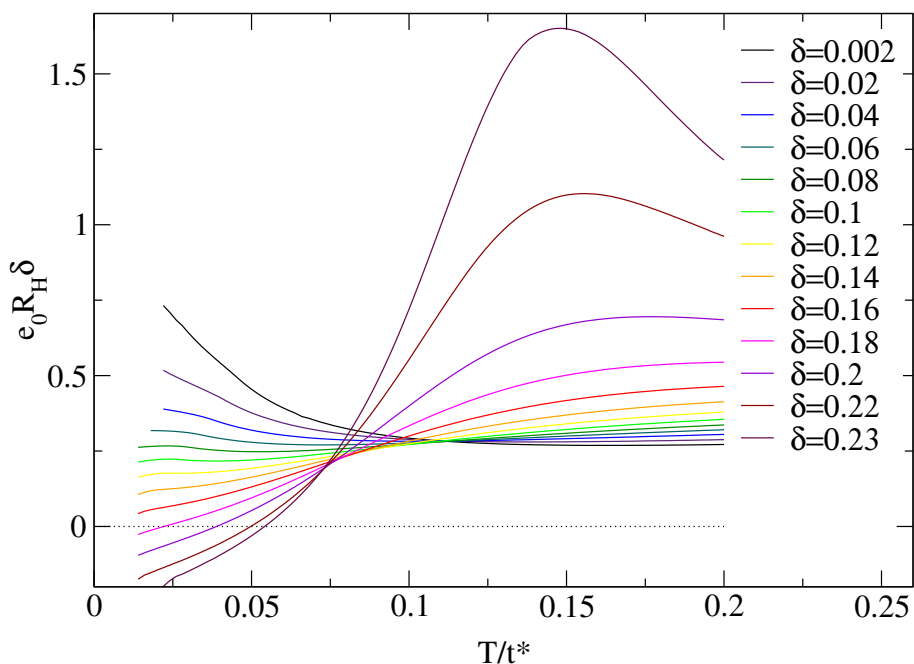


Figure 5.26: Hall number multiplied by doping vs temperature for various doping concentrations. It is positive at low doping and gets negative in the overdoped regime and low temperature. Close to the Mott-Hubbard transition and zero temperature it approaches classical limit $R_H = 1/(e_0\delta)$.

at the point where effective chemical potential $\bar{\mu}$ gets negative ($\delta \sim 17\%$) and the Fermi surface becomes electron-like. However, it is negative only in the low temperature region, while it rapidly converges to a positive value beyond the high energy scale t^* even in the far overdoped regime. This is because the system is Fermi liquid only for low enough temperatures where quasiparticles exist while electrons behave like almost independent spins with hole-like character for temperatures above the Fermi liquid characteristic temperature.

For doping above 20%, Hall number of the t-J model is very similar to that found in the infinite- d Hubbard model for large but finite U [71]. It starts at the non-interacting value (at $T = 0$) and goes through a maximum roughly located at $T \approx 0.15t^* = J$. The position of the maximum cannot be related to J because it is irrelevant for such large doping and because infinite- d Hubbard model does not capture magnetic exchange interaction, but has maximum at the same location. It was argued in Ref. [71] that the decrease of the Hall constant as a function of temperature beyond its maximum is due to the excitation of charge across the Mott-Hubbard gap. This is certainly not the case in the t-J model because double-occupancy of a lattice site is not allowed here. The only scale in this model at large doping

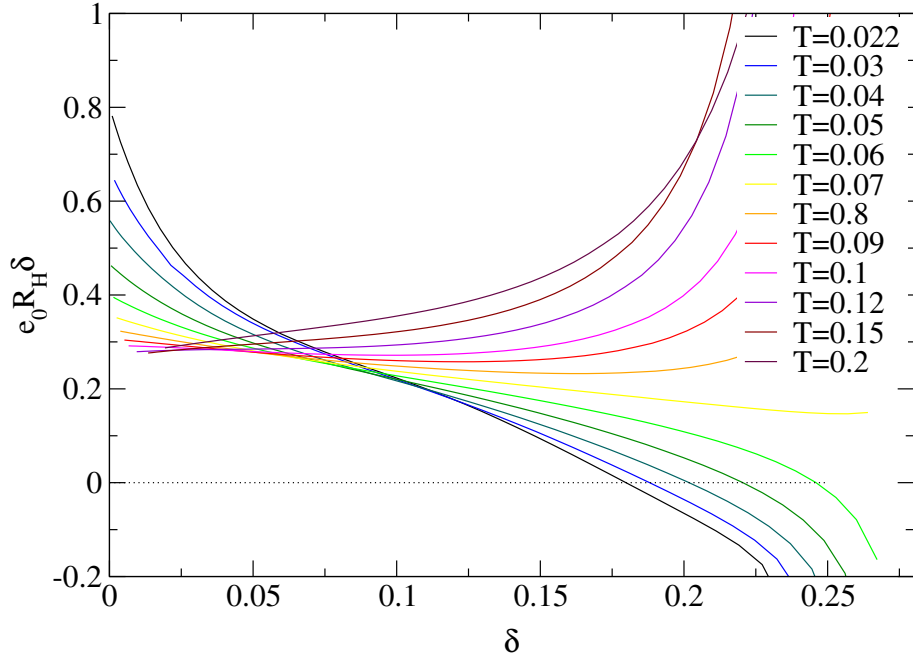


Figure 5.27: Doping dependence of the Hall number for various temperatures. For small doping and low temperature, R_H diverges as $1/\delta$ and changes sign when the Fermi surface becomes electron-like. This happens around 17% in our case.

is the Fermi liquid characteristic temperature. It was estimated in chapter 5.2 to be just around J for largest doping shown (see Fig. 5.9). This scale therefore might determine the position of the maximum of the Hall coefficient shown in Fig. 5.26.

The Hall number in the low doping regime is experimentally and theoretically far more interesting because it shows unusual temperature and doping dependence. Experiments on cuprates demonstrate that the Hall number is hole-like and approximately follows the semiclassical relation $R_H = 1/(e_0\delta)$, which cannot be explained with a simple Drude or Fermi liquid theory. At the same time, R_H monotonically decreases with increasing temperature as is evident from Fig. 5.28. The EDMFT results qualitatively agree with the experiment, at least for sufficiently low doping. The Hall number is positive up to overdoped regime and follow the semiclassical relation. It also monotonically decreases with increasing temperature up to 10% doping. Finally, R_H becomes negative in the overdoped regime which is consistent with the experiment.

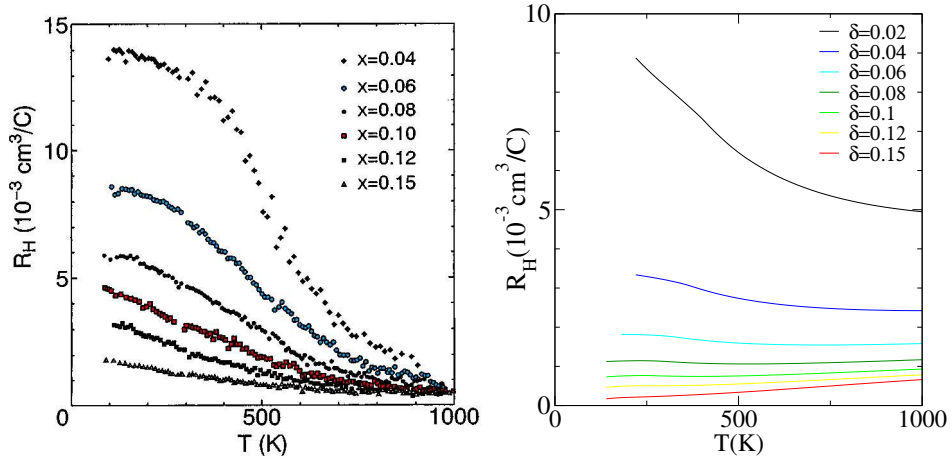


Figure 5.28: left: Experimental results for the temperature dependence of the Hall number R_H for LSCO (from Ref. [79]). right: Corresponding EDMFT+NCA results.

Chapter 6

Anderson impurity model at finite Coulomb interaction U : generalized NCA

Anderson impurity models have been of considerable interest recently as generic models of local systems with internal degrees of freedom coupled to a Fermi gas. Although first introduced as models for magnetic impurities in metals [80], they describe two-level systems in metals [81], quantum dots in mesoscopic structures [82, 83, 84] and strongly correlated lattice systems in the local approximation of the Dynamic Mean Field Theory (DMFT) [5] as well. In a nutshell, the Anderson model features one or several local levels hybridizing with the conduction electron states of the metal. Multiple occupancy of the local levels is inhibited by the strong Coulomb repulsion U between electrons in the local states. As a consequence, the local levels are approximately singly occupied, giving rise to a magnetic moment or an equivalent degree of freedom. Due to the coupling to the conduction electron system, the local moment is screened [80], or in a multi-channel situation forms a more complicated many-body state [85].

Most investigations of Anderson models have concentrated on the case of infinite Coulomb repulsion U where double occupancy of impurity site is prohibited. The t-J model, infinite- U Hubbard model and t-model are generic lattice systems that can be mapped onto the infinite- U Anderson impurity model in the limit of large dimensions. In previous chapters, we have concentrated on the t-J lattice, which does not require this kind of generalization of the local system. Instead we included non-local magnetic interaction and ended up with different generalization of the impurity model, where local degree of freedom is coupled to both boson and fermion bath. In order to treat Hubbard or Anderson lattice, even on the level of usual

DMFT, the finite- U generalization of the local system is needed.

In the case of infinite U impurity models, the restriction of the local Hilbert space to electron occupation $n_d \leq 1$ allows for an economical treatment in terms of pseudo-particle representations [86, 87] and a projection onto the physical sector of Hilbert space. In this framework, the simplest approximation consists of second-order self-consistent perturbation theory in the hybridization, the so-called Non-Crossing Approximation (NCA) [88, 89, 90]. Although the NCA has its limitations, it is a valuable tool for extracting the complex many-body physics of Anderson impurity models. In the single channel case the NCA accounts correctly for the formation of a Kondo resonance at the Fermi level below the Kondo temperature T_K [91], even though the appearance of a local Fermi liquid state at temperatures $T \ll T_K$ is not captured in this approximation [92]. In the multichannel case even the correct low temperature power law behavior is obtained in NCA [93]. However, in order to capture, e.g., the physics of the upper and the lower Hubbard bands in a DMFT description of the Hubbard model and the Mott-Hubbard metal-insulator transition, it is essential to consider the case of large but finite U . It is therefore desirable to develop a generalization of NCA to the case of finite Coulomb interaction. In the following we present a straightforward generalization of NCA, which conserves the symmetry of virtual transitions to the empty local level or doubly occupied local level states. This is essential for recovering the correct Kondo temperature T_K , as pointed out by Pruschke and Grewe [94] and, as will be shown, requires an infinite summation of a certain class of crossing diagrams [95]. We find that inclusion of only the first crossing term in this resummation [94], while contributing the larger part of the change of T_K , is not sufficient to provide a qualitatively correct Kondo temperature.

6.1 Pseudoparticle representation of the model

The model we consider describes a local impurity level (called d-level in the following), hybridizing with the conduction electron states. The energy E_d of the level may be located below or above the Fermi energy. Two electrons with spins \uparrow and \downarrow on the local level experience a Coulomb interaction U . The local states will be assumed to be created by pseudo-particle operators f_σ^\dagger (singly occupied state with spin σ), b^\dagger (empty state) and a^\dagger (doubly occupied state) acting on a vacuum state without any impurity. We choose f_σ to be fermion and a, b to be boson operators, where b will be called the “light” and a the “heavy” boson. The creation operator for the local physical electron can then be written as $d_\sigma^\dagger = f_\sigma^\dagger b + \sigma a^\dagger f_{-\sigma}$, where the pseudo-particle occupation

numbers must satisfy the operator constraint

$$Q = a^\dagger a + b^\dagger b + \sum_{\sigma} f_{\sigma}^\dagger f_{\sigma} = 1, \quad (6.1)$$

expressing the fact that at any instant of time the impurity is in exactly one charge state, empty, singly, or doubly occupied, respectively. The fermion operators $c_{\vec{k}\sigma}^\dagger$ create electrons in conduction electron states $|\vec{k}\sigma\rangle$ with energy ϵ_k . The Hamiltonian then takes the form

$$\begin{aligned} H = & \sum_{\vec{k},\sigma} \epsilon_{\vec{k}} c_{\vec{k}\sigma}^\dagger c_{\vec{k}\sigma} + E_d(2a^\dagger a + \sum_{\sigma} f_{\sigma}^\dagger f_{\sigma}) + \\ & + Ua^\dagger a + \sum_{\vec{k},\sigma} V(c_{\vec{k}\sigma}^\dagger b^\dagger f_{\sigma} + \sigma c_{\vec{k}\sigma}^\dagger f_{-\sigma}^\dagger a + h.c.), \end{aligned} \quad (6.2)$$

where V is the hybridization matrix element. For later use we define the conduction electron density of states at the Fermi energy as $\mathcal{N}(0)$ and the effective hybridization $\Gamma = \pi\mathcal{N}(0)V^2$.

6.2 Gauge Symmetry and Projection onto the Physical Hilbert Space

The model described by the auxiliary particle Hamiltonian (6.2) is invariant under simultaneous, local $U(1)$ gauge transformations, $f_{\sigma} \rightarrow f_{\sigma} e^{i\phi(t)}$, $b \rightarrow b e^{i\phi(t)}$, $a \rightarrow a e^{i\phi(t)}$, where $\phi(t)$ is an arbitrary, time-dependent phase. This gauge symmetry guarantees the conservation of the local charge Q in time. In order to project onto the physical subspace $Q = 1$, it is therefore sufficient to carry out the projection at time $t \rightarrow -\infty$, if the gauge symmetry is implemented exactly. One starts with the grandcanonical ensemble with respect to Q and the associated chemical potential $-\lambda$. The projection is achieved by taking the limit $\lambda \rightarrow \infty$ of any grandcanonical expectation value of a physical operator \hat{A} acting in the impurity Hilbert space

$$\langle \hat{A} \rangle = \lim_{\lambda \rightarrow \infty} \frac{\langle \hat{A} \rangle_G}{\langle \hat{Q} \rangle_G}. \quad (6.3)$$

Here the subscript G denotes the grandcanonical ensemble. The extra factor \hat{Q} in the denominator of Eq. (6.3) has been introduced to project out the $Q = 0$ subspace. Note that in the numerator this factor can be omitted, since any physical operator \hat{A} acting on the impurity states consists of powers of d_{σ}^\dagger , d_{σ} , which annihilate any state in the $Q = 0$ subspace, $d_{\sigma}^\dagger |Q = 0\rangle = 0$,

$d_\sigma|Q = 0\rangle = 0$. A detailed description of the projection procedure is given in Ref. [91]. Expectation values in the grandcanonical ensemble may be calculated straightforwardly in perturbation theory in the hybridization V , making use of Wick's theorem. The usual resummation techniques may be applied. Thus the imaginary time single particle Green's functions

$$G_{f\sigma}(\tau_1 - \tau_2) = -\langle \hat{T}[f_\sigma(\tau_1)f_\sigma^\dagger(\tau_2)] \rangle_G \quad (6.4)$$

and analogously for the two bosons a, b , may be expressed in terms of the self-energies $\Sigma_{f,b,c}(i\omega)$ as

$$\begin{aligned} G_{f\sigma}(i\omega) &= [i\omega - \lambda - E_d - \Sigma_f(i\omega)]^{-1} \\ G_b(i\omega) &= [i\omega - \lambda - \Sigma_b(i\omega)]^{-1} \\ G_a(i\omega) &= [i\omega - \lambda - 2E_d - U - \Sigma_a(i\omega)]^{-1}. \end{aligned} \quad (6.5)$$

The local conduction electron Green's function is given by

$$G_{c\sigma}(i\omega) = \left\{ \left[G_{c\sigma}^0(i\omega) \right]^{-1} - \Sigma_{c\sigma}(i\omega) \right\}^{-1} \quad (6.6)$$

with

$$G_{c\sigma}^0(i\omega) = \sum_{\vec{k}} G_{c\sigma}^0(\vec{k}, i\omega) = \sum_{\vec{k}} [i\omega - \epsilon_k]^{-1}. \quad (6.7)$$

The physical d-electron Green's function is proportional to the single-particle conduction electron t -matrix $t_{c\sigma}(i\omega)$, and is related to the grandcanonical (unprojected) $\Sigma_{c\sigma G}$ as

$$G_{d\sigma}(i\omega) = \frac{1}{V^2} t_{c\sigma}(i\omega) = \frac{1}{V^2} \lim_{\lambda \rightarrow \infty} e^{\beta\lambda} \Sigma_{c\sigma G}(i\omega, \lambda), \quad (6.8)$$

where β is the inverse temperature. The physical (projected onto the $Q = 1$ subspace) local conduction electron self-energy is then obtained from the t -matrix as

$$\Sigma_{c\sigma}(i\omega) = \frac{V^2 G_{d\sigma}(i\omega)}{1 + V^2 G_{c\sigma}^0(i\omega) G_{d\sigma}(i\omega)}. \quad (6.9)$$

6.3 Generating Functional

Gauge invariant approximations conserving the local charge Q may be derived from a Luttinger-Ward generating functional Φ . For a given approximation the functional Φ is defined by a sum of closed skeleton diagrams. The self-energies Σ_μ , $\mu = a, b, f, c$, are obtained by taking the functional derivatives

$$\Sigma_\mu = \frac{\delta\Phi}{\delta G_\mu}. \quad (6.10)$$

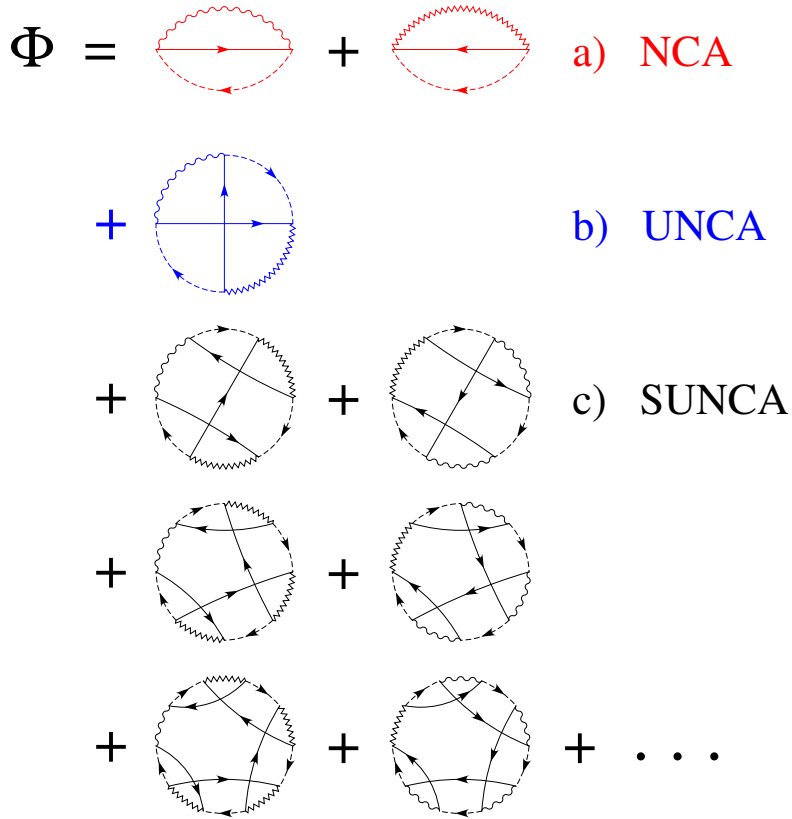


Figure 6.1: Diagrammatic representation of the generating functional to describe the Anderson impurity model at finite U . Throughout this paper, solid, dashed, wiggly and zig-zag lines correspond to conduction electron c , pseudo-fermion f , light boson b , and heavy boson a propagators, respectively. a) NCA including light and heavy boson lines. a)–b) Finite- U NCA (UNCA). This approximation amounts to renormalizing only one of the vertices in each of the self-energy diagrams of Fig. 6.3 and keeping only one (light or heavy boson) rung in the corresponding vertex function (see text). a)–c) Symmetrized finite- U NCA (SUNCA).

The “Non-crossing Approximation” (NCA) in the limit $U \rightarrow \infty$ is defined by the single lowest order diagram (2nd order in V) containing a light boson line (the first diagram of Fig. 1). In the limit of small hybridization element $V_{\vec{k}}$, it appears to be justified to keep only the lowest order contribution in V . However, as discussed in Refs. [92, 96, 97], the singular behavior of vertex functions may require to include these as well. This turns out to be necessary in the single channel model where the formation of a many-body resonance state is essential for recovering the Fermi liquid behavior, and less so in the multi-channel models. Including an infinite class of skeleton diagrams in Φ (in a “Conserving T-matrix Approximation” (CTMA)), which allows to capture a singular structure in the spin and charge excitation sectors, the low temperature Fermi liquid phase of the single channel Anderson model is recovered [92].

Here we are interested in constructing a simpler generalization of NCA to describe the case of finite U . It seems straightforward to define such an approximation on the NCA level by adding to the second order skeleton diagram for Φ containing the light boson (the first diagram in Fig. 1 a)) the corresponding diagram containing the heavy boson (the second diagram in Fig. 1 a)). This approximation and certain extensions motivated by perturbative arguments [94] or by a $1/N$ expansion (N being the spin degeneracy) [98] have been considered sometime ago. However, in the case of finite U NCA was found to fail badly: Not even the Kondo energy scale is recovered in the so-defined approximation. The reason for this failure is obvious: In the Kondo regime ($n_d \lesssim 1$) the local spin is coupled to the conduction electron spin density at the impurity through the antiferromagnetic exchange coupling

$$J = V^2 \left(-\frac{1}{E_d} + \frac{1}{E_d + U} \right). \quad (6.11)$$

The two terms on the r.h.s. of this relation arise from virtual transitions into the empty and doubly occupied local level, which e.g. contribute equally in the symmetric case $|E_d| = E_d + U$. The symmetric occurrence of these two virtual processes in all intermediate states is not included in the simple extension of NCA proposed above. Rather, the self-energy insertions in each of the two diagrams contain always only one of the processes, leading to an effective J which is only one half of the correct value. Correspondingly, the Kondo temperature $T_K \sim \exp[-1/(2\mathcal{N}(0)J)]$ comes out to scale as the square of the correct value, which can be orders of magnitude too small.

To correct this deficiency it is necessary to include additional diagrams, restoring the symmetry between the two virtual processes. As a first step one may add the next order skeleton diagram to Φ (Fig. 6.1 b)). As we will

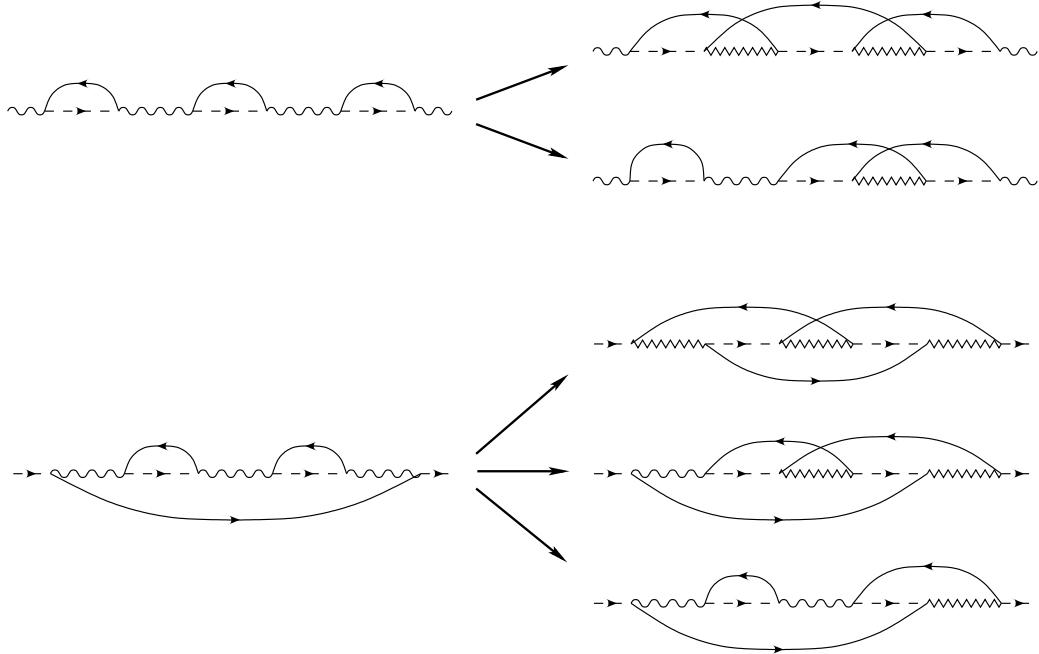


Figure 6.2: Two examples of how diagrams involving hybridization into the doubly occupied impurity state are generated from the bare noncrossing diagrams of the infinite U case by replacing light with heavy boson lines (see text).

show below, this approximation, later referred to as UNCA, helps to recover a large part of the correct behavior of T_K [94]. However, as seen from the preceding discussion, for a completely symmetric treatment of empty and doubly occupied intermediate states one must first consider the diagrams of bare perturbation theory instead of skeleton diagrams. A symmetric class of diagrams is generated by replacing a light boson line with a heavy boson line in each of the bare (non-skeleton) diagrams comprising the NCA, and vice versa (An example is shown in Fig. 6.2). Each replacement leads to a crossing of conduction electron lines spanning one fermion and at most two boson lines. A conserving approximation is then constructed by substituting renormalized propagators for the bare ones and keeping only skeleton diagrams. The resulting generating functional Φ is shown diagrammatically in Fig. 6.1 a)–c). These diagrams look similar to the CTMA diagrams mentioned above, but contain one light boson line and an arbitrary number of heavy boson lines, or vice versa. Diagrams with, for example, two light boson lines and an arbitrary number of heavy boson lines (and conduction electron lines spanning at most one fermion line) are reducible and do not appear. We will call the approximation defined by the generating functional given by the sum of the diagrams of Fig 6.1 “Symmetrized finite- U NCA” (SUNCA).

$$\begin{aligned}
 \Sigma_b &= \text{Diagram 1} + \text{Diagram 2} - \text{Diagram 3} \\
 \Sigma_a &= \text{Diagram 1} + \text{Diagram 2} - \text{Diagram 3} \\
 \Sigma_f &= \text{Diagram 1} + \text{Diagram 2} - 2 \text{Diagram 3} \\
 V^2 G_d &= \text{Diagram 1} + \text{Diagram 2} - 2 \text{Diagram 3}
 \end{aligned}$$

Figure 6.3: Diagrammatic representation of the auxiliary particle self-energies of SUNCA in terms of the renormalized hybridization vertices, defined in Fig. 6.4. In each line the third diagram is subtracted in order to avoid double counting of terms within the first two diagrams.

The above approximation corresponding to the CTMA at $U \rightarrow \infty$, termed “Symmetrized finite- U Conserving T-matrix Approximation” (SUCTMA) is thus defined in a natural way by summing up all skeleton Φ diagrams containing a single closed ring of auxiliary particle propagators with an arbitrary number of light or heavy boson lines, dressed by conduction electron lines spanning only one fermion line. Thus, the SUCTMA is defined by adding to the diagrams of the SUNCA the CTMA diagrams with (only) light boson lines or (only) heavy boson lines. The SUCTMA equations have not yet been evaluated.

6.4 Results of SUNCA

As discussed above, the self-energies Σ_μ are obtained by functional differentiation of the generating functional with respect to the Green’s functions G_μ . The functional Φ defined by Fig. 6.1 leads to an infinite series of diagrams for Σ_α , which may be conveniently presented in terms of three-point vertex functions (the filled semicircles with three legs: one boson and two fermion lines), see Fig. 6.3. It is necessary to subtract a diagram of 4th order in V in each case to avoid double counting. On the level of SUNCA and SUCTMA the vertex functions consist of ladder summations, with light or heavy boson lines as rungs, and are defined diagrammatically in Fig. 6.4. Note that keeping only a single light or heavy boson rung in these vertex

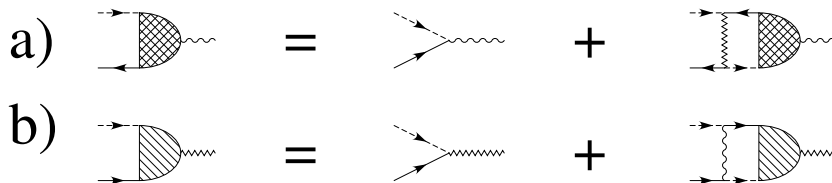


Figure 6.4: Diagrammatic representation of the Bethe–Salpeter equations for a) the renormalized light boson (empty impurity) and b) the renormalized heavy boson (doubly occupied impurity) vertex, as generated by the SUNCA Luttinger–Ward functional (Fig. 1).

functions corresponds to UNCA.

The expressions for the self-energies Σ_μ defined by Figs. 6.3 and 6.4, together with the definition of the Green’s functions, Eqs. (6.5), constitute a set of nonlinear integral equations for $\Sigma_\mu(\omega)$, $\mu = a, b, f$. The local conduction electron self-energy Σ_c does not appear in any internal Green’s functions because it contains at least one auxiliary particle loop, i.e. carries a factor $\exp(-\beta\lambda)$ and thus vanishes due to the exact projection onto the physical Hilbert space ($\lambda \rightarrow \infty$) [91]. G_d and therefore Σ_c may be calculated at the end via Eqs. (6.8), (6.9) by using the self-consistently determined G_α , $\alpha = a, b, f$. The SUNCA equations are given explicitly in appendix A. Although these equations are more involved than the regular NCA, they are numerically considerably more easily tractable than the CTMA equations [92, 96, 97], since SUNCA contains only renormalized three-point vertices (see Fig. 6.3) as compared to four-point vertex functions occurring in CTMA [92]. We solved the SUNCA equations numerically in the real frequency representation, i.e. after analytic continuation from Matsubara frequencies ω_n to the real frequency axis.

As a first important characteristic feature of the pseudo-particles we note that the single-particle excitation spectrum is powerlaw divergent, $G_\mu(\omega) \sim \omega^{-\alpha_\mu}$, $\mu = a, b, f$ reflecting the abundance of low energy excitations forced by the constraint. At finite temperature T these singularities are cut off at the scale $\omega \sim T$. As observed in earlier work [92, 99, 100, 101], the values of the exponents α_μ are characteristic of the state of the system. In the single channel case, when the ground state is a local Fermi liquid, the exponents may be inferred from the Friedel sum rule relating the scattering phase shifts $\eta_{\mu,\sigma}$ to the number of electrons bound to the impurity in each channel $\Delta n_{\mu,\sigma} = \eta_{\mu\sigma}/\pi$. The exponents α_μ in turn are related to the $\eta_{\mu,\sigma}$ by the general result first derived for the x-ray edge singularities [102], $\alpha_\mu = 1 - \sum_\sigma (\eta_{\mu\sigma}/\pi)^2$. This is so, since e.g. the heavy boson Green’s function, describing the transition amplitude for a doubly occupied impurity to be created at time $t = 0$ and

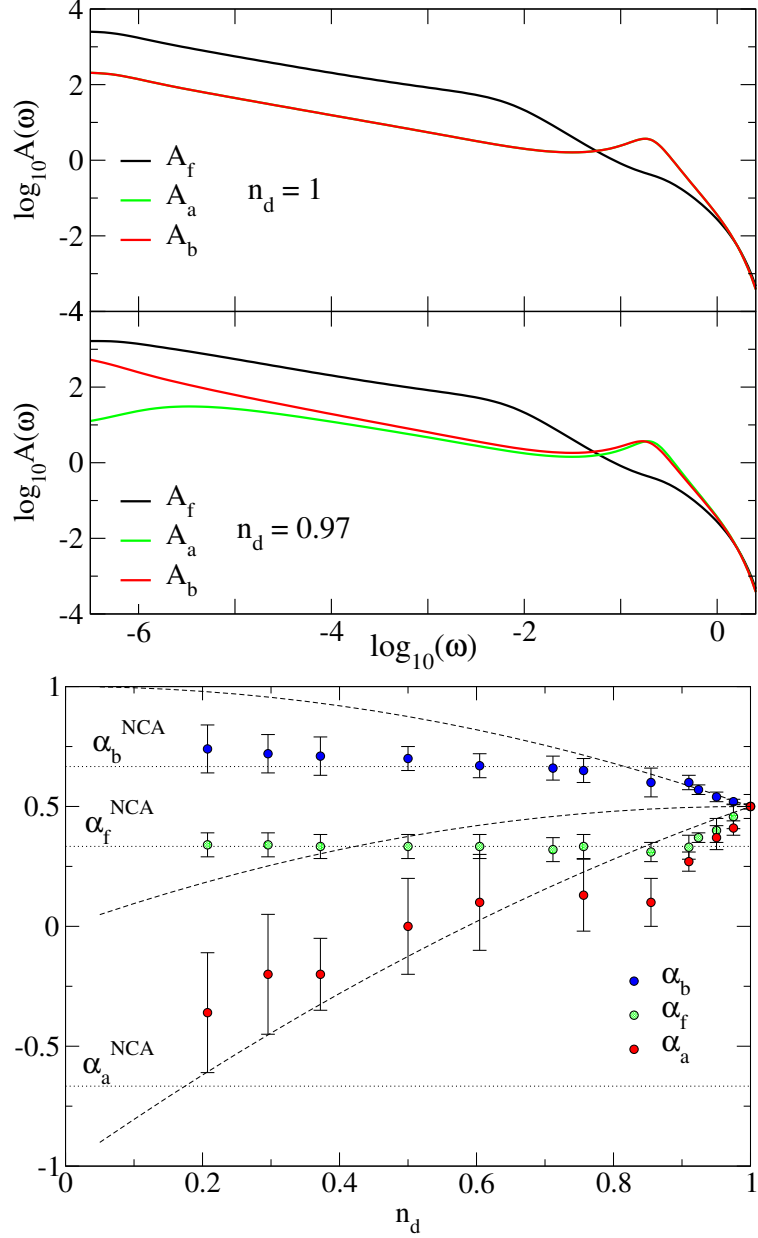


Figure 6.5: Upper panel: Log-log plots of pseudo-fermion (A_f), heavy (A_a) and light (A_b) slave boson spectral functions in the Kondo regime. The singular divergence below T_K is clearly visible in the plot. Lower panel: Infrared threshold exponents of the auxiliary particle spectral functions in dependence of the impurity occupation n_d , for fixed values of Γ and U and varying E_d . Dashed curved lines: exact results (Eq. (12)); horizontal lines: NCA results; data points with error bars: SUNCA results. In the Kondo limit ($n_d \rightarrow 1$) the exact exponents are recovered, while in the mixed valence and empty impurity regime the SUNCA results for α_f and α_b cross over to the NCA values.

removed at a later time is proportional to the overlap of the free Fermi sea of conduction electrons with the ground state of the Anderson model. The change in the occupation of the local level due to the hybridization with the conduction band $\Delta n_{\mu\sigma}$ is the difference between the $t = 0$ initial impurity occupation $n_{\mu\sigma}(t = 0)$ (without hybridization) and the occupation in the ground state of the Anderson impurity model $n_{d\sigma} = n_d/2$, i.e. it depends on the initial conditions of the different Green's functions G_μ , $\mu = a, b, f$. Thus we have $\Delta n_{a,\sigma} = \frac{2-n_d}{2}$, $\Delta n_{f,\sigma} = \delta_{\sigma,\sigma_0} - \frac{1}{2}n_d$ (where σ_0 is the spin of the fermion in the Green's function $G_{f\sigma_0}$), and $\Delta n_{b,\sigma} = -\frac{n_d}{2}$. The infrared threshold exponents of $G_\mu(\omega)$ are therefore given by

$$\begin{aligned}\alpha_a &= -1 + 2n_d - \frac{n_d^2}{2} \\ \alpha_b &= 1 - \frac{n_d^2}{2} \\ \alpha_f &= n_d - \frac{n_d^2}{2}.\end{aligned}\tag{6.12}$$

In Fig. 6.5 we show the exponents α_μ for different n_d , as obtained from a numerical solution of the SUNCA equations. Also shown is the exact result given by Eq. (6.12) (dashed lines), and the analytical result that can be extracted analytically from the NCA equations (defined by the first two diagrams in Fig. 1) in analogy to Ref. [103]. The numerical results of SUNCA (data points) are seen to approach the exact result in the limit $n_d \rightarrow 1$, but in the case of α_b and α_f appear to follow the NCA result rather than the exact result for $n_d \leq 0.8$. The results for the exponent α_a trace the exact behavior in reasonable agreement. Clearly the SUNCA does much better than the simple NCA. From our experience [92] with the Anderson model in the limit $U \rightarrow \infty$, we expect that the correct exponents should be recovered in SUCTMA.

We now turn to the d-electron spectral function $A_d(\omega) = \frac{1}{\pi}\text{Im}G_d(\omega - i0)$. Fig. 6.6 shows the results for $A_d(\omega)$ for the symmetric Anderson model in the Kondo regime ($n_d \approx 1$) at a very low temperature of $T \simeq 10^{-2}T_K$. Shown are the results obtained from the simple NCA (diagrams of first line in Fig. 1), the perturbatively corrected version UNCA (including the diagram in the second line of Fig. 1) and the full SUNCA. The inset shows that the width of the Kondo resonance peak, which is a measure of T_K , comes out orders of magnitude different in the three approximations. In order to compare the numerical results with the exact expression for T_K ,

$$T_K = \min\left\{\frac{1}{2\pi}U\sqrt{I}, \sqrt{D\Gamma}\right\}e^{-\pi/I}\tag{6.13}$$

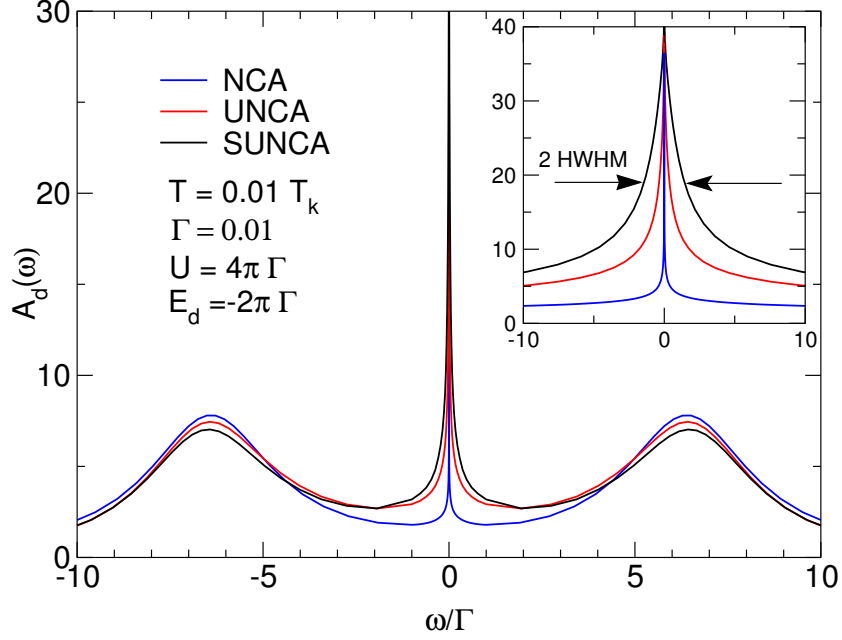


Figure 6.6: Local electron spectral function calculated using NCA, UNCA, and SUNCA. The Kondo temperature is determined as the HWHM of the Kondo peak (see inset). It is seen that in NCA the Kondo peak width comes out orders of magnitude too low.

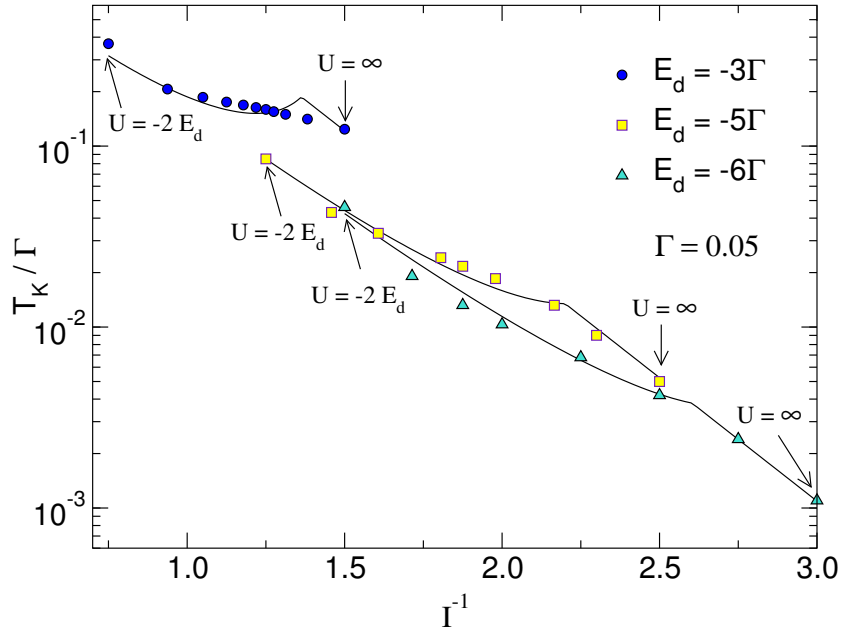


Figure 6.7: Kondo Temperature for various parameters E_d , U and fixed Γ . Solid lines represent the exact results, Eqs. (13), (14). Data points are the SUNCA results determined from the width of the Kondo peak in the d-electron spectral function.

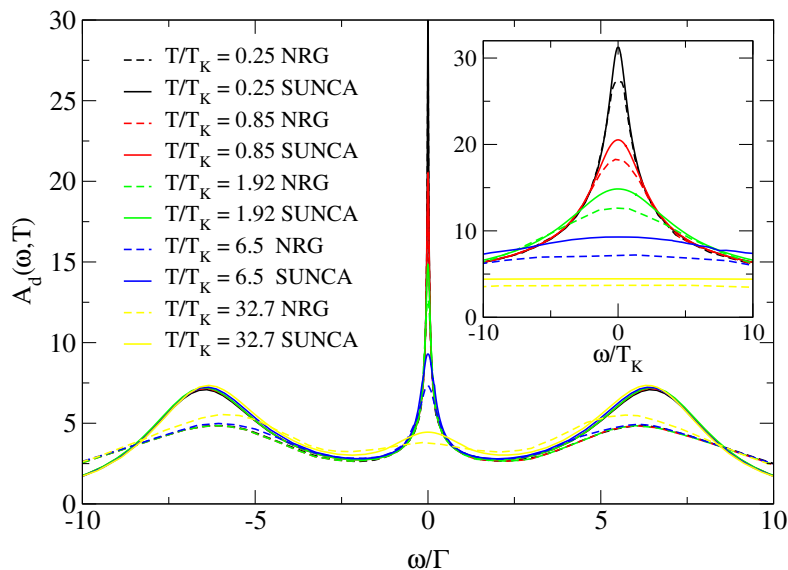


Figure 6.8: Comparison between SUNCA and NRG impurity spectral function for various temperatures. The NRG method is essentially exact in the low-energy region while SUNCA slightly overestimates the zero frequency value of the Abrikosov-Suhl resonance. However, the width of the peak (i.e. the Kondo temperature) is correct within SUNCA. The high frequency discrepancy (around E_d and $E_d + U$) is due to the fact that NRG does not resolve high-energy structure very accurately.

where

$$I = 2 \left[\frac{\Gamma}{|E_d|} + \frac{\Gamma}{E_d + U} \right], \quad (6.14)$$

we determine T_K as the half width of the Kondo resonance at half maximum (HWHM).

In Fig. 6.7 the results for T_K/Γ obtained in this way for a fixed value of $\Gamma = 0.05$ (in units of D) and several values of E_d/Γ , as a function of $I(U/\Gamma)$ (data points) are compared with the exact values Eqs. (6.13), (6.13) (solid lines). The agreement is excellent, demonstrating that the SUNCA provides the correct scale T_K for a wide range of parameters E_d and U .

*CHAPTER 6. ANDERSON IMPURITY MODEL AT FINITE
COULOMB INTERACTION U : GENERALIZED NCA*

Chapter 7

Conclusions

In first five chapters we described in detail the recently introduced Extended dynamical mean field theory (EDMFT) [6, 8] and explained its assumptions and limitations. We solved the EDMFT equations for the paramagnetic metallic state of t - J model within a Non-crossing approximation and calculated various thermodynamic quantities, transport and single-particle response functions. The results are compared to the Exact diagonalization (ED) results for small 2D system of 20 sites.

Last chapter introduces novel method to describe Anderson impurity model at finite on-site repulsion U arising in DMFT studies of the Hubbard and related lattice models.

The EDMFT is an extension of very successful Dynamical mean field theory (DMFT) which, however, takes full account of only local quantum fluctuations but fails to capture the dynamical effects of intersite interactions, in either the charge channel (e.g., nearest-neighbor repulsion) or spin channel (exchange). The EDMFT, on the other hand, treats the inter-site quantum fluctuations on the same footing with local ones. This is particularly important in case of the $t - J$ model where the exchange coupling J competes with the kinetic term t . For the correct description of the model, it is crucial to preserve the symmetry between both terms, and take into account the dynamical effect of the non-local exchange fluctuations as well.

To keep the symmetry between the local and non-local term of the $t - J$ model, EDMFT reduces the correlated lattice to a self-consistent impurity problem, where the local moment is coupled to both fermionic and bosonic bath. The fermionic bath gives rise to a Kondo interaction that tends to quench the local moments whereas the bosonic bath mimics the RKKY interaction that promotes local-moment ordering. For large doping, where Kondo screening prevails, the low-energy properties can be explained within a Fermi-liquid picture. In the opposite limit of RKKY domination, a pseudogap opens

in one particle spectra which determines the properties of the metal in the vicinity of the Mott-Hubbard transition. The conventional $d \rightarrow \infty$ metal-insulator transition with diverging effective mass is thus crucially modified here. The region, where both interactions are about equally important, is characterized by the largest low temperature entropy and largest scattering rate at the chemical potential. This point ($\delta \sim 15\%$) corresponds to optimum doping in cuprates.

The most serious limitation of EDMFT is that it mainly freezes spatial fluctuations so that the single particle self-energy and irreducible spin cumulant are momentum independent. However, this weakness of the method might not be crucial to explain many anomalous properties of strongly correlated systems. Indeed, as proposed by Varma *et al.* [10], the normal state properties of cuprates can be well explained by momentum independent self-energy of marginal Fermi liquid type. The assumptions of EDMFT might therefore be justified by the success of the marginal Fermi liquid theory.

To investigate the novel effective impurity model, corresponding to an Anderson impurity problem with an additional self-consistent bosonic bath, we employed the diagrammatic theory for quantum impurities with strong on-site repulsion. The method is based on auxiliary particle technique, where Wick's theorem is valid, which offers straightforward generalization of existing approximations to the model considered here. A Luttinger-Ward functional for a conserving approximation was proposed in section 4.3, based on the so-called Non-Crossing Approximation for Anderson impurity model.

The simplest conserving approximation, which neglects all crossing diagrams but keeps symmetry between Kondo and RKKY interaction, was numerically evaluated and used to study various physical properties of the $t - J$ model within EDMFT. The lowest order approximation does not work down to zero temperature. In the Fermi-liquid regime it is known to work down to $T \gtrsim 0.2 \varepsilon^*$, where ε^* is the characteristic energy scale of the metal and is equal to J for doping around 25%. In the opposite limit of low doping, the method also suffers from the absence of the vertex corrections and is limited to temperatures higher than $T \sim 0.2J$.

The thermodynamic properties of the $t - J$ model were obtained from the free-energy of the lattice system that can be expressed by the free-energy of the impurity model, single-particle Green's functions and spin susceptibility alone. As a function of doping, the entropy shows a rather broad maximum at the hole density of 15%, corresponding to optimum doping in cuprates. The degeneracy temperature, associated with the release of the entropy, is relatively small $T_{deg} < J$. The chemical potential increases with increasing temperature in the underdoped regime while it decreases with temperature in the overdoped regime. The point, where μ is temperature independent co-

incides with the point of maximal entropy and characterizes optimum doping. It is important to stress that the excellent agreement is found between the exact diagonalization and EDMFT results for all temperatures and all dopings considered.

The Mott insulating gap of the half-filled $t - J$ model is slowly destroyed with adding holes to the system but a remnant of the gap persists up to the overdoped regime. The non-Fermi liquid state with a large pseudogap of order J is found in the underdoped region of the $t - J$ model. A small shoulder with weight 2δ appears above the chemical potential and approaches the Fermi energy with doping. In the overdoped regime, it finally merges with the Hubbard sideband and a broad quasiparticle peak emerges above the chemical potential. For doping $\delta \gtrsim 24\%$, $t - J$ model is found to be a Fermi-liquid with a characteristic energy scale ε^* of order J . In this region, RKKY interaction becomes unimportant and therefore the impurity model is equivalent to the usual Anderson impurity model with a well defined Kondo temperature ε^* that monotonically increases with doping.

The EDMFT results for the t - J model suggest that the Luttinger theorem is not satisfied for doping below 20%. The deviation from the Luttinger volume is quite pronounced at low doping and seems to support a simple rigid picture of doping the Mott insulator as proposed already by Hubbard: at half filling, the chemical potential is between the Hubbard bands and the effect of doping is that the chemical potential gradually cuts into the top of the lower Hubbard band. The Fermi surface is hole-like and centered around (π, π) for underdoped and optimum doped case, while it is electron-like for the overdoped system.

The change of the Fermi surface from hole-like to electron-like is closely related to the change of sign of the Hall coefficient from positive to negative occurring for doping slightly above the optimum doping. The Hall number diverges as $1/(e_0\delta)$ close to the Mott-Hubbard transition consistent with the simple semiclassical picture of doping with independent hole carriers and in agreement with experiments on cuprates. For low doping system, the Hall number is found to monotonically decrease with increasing temperature again in agreement with experiments.

In chapter 6 we have proposed a conserving scheme to describe the Anderson impurity model at finite on-site repulsion U within the auxiliary particle method. In order to incorporate the correct value of the spin exchange coupling J into the theory and, hence, to obtain the correct size of the low-energy scale T_K , it is necessary to treat fluctuation processes into the empty and into the doubly occupied intermediate state on equal footing at the level of bare perturbation theory. The simplest Luttinger–Ward functional which is completely symmetric in this respect consists of an infinite series of skeleton

diagrams, corresponding to ladder-type vertex renormalizations in the self-energies. Although considerably more involved than the regular NCA, this approximation, termed “symmetrized finite- U NCA” (SUNCA), is numerically tractable on a typical workstation. We find that SUNCA recovers the correct Kondo temperature over a wide range of the parameters of the Anderson model E_d , U , and Γ , while simplified approximations (NCA, UNCA) produce a low-energy scale typically orders of magnitude smaller than the exact value. This result is especially relevant for a correct description of the low temperature properties of strongly correlated lattice models by a diagrammatic many-body technique, since in the limit of infinite dimensions these models reduce to a selfconsistent, finite- U single-impurity problem. Applications of the present theory to such models are currently in progress.

In conclusion, in this work we have applied the Extended dynamical mean field theory to the $t - J$ model. Single-particle spectra, thermodynamic and transport properties were calculated and compared to the Exact diagonalization results. Our results show that several anomalous properties of cuprates are captured in the $t - J$ model and simple local EDMFT theory.

Appendix A

Weiss fields

The lattice self-energy and irreducible spin cumulant become local quantities in the limit of large dimensions as has been shown in chapter 3. The lattice Green's function and spin susceptibility can therefore be written as

$$G_{\mathbf{k}} = 1/(\xi - \varepsilon_{\mathbf{k}}) \quad \xi = \omega + \mu - \Sigma(\omega) \quad (\text{A.1})$$

$$\chi_{\mathbf{q}} = 1/(\zeta + J_{\mathbf{q}}) \quad \zeta = M^{-1}. \quad (\text{A.2})$$

It is then straightforward to check the following identities for the Green's function

$$\sum_{\mathbf{k}} \varepsilon_{\mathbf{k}} G_{\mathbf{k}} = \sum_{\mathbf{k}} \frac{\varepsilon_{\mathbf{k}} - \xi + \xi}{\xi - \varepsilon_{\mathbf{k}}} = -1 + \xi \sum_{\mathbf{k}} G_{\mathbf{k}} = -1 + \xi G_{oo} \quad (\text{A.3})$$

$$\sum_{\mathbf{k}} \varepsilon_{\mathbf{k}}^2 G_{\mathbf{k}} = \sum_{\mathbf{k}} \frac{\varepsilon_{\mathbf{k}}(\varepsilon_{\mathbf{k}} - \xi) + \varepsilon_{\mathbf{k}}\xi}{\xi - \varepsilon_{\mathbf{k}}} = \xi \sum_{\mathbf{k}} \frac{\varepsilon_{\mathbf{k}}}{\xi - \varepsilon_{\mathbf{k}}} = -\xi + \xi^2 G_{oo} \quad (\text{A.4})$$

as well as the corresponding relations for the susceptibility

$$\sum_{\mathbf{q}} J_{\mathbf{q}} \chi_{\mathbf{q}} = 1 - \zeta \chi_{oo} \quad (\text{A.5})$$

$$\sum_{\mathbf{q}} J_{\mathbf{q}}^2 \chi_{\mathbf{q}} = -\zeta + \zeta^2 \chi_{oo}. \quad (\text{A.6})$$

The expressions (2.13) and (3.10) for the Weiss fields can be greatly simplified using the above relations

$$\begin{aligned} \mathcal{G}_0^{-1} &= \omega + \mu - \sum_{ij} t_{io} t_{oj} \left(G_{ij} - \frac{G_{io} G_{oj}}{G_{oo}} \right) = \\ &= \omega + \mu - \left(\sum_{\mathbf{k}} \varepsilon_{\mathbf{k}}^2 G_{\mathbf{k}} - \frac{(\sum_{\mathbf{k}} \varepsilon_{\mathbf{k}} G_{\mathbf{k}})^2}{G_{oo}} \right) = \Sigma + G_{oo}^{-1} \end{aligned} \quad (\text{A.7})$$

$$\begin{aligned} \chi_0^{-1} &= \sum_{ij} J_{io} J_{oj} \left(\chi_{ij} - \frac{\chi_{io} \chi_{oj}}{\chi_{oo}} \right) = \\ &\left(\sum_{\mathbf{q}} J_{\mathbf{q}}^2 \chi_{\mathbf{q}} - \frac{\left(\sum_{\mathbf{q}} J_{\mathbf{q}} \chi_{\mathbf{q}} \right)^2}{\chi_{oo}} \right) = M^{-1} - \chi_{oo}^{-1} \end{aligned} \quad (\text{A.8})$$

Appendix B

Equation of motion

All local correlation functions can be obtained from the local action (3.8) alone. Once Luttinger-Ward functional for a particular approximation is written down, one should be able to identify diagrams for any one or two particle correlation function, particularly local Green's function and local magnetic susceptibility. The objective of this appendix is to show that local Green's function is proportional to the grand-canonical conduction electron self-energy, which is built out of diagrams obtained by cutting a single conduction electron line in Luttinger-Ward functional. Similarly, local susceptibility is proportional to the grand-canonical boson self-energy that consists of diagrams obtained by cutting single boson line in the same Luttinger-Ward functional.

The conduction electron Green's function is defined as

$$G_k(\tau - \tau') = - \left\langle T_\tau c_{k\sigma}(\tau) c_{k\sigma}^\dagger(\tau') \right\rangle, \quad (\text{B.1})$$

where $c_{k\sigma}$ destroys a conduction electron with momentum k and spin σ .

The time development of any operator is governed by its commutator with Hamiltonian

$$\begin{aligned} \frac{\partial}{\partial \tau} c_{k\sigma} &= [H, c_{k\sigma}] = -\varepsilon_k c_{k\sigma} - V c_{o\sigma} \\ \frac{\partial}{\partial \tau} c_{k\sigma}^\dagger &= [H, c_{k\sigma}^\dagger] = \varepsilon_k c_{k\sigma}^\dagger + V c_{o\sigma}^\dagger, \end{aligned} \quad (\text{B.2})$$

where H is the full impurity Hamiltonian (3.12). Time derivative of the conduction electron Green's function then follows

$$- \left(\frac{\partial}{\partial \tau} + \varepsilon_k \right) G_k(\tau - \tau') = \delta(\tau - \tau') + V G_{ok}(\tau - \tau') \quad (\text{B.3})$$

APPENDIX B. EQUATION OF MOTION

and G_{ok} is proportional to the amplitude for the conduction electron with momentum k and spin σ to be created at time τ' and destroyed at the impurity at time τ

$$G_{ok}(\tau - \tau') = - \left\langle T_\tau c_{o\sigma}(\tau) c_{k\sigma}^\dagger(\tau') \right\rangle. \quad (\text{B.4})$$

The time derivative of latter Green's function is proportional to the local Green's function

$$\left(\frac{\partial}{\partial \tau'} - \varepsilon_k \right) G_{ok}(\tau - \tau') = V G_{oo}(\tau - \tau') \quad (\text{B.5})$$

The corresponding equations for the free particle propagators are

$$\begin{aligned} - \left(\frac{\partial}{\partial \tau} + \varepsilon_k \right) g_k(\tau - \tau') &= \delta(\tau - \tau') \\ \left(\frac{\partial}{\partial \tau'} - \varepsilon_k \right) g_k(\tau - \tau') &= \delta(\tau - \tau'). \end{aligned} \quad (\text{B.6})$$

Combining these equation together, the exact relation between local and conduction-electron Green's function is obtained

$$G_k(\imath\omega) = g_k(\imath\omega) + g_k(\imath\omega) V G_{oo}(\imath\omega) V g_k(\imath\omega). \quad (\text{B.7})$$

The equation (B.7) is valid for the grand-canonical ensemble as well as for the canonical (i.e. physical $Q = 1$) subspace. Once the local Green's function is known, the physical ($Q = 1$) conduction electron Green's function can be obtained. The relation (B.7) is even more important in the grand-canonical ensemble. In the $Q = 0$ subspace (i.e. without impurity) G_{oo} vanishes, therefore $G_{oo} = \mathcal{O}(e^{-\beta\lambda})$. The grand-canonical conduction electron Green's function is thus $G_k = g_k + \mathcal{O}(e^{-\beta\lambda})$ and comparison of Eq. (B.7) with the Dyson equation

$$G_k(\imath\omega) = g_k(\imath\omega) + g_k(\imath\omega) \Sigma_k^c(\imath\omega) G_k(\imath\omega) \quad (\text{B.8})$$

assures that the local Green's function is proportional to the conduction electron self-energy, since both vanish in the $Q = 0$ subspace and are thus of the order $\mathcal{O}(e^{-\beta\lambda})$

$$G_{oo}(\imath\omega) = \frac{1}{V^2} \Sigma_k^c(\imath\omega). \quad (\text{B.9})$$

In the case of k independent hopping matrix elements $V_k = V$, grand canonical conduction-electron self-energy $\Sigma_k^c(\imath\omega)$ is also k independent and can be denoted just by Σ_c . The equation (B.9) is important, since it establishes

the relationship between the local physical ($Q = 1$) spectral function and Luttinger-Ward functional for a chosen approximation. The self-energy diagrams for any type of particle is obtained just by cutting the corresponding propagators in the Luttinger-Ward functional ($\Sigma = \delta\Phi/\delta G$), whereas it is much less trivial to draw the right diagrams for any other correlation function and keep the approximation conserving.

There exists a certain symmetry between boson and fermion bath in the Eq. (3.12). In the case of fermions, impurity creation operator $c_{o\sigma}$ is coupled to the bath, while in the boson case, the impurity spin \vec{S}_o couples to the free vector bosonic bath. It is therefore not surprising that the spin susceptibility is just proportional to the grand canonical boson self-energy.

The time derivative of the bosonic operators is obtained by their commutator with the impurity Hamiltonian (3.12)

$$\frac{\partial}{\partial\tau}\Phi_q^\alpha = [H, \Phi_q^\alpha] = -w_q\Phi_q^\alpha - g S_f^\alpha \quad (\text{B.10})$$

$$\frac{\partial}{\partial\tau}\Phi_q^{\alpha\dagger} = [H, \Phi_q^{\alpha\dagger}] = w_q\Phi_q^{\alpha\dagger} + g S_f^\alpha \quad (\text{B.11})$$

The boson Green's function can be defined by

$$G_{\Phi_q^\alpha}(\tau - \tau') = -\left\langle T_\tau \vec{\Phi}_q^\alpha(\tau) \vec{\Phi}_q^\alpha(\tau') \right\rangle \quad (\text{B.12})$$

and its time derivative is

$$-\left(\frac{\partial}{\partial\tau} + w_q\right) G_{\Phi_q^\alpha}(\tau - \tau') = \delta(\tau - \tau') + g G_{S^\alpha\Phi_q^\alpha}(\tau - \tau'). \quad (\text{B.13})$$

The obtained correlation function $G_{S^\alpha\Phi_q^\alpha}$ takes the form

$$G_{S^\alpha\Phi_q^\alpha}(\tau - \tau') = -\left\langle T_\tau \vec{S}^\alpha(\tau) \vec{\Phi}_q^\alpha(\tau') \right\rangle \quad (\text{B.14})$$

and its time derivative with respect to τ' is finally proportional to the local susceptibility

$$\left(\frac{\partial}{\partial\tau'} - w_q\right) G_{S^\alpha\Phi_q^\alpha}(\tau - \tau') = -g \chi_{oo}^{\alpha\alpha}(\tau - \tau'). \quad (\text{B.15})$$

Non-interacting ($Q = 0$ subspace) Green's functions obey the following equation of motion

$$\begin{aligned} -\left(\frac{\partial}{\partial\tau} + w_q\right)g_{\Phi_q^\alpha}(\tau - \tau') &= \delta(\tau - \tau') \\ \left(\frac{\partial}{\partial\tau'} - w_q\right)g_{\Phi_q^\alpha}(\tau - \tau') &= \delta(\tau - \tau') \end{aligned} \quad (\text{B.16})$$

APPENDIX B. EQUATION OF MOTION

Combining (B.13), (B.15) and (B.16) and using the Fourier representation, a closed relation between boson Green's function and local impurity susceptibility is obtained

$$G_{\Phi_q^\alpha}(i\omega) = g_{\Phi_q^\alpha}(i\omega) - g^2 g_{\Phi_q^\alpha}(i\omega) \chi_{oo}^{\alpha\alpha}(i\omega) g_{\Phi_q^\alpha}(i\omega). \quad (\text{B.17})$$

The last relation can be compared to the Dyson equation for bosons in the bath

$$G_{\Phi_q^\alpha}(i\omega) = g_{\Phi_q^\alpha}(i\omega) + g_{\Phi_q^\alpha}(i\omega) \Sigma_\Phi(i\omega) G_{\Phi_q^\alpha}(i\omega). \quad (\text{B.18})$$

In the grand canonical ensemble $\Sigma_\Phi = \mathcal{O}(e^{-\beta\lambda})$ and $G_{\Phi_q^\alpha} = g_{\Phi_q^\alpha} + \mathcal{O}(e^{-\beta\lambda})$, finally after projecting onto the physical subspace ($\lambda \rightarrow \infty$) the important relation is obtained

$$\chi_{oo}^{\alpha\alpha}(i\omega) = -\frac{1}{g^2} \Sigma_\Phi(i\omega). \quad (\text{B.19})$$

Appendix C

Derivation of NCA equations

For pedagogical reasons, a detailed derivation of the NCA equations together with the projection on to the physical subspace will be presented here.

$$\Sigma_f = \text{diagram 1} + \text{diagram 2}$$

Figure C.1: Pseudo-fermion self-energy within NCA.

Consider first the left diagram in Fig. C.1. Following the standard diagrammatic rules for evaluating Feynman diagrams at finite temperature we get for the pseudo-fermion self-energy

$$\Sigma_{fs}(i\omega) = -\frac{V^2}{\beta} \sum_{i\omega'} G_{cs}(i\omega') G_b(i\omega - i\omega') = -V^2 \oint \frac{dz}{2\pi i} f(-z) G_{cs}(z) G_b(i\omega - z)$$

In summation over Matsubara frequencies, the Fermi function with minus sign $f(-z)$ was chosen. As it will be shown below, this choice guarantees that only integral over conduction electron branch-cut survives after the projection onto the physical subspace. Alternatively, if $f(z)$ is taken instead of $f(-z)$, both integrals (over conduction electron branch-cut and pseudo-boson branch-cut) would give a nonzero contribution after the projection onto the physical subspace. The sum of both terms naturally gives identical result. Hence, we will take $f(-z)$ and consider only the integral over conduction electron branch-cut for the moment. Later, we will show that the other contribution vanishes after the projection onto the physical subspace.

For the first term we get

$$\Sigma_{fs}(i\omega) = -V^2 \int \frac{d\xi}{\pi} f(-\xi) \text{Im} G_{cs}(\xi) G_b(i\omega - \xi).$$

The analytic continuation to real frequencies is trivial in this case: it is done by replacing $i\omega$ with $\omega + i\delta$ at all places

$$\Sigma_{fs}(\omega + i\delta) = \int d\xi f(-\xi) A_{cs}(\xi) G_b(\omega - \xi + i\delta). \quad (\text{C.1})$$

The projection onto the physical subspace is somewhat more tedious. A term was added to the original Hamiltonian $+\lambda Q$, which pushes all structure of the auxiliary Green's functions and auxiliary self-energies to infinity when λ goes to infinity. In another words, the eigenvalues of $H + \lambda Q$ scale to infinity as λQ . It is therefore convenient to redefine arguments of the auxiliary quantities such that the structure will appear around zero. Hence, the transformation of frequencies in arguments of the auxiliary functions is performed $\omega \rightarrow \omega + \lambda$ and after that λ is assumed to go to infinity. After the projection, the pseudo-fermion and pseudo-boson Green's functions become

$$G_f(i\omega) = \frac{1}{i\omega + \mu - \Sigma_f(i\omega)}$$

$$G_b(i\omega) = \frac{1}{i\omega - \Sigma_b(i\omega)}.$$

This should be compare with the original definitions in Fig. 4.1. Note that the conduction electron and vector boson Green's functions do not contain λ and are not changed with the projection. This is because the operator number Q counts only auxiliary particles.

In the Eq. (C.1) only ω has to be transformed, but not ξ , since the conduction electron quantities do not involve λ . It is then clear, that the equation (C.1) remains unchanged after the projection.

On the other hand, the integral over the pseudo-boson branch-cut, that was omitted above, is proportional to $e^{-\beta\lambda}$ and vanishes in the physical subspace. To show that, let us write the self-energy contribution explicitly

$$\Sigma'_{fs}(i\omega) = -V^2 \int \frac{d\xi}{\pi} f(\xi - i\omega) (-1) \text{Im} G_b(\xi) G_{cs}(i\omega - \xi).$$

Now, both variables ω and ξ must be transformed, so that the structure of Σ'_f and G_b is shifted to zero. The Bose function is then replaced by $e^{-\beta(\lambda+\xi)}$ and

λ is limited to infinity. The result is then proportional to $e^{-\beta\lambda}$ and vanishes

$$\begin{aligned}\Sigma'_{fs}(\omega + i\delta) &= -V^2 \int \frac{d\xi}{\pi} n(\xi) \text{Im} G_b(\xi) G_{cs}(\omega - \xi + i\delta) = \\ &= -e^{-\beta\lambda} V^2 \int \frac{d\xi}{\pi} e^{-\beta\xi} \text{Im} G_b(\xi) G_{cs}(\omega - \xi + i\delta).\end{aligned}$$

The pseudo-fermion self-energy contribution depicted on the right in Fig. C.1 reduces to

$$\begin{aligned}\Sigma_{fs}(i\omega) &= -\frac{1}{4}g^2 \sum_{s',\alpha} \sigma_{ss'}^\alpha \sigma_{s's}^\alpha \frac{1}{\beta} \sum_{i\Omega} G_{\Phi^\alpha}(i\Omega) G_{fs'}(i\omega + i\Omega) = \\ &= -\frac{1}{4}g^2 \sum_{s',\alpha} \sigma_{ss'}^\alpha \sigma_{s's}^\alpha \oint \frac{dz}{2\pi i} n(z) G_{\Phi^\alpha}(z) G_{fs'}(z + i\omega) = \\ &= -\frac{1}{4}g^2 \sum_{s',\alpha} \sigma_{ss'}^\alpha \sigma_{s's}^\alpha \int \frac{d\xi}{\pi} n(\xi) \text{Im} G_{\Phi^\alpha}(\xi) G_{fs'}(\xi + i\omega).\end{aligned}$$

The integration was performed only around the Φ boson branch-cut. The other contribution, coming from the loop around pseudo-fermion branch-cut again vanishes after the projection. The analytic continuation is straightforward and gives

$$\Sigma_{fs}(\omega + i\delta) = \frac{1}{4} \int d\xi n(\xi) D_\Phi(\xi) [G_{fs}(\omega + \xi + i\delta) + 2G_{f\bar{s}}(\omega + \xi + i\delta)]. \quad (\text{C.2})$$

As before, the projection does not alter this term, since only ω is transformed, while ξ is left unchanged. Finally, the pseudo-fermion self-energy within NCA is equal to the sum of both diagrams given by Eq. (C.1) and (C.2).

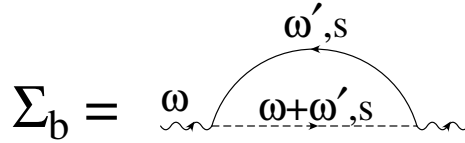


Figure C.2: pseudo-boson self-energy within NCA.

Using standard diagrammatic rules, one obtains for the pseudo-boson self-energy diagram depicted in Fig. C.2 the following expression

$$\Sigma_b(i\omega) = \frac{V^2}{\beta} \sum_{s,\omega'} G_{cs}(i\omega') G_{fs}(i\omega + i\omega') = -V^2 \sum_s \oint \frac{dz}{2\pi i} f(z) G_{cs}(z) G_{fs}(z + i\omega).$$

APPENDIX C. DERIVATION OF NCA EQUATIONS

As discussed above, only the integral around conduction electron branch-cut contributes to the auxiliary self-energies and gives

$$\Sigma_b(i\omega) = -V^2 \sum_s \int \frac{d\xi}{\pi} f(\xi) \text{Im} G_{cs}(\xi) G_{fs}(\xi + i\omega),$$

with analytic continuation to the real frequency

$$\Sigma_b(\omega + i\delta) = \sum_s \int d\xi f(\xi) A_{cs}(\xi) G_{fs}(\omega + \xi + i\delta). \quad (\text{C.3})$$

Again, the projection does not change the expression since only ω has to be transformed while ξ remains unchanged. The Eq. (C.3) is thus the final and only contribution to the pseudo-boson self-energy within NCA.

All physical quantities that vanish in the $Q = 0$ subspace, like the local Green's function or local susceptibility, are proportional to the $e^{-\beta\lambda}$, since in that case the relation (4.12) can be equivalently written as

$$\langle A \rangle = \lim_{\lambda \rightarrow \infty} \frac{\langle A \rangle_G}{\langle Q \rangle_G}. \quad (\text{C.4})$$

The grand-canonical expectation value of the number operator is

$$\langle Q \rangle_G = \int [f(\omega) \sum_s A_{fs}(\omega) + n(\omega) A_b(\omega)] d\omega.$$

In the limit $\lambda \rightarrow \infty$ this expression is simplified to

$$\langle Q \rangle_G = e^{-\beta\lambda} \int e^{-\beta\omega} [\sum_s A_{fs}(\omega) + A_b(\omega)] d\omega.$$

Furthermore, the frequency scale of the auxiliary particles can be conveniently chosen such that the

$$\int e^{-\beta\omega} [\sum_s A_{fs}(\omega) + A_b(\omega)] d\omega = 1 \quad (\text{C.5})$$

and therefore the expectation value of any physical operator that vanish in the $Q = 0$ subspace is

$$\langle A \rangle = \lim_{\lambda \rightarrow \infty} e^{\beta\lambda} \langle A \rangle_G. \quad (\text{C.6})$$

The conduction electron self-energy sketched in Fig. C.3 is

$$\begin{aligned} \Sigma_{cs}(i\omega) &= -\frac{V^2}{\beta} \sum_{i\omega'} G_{fs}(i\omega + i\omega') G_b(i\omega') = -V^2 \oint \frac{dz}{2\pi i} n(z) G_{fs}(z + i\omega) G_b(z) = \\ &= -V^2 \int \frac{d\xi}{\pi} [n(\xi) G_{fs}(\xi + i\omega) \text{Im} G_b(\xi) + n(\xi - i\omega) \text{Im} G_{fs}(\xi) G_b(\xi - i\omega)] \end{aligned}$$

$$\Sigma_{\mathbf{c}} = \begin{array}{c} \omega' \\ \text{wavy line} \\ \omega, s \text{ --- } \omega + \omega', s \end{array} \quad \Sigma_{\Phi}^{\alpha} = \begin{array}{c} \omega + \omega', s' \\ \text{dashed loop} \\ \omega \text{ --- } \omega', s \end{array}$$

Figure C.3: Local Green's function (conduction electron self-energy) and local susceptibility (boson self-energy) within NCA.

Here, we have integrated over both branch-cuts since they are equally important and carry a factor $e^{-\beta\lambda}$. The analytic continuation introduces in this case both, retarded and advanced Green's functions

$$\Sigma_{c_s}(\omega + i\delta) = -V^2 \int \frac{d\xi}{\pi} [n(\xi)G_{f_s}(\xi + \omega + i\delta) \text{Im} G_b(\xi) - f(\xi) \text{Im} G_{f_s}(\xi)G_b(\xi - \omega - i\delta)].$$

The projection transforms only ξ and leaves ω unchanged, hence the self-energy is proportional to $e^{-\beta\lambda}$ and reads

$$\Sigma_{c_s}(\omega + i\delta) = -e^{-\beta\lambda} V^2 \int \frac{d\xi}{\pi} e^{-\beta\xi} [G_{f_s}(\xi + \omega + i\delta) \text{Im} G_b(\xi) - \text{Im} G_{f_s}(\xi)G_b(\xi - \omega - i\delta)]$$

with the imaginary part equal to

$$\text{Im} \Sigma_{c_s}(\omega + i\delta) = -e^{-\beta\lambda} V^2 \pi \int d\xi e^{-\beta\xi} [A_{f_s}(\xi + \omega)A_b(\xi) + A_{f_s}(\xi)A_b(\xi - \omega)].$$

Finally, the grand-canonical (not yet fully projected) local Green's function is obtained just by dividing this expression by V^2 , as one can see from Eq. (B.9). However, the projection is still not finished in this case. It follows from Eq. (C.6), that in order to get physical spectral function, calculated only within the subspace $Q = 1$, we need to multiply the grand-canonical spectral function by $e^{\beta\lambda}$. Thus the local Green's function calculated within NCA is

$$\text{Im} G_{s_{oo}} = -\frac{\pi}{f(-\omega)} \int d\xi e^{-\beta\xi} A_{f_s}(\xi + \omega)A_b(\xi). \quad (\text{C.7})$$

Finally, we would like to obtain the expression for local magnetic susceptibility. The derivation closely follows the above derivation of local Green's function. Instead of conduction electron self-energy, the Φ boson self-energy

is required first

$$\begin{aligned}
 \Sigma_{\Phi z}(\omega) &= \frac{1}{4}g^2 \sum_{ss'} \sigma_{ss'}^z \sigma_{s's}^z \frac{1}{\beta} \sum_{\omega'} G_{f_s}(\omega') G_{f_{s'}}(\omega' + \omega) = \\
 &= -\frac{1}{4}g^2 \sum_s \oint \frac{dz}{2\pi i} f(z) G_{f_s}(z) G_{f_s}(z + \omega) = \\
 &= -\frac{1}{4}g^2 \sum_s \int \frac{d\xi}{\pi} [f(\xi) \text{Im} G_{f_s}(\xi) G_{f_s}(\xi + \omega) + \\
 &\quad f(\xi - \omega) G_{f_s}(\xi - \omega) \text{Im} G_{f_s}(\xi)].
 \end{aligned}$$

After the analytic continuation to the real frequency the self-energy reads

$$\Sigma_{\Phi z}(\omega + i\delta) = -\frac{1}{4}g^2 \sum_s \int \frac{d\xi}{\pi} f(\xi) \text{Im} G_{f_s}(\xi) [G_{f_s}(\xi + \omega + i\delta) + G_{f_s}(\xi - \omega - i\delta)].$$

The imaginary part can be further simplified

$$\text{Im} \Sigma_{\Phi z}(\omega + i\delta) = -e^{-\beta\lambda} \frac{\pi}{4} g^2 \sum_s \int d\xi e^{-\beta\xi} (e^{\beta\omega} - 1) A_{f_s}(\xi - \omega) A_{f_s}(\xi).$$

Projecting onto the physical subspace and taking into account Eq. (B.19) and (C.6), we finally obtain

$$\text{Im} \chi_{oo}(\omega + i\delta) = \frac{\pi}{4n(\omega)} \sum_s \int d\xi e^{-\beta\xi} A_{f_s}(\xi - \omega) A_{f_s}(\xi)$$

Appendix D

Friedel sum rule

The Luttinger theorem, or equivalently, the Friedel sum rule [104] for system of interacting fermions was first derived by Langer and Ambegaokar [105]. If well defined quasy-particles exist in the system that bear a one-to-one correspondence with a non-interacting problem, in our case a system of free electrons, the low energy and long wavelength exciations as well as the correlation and the response functions follow the same universal laws. The system is a Fermi liquid. Alternatively, in the language of perturbation theory, the systems has to vary in a continuous way when the interaction increases from zero to its actual value. It is thus possible to obtain the exact solution perturbing the system of non-interacting electrons. This solution can be formally represented with the exact Luttinger-Ward functional $\Phi(G)$ [48], which contains all possible vacuum skeleton diagrams build out of only exact Green's functions G . The functional derivative of Φ with respect to G yields the exact self-energy

$$\Sigma_{\alpha}(i\omega) = \frac{\delta\Phi}{\delta G_{\alpha}(i\omega)}. \quad (\text{D.1})$$

We may also write

$$\delta\Phi = \sum_{\alpha, i\omega} \Sigma_{\alpha}(i\omega) \delta G_{\alpha}(i\omega), \quad (\text{D.2})$$

where δG represents any displacement of the exact Green's function from its equilibrium value. Let us consider a particular transformation, where Green's functions are shifted for a small amount $\delta\lambda$

$$\delta G_{\alpha}(i\omega) = G_{\alpha}(i\omega + \delta\lambda) - G_{\alpha}(i\omega) = \frac{\partial G_{\alpha}(i\omega)}{\partial i\omega} \delta\lambda. \quad (\text{D.3})$$

APPENDIX D. FRIEDEL SUM RULE

The change in Φ induced by this change in G is zero since the functional is invariant under a frequency shifts

$$\delta\Phi = 0 = \delta\lambda \sum_{\alpha, \omega} \Sigma_{\alpha}(\omega) \frac{\partial G_{\alpha}(\omega)}{\partial \omega}. \quad (\text{D.4})$$

In passing to the limit $T \rightarrow 0$, we can simply make the replacement [106]

$$\frac{1}{\beta} \sum_{\omega} \rightarrow \int_{-\infty}^{\infty} \frac{dz}{2\pi i} \quad (\text{D.5})$$

since the separation between different ω values is $2\pi i/\beta$. The integration path is thus in the vertical direction in contrast to the usual integration along the real axis. However, a great deal of care has to be taken in using D.5 if the integrand has double or multiple poles on the path of integration. Integrating by parts Eq. (D.4), the Luttinger theorem is readily obtained

$$-\sum_{\alpha} \int_{-\infty}^{\infty} \frac{dz}{2\pi i} \Sigma_{\alpha}(z) \frac{\partial G_{\alpha}(z)}{\partial z} = \sum_{\alpha} \int_{-\infty}^{\infty} \frac{dz}{2\pi i} G_{\alpha}(z) \frac{\partial \Sigma_{\alpha}(z)}{\partial z} = 0. \quad (\text{D.6})$$

The integration can also be done along the real axis. To embrace the same simple poles than above, we need to close the contour to the left (integrating from $-\infty$ above the real axis to 0 and back to $-\infty$ below the real axis, corresponding to $f(\xi, T \rightarrow 0)$) or to the right (corresponding to $f(-\xi, T \rightarrow 0)$). As usually, a term $e^{-z\tau}$ with small $\tau \rightarrow 0^-$ is assumed to be added to the integral which requires closing the contour to the left

$$\int_{-\infty}^{\infty} \frac{dz}{2\pi i} g(z) e^{z0^+} = \int_{-\infty}^0 \frac{d\xi}{2\pi i} (g(\xi + i\delta) - g(\xi - i\delta)). \quad (\text{D.7})$$

The same Luttinger theorem on the real axis thus reads

$$\text{Im} \sum_{\alpha} \int_{-\infty}^0 \frac{d\omega}{\pi} G_{\alpha}(\omega + i\delta) \frac{\partial \Sigma_{\alpha}(\omega + i\delta)}{\partial \omega} = 0. \quad (\text{D.8})$$

Next, we would like to relate the average occupation number with the value of the quasiparticle peak at the Fermi energy at zero temperature. For that purpose we may write the occupation number as

$$n = \sum_{\alpha} G_{\alpha}(\tau = 0^-) = \frac{1}{\beta} \sum_{\alpha, \omega} G_{\alpha}(\omega) e^{i\omega 0^+}, \quad (\text{D.9})$$

where α is a spin variable in the impurity case or complete set of states $\{\mathbf{k}, \sigma\}$ in the lattice case.

Using the Dyson equation, the Green's function becomes

$$G_\alpha(i\omega) = \frac{1}{i\omega + \mu - \Lambda_\alpha(i\omega) - \Sigma_\alpha(i\omega)}, \quad (\text{D.10})$$

where we have separated the self-energy into proper (Σ) and improper (Λ) part. The latter comes from the noninteracting problem (when interaction is not yet present) and does not vanish at zero temperature and zero frequency. In the impurity case, the improper part is just the exact self-energy for the case $U = 0$ (i.e. the self-energy for the system we perturb on).

It is easy to see from the definition of the Green's function D.10 that the following equation holds

$$\frac{\partial}{\partial z} (G^{-1}(z) + \Lambda(z) + \Sigma(z)) = 1. \quad (\text{D.11})$$

Evaluating the derivative in D.11 and multiplying by G , we get

$$\begin{aligned} G(z) &= G(z) \left(-\frac{1}{G^2(z)} \frac{\partial G(z)}{\partial z} + \frac{\partial \Lambda(z)}{\partial z} + \frac{\partial \Sigma(z)}{\partial z} \right) \\ &= -\frac{\partial}{\partial z} \ln G(z) + G(z) \frac{\partial \Lambda(z)}{\partial z} + G(z) \frac{\partial \Sigma(z)}{\partial z} \end{aligned} \quad (\text{D.12})$$

Inserting the form D.12 for the Green's function into D.9 and changing the summation over Matsubara frequencies into the integral over the real axis, we obtain

$$n = \text{Im} \sum_\alpha \int \frac{d\xi}{\pi} f(\xi) \left[\frac{\partial}{\partial \xi} \ln G_\alpha(\xi) - G_\alpha(\xi) \frac{\partial \Lambda_\alpha}{\partial \xi} - G_\alpha(\xi) \frac{\partial \Sigma_\alpha}{\partial \xi} \right] \quad (\text{D.13})$$

In the zero temperature limit the last term vanishes due to the Luttinger theorem, while the first term can be evaluated exactly

$$\text{Im} \int_{-\infty}^0 \frac{d\xi}{\pi} \frac{\partial}{\partial \xi} \ln G_\alpha(\xi) = \frac{1}{\pi} \text{Im} \ln G_\alpha(\xi) \Big|_{-\infty}^0 = \frac{1}{\pi} \arg(G_\alpha(0)) - 1. \quad (\text{D.14})$$

We have used the fact that imaginary part of the Green's function drops exponentially while the real part decays much slower, usually as $1/\omega$.

The second term in Eq. (D.13) is usually zero in the impurity problem, since Λ is taken to be a constant or very slowly varying function up to cut-off being usually much larger than any other scale in the system. However, DMFT imposes self-consistency condition on Λ and therefore it becomes quite rapidly varying function of frequency. In general, it is composed of Hubbard bands (incoherent part) and also very pronounced quasiparticle

peak (coherent contribution), which is responsible for the large derivative $\partial\Lambda/\partial\xi$ on the chemical potential. The second term cannot be neglected in general and has to be incorporated in the generalized Friedel sum-rule

$$n_c = -\text{Im} \sum_{\alpha} \int_{-\infty}^0 \frac{d\xi}{\pi} G_{\alpha}(\xi) \frac{\partial\Lambda_{\alpha}}{\partial\xi} \quad (\text{D.15})$$

This term is connected with the change of the charge in the conduction band as a consequence of introducing an impurity in the system of free fermions. Using the identity $\arctan(1/x) = \pi/2 - \arctan(x)$, the generalized Friedel sum-rule can be written in its usual form

$$n - n_c = \sum_{\alpha} \left\{ \frac{1}{2} - \frac{1}{\pi} \arctan \left(\frac{\text{Re} G_{\alpha}(0)}{\text{Im} G_{\alpha}(0)} \right) \right\}. \quad (\text{D.16})$$

Until now, the derivation was completely general and holds for any system in equilibrium that bears a one-to-one correspondence with a system of free electrons. For a translational invariant system trace is assumed over a complete set of states from very beginning (Eq. D.2), so that for a lattice model, sum over all possible wave vectors $k = \{\mathbf{k}, \sigma\}$ must be performed in Eq. (D.16). The improper part of the self-energy Λ is zero in this case and therefore the Luttinger theorem reads

$$n = \sum_k \left\{ \frac{1}{2} - \frac{1}{\pi} \arctan \left(\frac{\text{Re} G_k(0)}{\text{Im} G_k(0)} \right) \right\} \quad (\text{D.17})$$

or equivalently

$$n = \sum_k \left\{ \frac{1}{2} - \frac{1}{\pi} \arctan \left(\frac{\mu - \varepsilon_k - \text{Re} \Sigma_k(0)}{\text{Im} \Sigma_k(0)} \right) \right\}. \quad (\text{D.18})$$

Since the imaginary part of the self-energy goes to zero at the chemical potential and zero temperature the Eq. (D.18) can be further simplified to

$$n = \sum_k \Theta(\mu - \varepsilon_k - \text{Re} \Sigma_k(0)). \quad (\text{D.19})$$

Thus, the volume enclosed by the Fermi surface is not changed with the interaction, while the shape is changed if the self-energy is \mathbf{k} dependent. In the case of local self-energy, the shape is also preserved and the effective chemical potential $\mu - \text{Re} \Sigma(0) = \mu_0$ is equal to the noninteracting chemical potential corresponding to the same filling.

Now, we would like to invert the Eq. (D.16) and calculate the Green's function at the chemical potential knowing the change of the occupation. This can be easily done in the impurity case, where it takes the form

$$\frac{\text{Im } G(0)}{\text{Re } G(0)} = \tan\left(\frac{\pi}{2}(n - n_c)\right). \quad (\text{D.20})$$

Here we have assumed that the spin symmetry breaking does not occur, so that $G_{\uparrow} = G_{\downarrow}$.

Local (impurity) Green's function at the chemical potential can also be expressed in terms of the self-energy

$$\begin{aligned} \text{Im } G(0) &= \frac{\text{Im } \Lambda(0)}{[\text{Re}(\mu - \Sigma(0) - \Lambda(0))]^2 + [\text{Im } \Lambda(0)]^2} \\ \text{Re } G(0) &= \frac{\text{Re}(\mu - \Sigma(0) - \Lambda(0))}{[\text{Re}(\mu - \Sigma(0) - \Lambda(0))]^2 + [\text{Im } \Lambda(0)]^2}, \end{aligned} \quad (\text{D.21})$$

where we have assumed that $\text{Im } \Sigma(0) = 0$. Inserting D.21 into D.20, we get

$$\frac{\text{Im } \Lambda(0)}{\text{Re}(\mu - \Sigma(0) - \Lambda(0))} = \tan\left(\frac{\pi}{2}(n - n_c)\right). \quad (\text{D.22})$$

Finally, the imaginary part of the Green's function can be reduced to

$$\text{Im } G(0) = \frac{\text{Im } \Lambda(0)}{[\text{Im } \Lambda(0)]^2 (1 + \tan^{-2}(\frac{\pi}{2}(n - n_c)))} = \frac{\sin^2(\frac{\pi}{2}(n - n_c))}{\text{Im } \Lambda(0)}. \quad (\text{D.23})$$

Hence, the value of the impurity Green's at the chemical potential and zero temperature is entirely determined by the change in number of electrons due to the introduction of the impurity $n - n_c$ and the hybridization matrix elements $\text{Im } \Lambda(\omega) = -\pi \sum_k |V_k|^2 \delta(\omega - \varepsilon_k)$.

Appendix E

Density of states

It is convenient to replace the momentum sum by an energy integration where possible. In many calculations within EDMFT, the density of states $D(\varepsilon)$ is sufficient. However, to study transport properties, one needs to define additional functions like $\Phi_{xx}(\varepsilon)$ and $\Phi_{xy}(\varepsilon)$, given by

$$D(\varepsilon) = \frac{1}{N} \sum_{\mathbf{k}} \delta(\varepsilon - \varepsilon_{\mathbf{k}}) \quad (\text{E.1})$$

$$\Phi_{xx}(\varepsilon) = \frac{1}{N} \sum_{\mathbf{k}} (2t)^2 \sin^2(k_x) \delta(\varepsilon - \varepsilon_{\mathbf{k}}) \quad (\text{E.2})$$

$$\Phi_{xy}(\varepsilon) = \frac{1}{N} \sum_{\mathbf{k}} (2t)^3 \sin^2(k_x) \cos(k_y) \delta(\varepsilon - \varepsilon_{\mathbf{k}}). \quad (\text{E.3})$$

For the two dimensional square lattice, those densities can be expressed by elementary functions as follows

$$D(x) = \frac{1}{2t\pi^2} \frac{1}{|x|} K(1 - 1/x^2) \quad (\text{E.4})$$

$$\Phi_{xx}(x) = \frac{2t}{\pi^2} [2|x|E(1 - 1/x^2) + 2K(1 - 1/x^2) - 2\Pi(1 - 1/|x|, 1 - 1/x^2)]$$

$$\Phi_{xy}(x) = 2 \left(\frac{2t}{\pi} \right)^2 (x^2 E(1 - 1/x^2) - K(1 - 1/x^2)) \text{Sign}(x). \quad (\text{E.5})$$

Here, $K(x)$, $E(x)$ and $\Pi(x)$ are complete elliptic integrals of first, second and third kind and $x = \varepsilon/(4t)$.

Appendix F

Internal and free energy

The internal energy of lattice system can quite generally be calculated from the Green's functions alone [47]. It is easy to see this by considering the following commutator

$$\sum_k c_k^\dagger [V, c_k], \quad (\text{F.1})$$

where c_k represent the complete set of states and V is the interaction part of the Hamiltonian. For most two particle interactions, like Coulomb interaction or magnetic exchange interaction, this commutator is equal to $-2V$. Note that in the case of interaction between electrons and phonons the commutator is equal to $-V$.

This commutator can also be calculated for the non-interacting part of the Hamiltonian H_0 and in the case of the tight-binding $H_0 = \sum_k (\varepsilon_{\mathbf{k}} - \mu) n_k$ explicitly read

$$\sum_k c_k^\dagger [H_0, c_k] = -H_0 = -\sum_k (\varepsilon_{\mathbf{k}} - \mu) n_k = -\sum_k (\varepsilon_{\mathbf{k}} - \mu) G_k(\tau \rightarrow 0^-) \quad (\text{F.2})$$

On the other hand, the time derivative of the Green's function involves commutator with a full Hamiltonian

$$\left(\frac{\partial G_k(\tau)}{\partial \tau} \right)_{\tau \rightarrow 0^-} = \left\langle c_k^\dagger [H, c_k] \right\rangle. \quad (\text{F.3})$$

Combining equations (F.1), (F.2) and (F.3) we readily obtain

$$\begin{aligned} \langle -2V \rangle &= \sum_k \left\langle c_k^\dagger [H - H_0, c_k] \right\rangle = \sum_k \left[\left(\frac{\partial}{\partial \tau} + \varepsilon_{\mathbf{k}} - \mu \right) G_k(\tau) \right]_{\tau \rightarrow 0^-} = \\ &= \frac{1}{\beta} \sum_{k, \nu\omega} (-\nu\omega + \varepsilon_{\mathbf{k}} - \mu) G_k(\nu\omega) e^{\nu\omega 0^+}. \end{aligned} \quad (\text{F.4})$$

Thus, the average of the potential energy is given by

$$\langle V \rangle = \frac{1}{2\beta} \sum_{k, i\omega} (i\omega + \mu - \varepsilon_{\mathbf{k}}) G_k(i\omega) e^{i\omega 0^+}. \quad (\text{F.5})$$

For the tight binding H_0 , the kinetic energy part is

$$\langle H_0 \rangle = \frac{1}{\beta} \sum_{k, i\omega} (\varepsilon_{\mathbf{k}} - \mu) G_k(i\omega) e^{i\omega 0^+}, \quad (\text{F.6})$$

which can be combined with (F.5) to yield the internal energy

$$E = \langle H \rangle + \mu N = \frac{1}{2\beta} \sum_{k, i\omega} (i\omega + \varepsilon_{\mathbf{k}} + \mu) G_k(i\omega) e^{i\omega 0^+}. \quad (\text{F.7})$$

Within a local theory like EDMFT, the free energy of the lattice system can be obtained from the free energy of the corresponding impurity problem and the local Green's functions (fermionic and bosonic) alone. The proof usually considers free-energy as a functional of Green's functions and involves Luttinger-Ward potential. The main idea is that the interactions considered in a dynamical mean field theory are only those defined within the unit cell. Diagrammatically, DMFT retains only local diagrams, i.e., those whose internal propagators and vertices just connect points within the same unit cell, therefore the Luttinger-Ward potential is local. In other words, the Luttinger-Ward potential is common for both lattice and impurity problem and can thus be eliminated.

The situation is not so simple in the context of the EDMFT because some long range vertices are retained in this theory. Not only that the Luttinger-Ward functional is not local, it even doesn't exist at least not in the picture we have presented earlier. It does exist before taking the infinite d limit, the momentum dependent diagrams are then of leading order for the two particle vertex function while they are subleading in the context of self-energy.

An alternative derivation of EDMFT equations is possible, where bosonic fields that maintain nonlocal interaction, are introduced before the limit of large dimensions is taken. In this case, two essential steps (i.e. large d limit and Hubbard-Stratonovich transformation) needed to obtain EDMFT equations are interchanged. The advantage of this procedure is that the lattice model with bosons more closely resembles the impurity model. After the limit of large d is taken, only the local component of self-energies survives. But in this case, boson Green's function, which is naturally momentum dependent, replaces the two particle vertex in Fig. F.1. The same approximation is Φ -derivable in this picture and is completely local so that the Luttinger-Ward functional is common to both the lattice and impurity model.

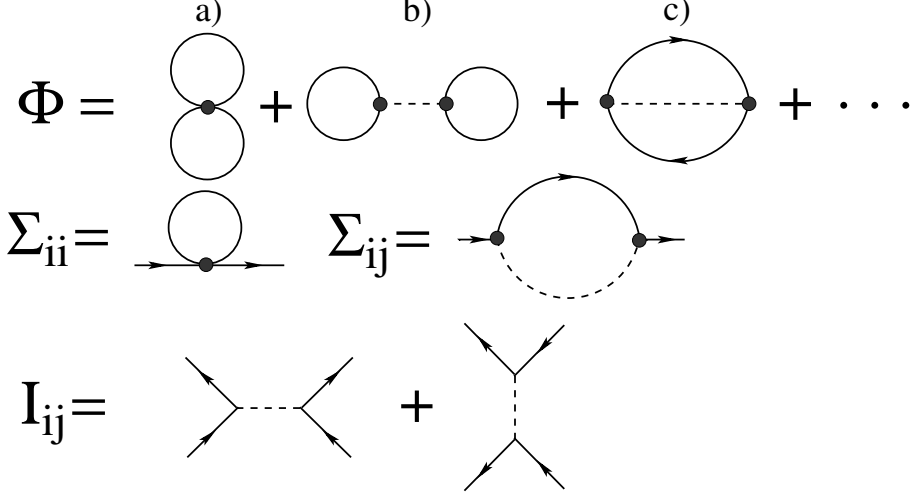


Figure F.1: The Luttinger-Ward functional Φ for EDMFT before taking the limit of large z is shown in the first line. The first term (a) is the local on-site part while the second (b) and the third (c) terms correspond to Hartree and Fock non-local contributions, respectively. The local self-energy Σ_{ii} is then of leading order within EDMFT, the Hartree self-energy is exactly zero (not shown) and the Fock term Σ_{ij} is subleading. The non-local part of the irreducible two-particle vertex I_{ij} , coming from the Hartree and Fock term, is of leading order.

Replacing the non-local interaction J_{ij} in the action (3.3) by the Hubbard-Stratonovich fields Φ , we obtain

$$S = \int_0^\beta d\tau \left[\sum_{i,\sigma} c_{i\sigma}^\dagger(\tau) \left(\frac{\partial}{\partial \tau} - \mu \right) c_{i\sigma}(\tau) - \sum_{ij,\sigma} t_{ij} c_{i\sigma}^\dagger(\tau) c_{j\sigma}(\tau) + \sum_i U n_{i\uparrow}(\tau) n_{i\downarrow}(\tau) + \sum_{\mathbf{q}} w_{\mathbf{q}} \Phi_{\mathbf{q}}^\dagger(\tau) \Phi_{\mathbf{q}}(\tau) + g \sum_i \mathbf{S}_i(\tau) (\Phi_i^\dagger(\tau) + \Phi_i(\tau)) \right],$$

where the boson free-particle energy $w_{\mathbf{q}} = -2g^2/J_{\mathbf{q}}$.

Boson Green's function $\mathcal{D}_{\mathbf{q}\alpha}$ is closely related to the spin susceptibility, i.e.,

$$\mathcal{D}_{\mathbf{q}\alpha} = \mathcal{D}_{\mathbf{q}\alpha}^0 - \mathcal{D}_{\mathbf{q}\alpha}^0 g \chi_{\mathbf{q}}^{\alpha\alpha} g \mathcal{D}_{\mathbf{q}\alpha}^0. \quad (\text{F.8})$$

Here, $\mathcal{D}_{\mathbf{q}\alpha}^0$ is noninteracting boson Green's function for instantaneous interaction, which in our case reads $\mathcal{D}_{\mathbf{q}}^0 = J_{\mathbf{q}}/g^2$. A diagrammatic representation of the above equation is shown in Fig. F.2, where shaded ellipse represents the spin susceptibility $\chi_{\mathbf{q}}^{\alpha\alpha}$.

Using the Dyson equation $\Pi_{\mathbf{q}} = \mathcal{D}_{\mathbf{q}}^0{}^{-1} - \mathcal{D}_{\mathbf{q}}^{-1}$, we can express boson self

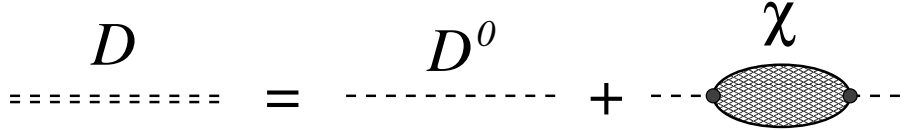


Figure F.2: Diagrammatic representation of Eq. (F.8). The double and single dashed lines represent fully dressed (\mathcal{D}_q) and noninteracting (\mathcal{D}_q^0) boson Green's functions, respectively. Shaded ellipse is spin spin susceptibility and small black circle is vertex g .

energy in terms of spin susceptibility

$$\Pi_q = -\frac{g^2}{\chi_q^{-1} - J_q}, \quad (\text{F.9})$$

where q is compact notations for $\{\mathbf{q}, \alpha\}$. Inserting the form of the noninteracting propagator \mathcal{D}_q^0 into Eq. (F.8), we also get

$$\mathcal{D}_q = \frac{1}{g^2} J_q \chi_q (\chi_q^{-1} - J_q), \quad (\text{F.10})$$

therefore the product of self-energy and Green's function is just

$$\Pi_q \mathcal{D}_q = -J_q \chi_q. \quad (\text{F.11})$$

In the limit of large dimensions, boson self-energy becomes a local quantity $\Pi_q = \Pi_{ii}$. From Eq. (F.9) we can see that the irreducible spin cumulant M_q , defined by

$$\chi_q = \frac{1}{M_q^{-1} + J_q}$$

is also local and just proportional to the boson self-energy

$$\Pi_{ii} = -g^2 M_{ii}. \quad (\text{F.12})$$

This proves that the approximation made in chapter 3.3, where we took a local irreducible spin cumulant, is equivalent to the usual large d limit of wave vector independent self-energies.

The important consequence of local self-energies $\Sigma_{ij} = \Sigma_{ii} \delta_{ij}$ and $\Pi_{ij} = \Pi_{ii} \delta_{ij}$ is that the Luttinger-Ward functional $\Phi[G_{ij}, \mathcal{D}_{ij}]$ is also local. It is the sum of all vacuum-to-vacuum skeleton graphs with the property

$$\Sigma_{ij}(\omega) = \frac{\delta \Phi}{\delta G_{ij}(\omega)} \quad (\text{F.13})$$

$$\Pi_{ij}(\omega) = -2 \frac{\delta \Phi}{\delta \mathcal{D}_{ij}(\omega)}. \quad (\text{F.14})$$

Thus, the Luttinger-Ward functional can be collapsed to a single site since it depends only on the local Green's functions G_{ii} and \mathcal{D}_{ii}

$$\Phi = \sum_i \Phi(G_{ii}, \mathcal{D}_{ii}). \quad (\text{F.15})$$

Now, we can write the thermodynamic potential in terms of Φ , G_k and \mathcal{D}_q as

$$\Omega = \frac{1}{\beta} \Phi + \frac{1}{\beta} \sum_{k,\omega} [\ln G_k - \Sigma_k G_k] - \frac{1}{2} \frac{1}{\beta} \sum_{q,\omega} [\ln \mathcal{D}_q - \Pi_q \mathcal{D}_q], \quad (\text{F.16})$$

where q and k are compact notations for $\{\mathbf{q}, \alpha\}$ and $\{\mathbf{k}, \sigma\}$, respectively. Only this functional form of Ω is stationary under small variation of G_k or \mathcal{D}_q , i.e.,

$$\frac{\delta \Omega}{\delta G_k} = 0 \quad \text{and} \quad \frac{\delta \Omega}{\delta \mathcal{D}_q} = 0. \quad (\text{F.17})$$

Substituting Eq. (F.10) and (F.11) in (F.16), we get

$$\Omega = \frac{1}{\beta} \Phi + \frac{1}{\beta} \sum_{k,\omega} [\ln G_k - \Sigma_k G_k] - \frac{1}{2} \frac{1}{\beta} \sum_{q,\omega} [\ln(\chi_q(\chi_q^{-1} - J_{\mathbf{q}})) + J_{\mathbf{q}} \chi_q]. \quad (\text{F.18})$$

Taking into account that M and Σ are local, Eq. (F.18) can be reduced to

$$\Omega = \frac{1}{\beta} \Phi + \frac{1}{\beta} \sum_{k,\omega} [\ln G_k - \Sigma G_{oo}] - \frac{1}{2} \frac{1}{\beta} \sum_{q,\omega} [\ln(\chi_q M^{-1}) - M^{-1} \chi_{oo}]. \quad (\text{F.19})$$

Now, we would like to compare expression (F.19) with the impurity thermodynamic potential, which may also be expressed as a functional of electron and boson Green's functions by

$$\Omega = \frac{1}{\beta} \Phi[G_{oo}, D_{oo}] + \frac{1}{\beta} \sum_{\omega} \text{Tr}[\ln G - \Sigma G] - \frac{1}{2} \frac{1}{\beta} \sum_{\omega} \text{Tr}[\ln G_{\Phi} - \Sigma_{\Phi} G_{\Phi}]. \quad (\text{F.20})$$

Here G denotes the whole set of electron Green's functions (impurity and electronic bath) while G_{Φ} stands for Green's functions of the bosonic bath. A straightforward calculation gives the following relations

$$\begin{aligned} \det[G] &= \det[G_c^0] \prod_{\sigma} G_{oo} \\ \text{Tr}[\Sigma G] &= \sum_{\sigma} \Sigma G_{oo} \\ \det[G_{\Phi}] &= \det[G_{\Phi}^0] \prod_{\alpha} \chi_{oo} M^{-1} \\ \text{Tr}[\Sigma_{\Phi} G_{\Phi}] &= \sum_{\alpha} (M^{-1} \chi_{oo} - 1), \end{aligned} \quad (\text{F.21})$$

where G_c^0 and G_Φ^0 denote the Green's functions of the electronic and bosonic baths in the absence of the impurity, respectively. Inserting relations (F.21) in (F.22), we get

$$\Omega_{imp} = \frac{1}{\beta} \Phi[G_{oo}, \mathcal{D}_{oo}] + \frac{1}{\beta} \sum_{\sigma\omega} [\ln G_{oo} - \Sigma G_{oo}] - \frac{1}{2} \frac{1}{\beta} \sum_{\alpha\omega} [\ln(\chi_{oo} M^{-1}) - M^{-1} \chi_{oo}]. \quad (\text{F.22})$$

The crucial point in combining Eqs. (F.19) and (F.22) is that the Luttinger-Ward functional Φ of the lattice model is just N -times the impurity functional $\Phi[G_{oo}, \mathcal{D}_{oo}]$ (see Eq. F.15) and can therefore be eliminated. Thus, the thermodynamic potential can be calculated from the impurity free-energy Ω_{imp} , self-energy Σ and and irreducible spin cummulant M by

$$\Omega = \Omega_{imp} + \frac{1}{\beta} \sum_{k,\omega} (\ln G_k - \ln G_{oo}) - \frac{1}{2} \frac{1}{\beta} \sum_{q,\omega} (\ln \chi_q - \ln \chi_{oo}), \quad (\text{F.23})$$

where $G_k(i\omega) = 1/(i\omega + \mu - \varepsilon_{\mathbf{k}} - \Sigma(i\omega))$ and $\chi_q(i\omega) = 1/(M^{-1}(i\omega) + J_{\mathbf{q}})$ are lattice Green's function and spin susceptibility, respectively.

For completeness, let us briefly mention how to calculate the impurity free-energy within a self-consistent auxiliary method that was presented in chapter 4.2. The impurity part of Ω is the difference between the free-energy of the system with ($Q = 1$) and without ($Q = 0$) the impurity. It can be expressed by auxiliary spectral functions as

$$e^{-\beta\Omega_{imp}} = \frac{Z_{Q=1}}{Z_{Q=0}} = \int d\omega e^{-\beta\omega} \left[\sum_{\sigma} A_{f\sigma}(\omega) + A_b(\omega) \right], \quad (\text{F.24})$$

where A_f and A_b are pseudo-fermion and pseudo-boson spectral functions, respectively.

Appendix G

SUNCA equations

In this appendix we explicitly give the self-consistent SUNCA equations which, together with the definitions Eqs. (6.5) of the Green's functions, determine the auxiliary particle self-energies. We also give the expression for the physical d-electron spectral function in terms of the auxiliary particle propagators.

We first define the ladder vertex functions T_a , T_b with heavy boson a and light boson b rungs, respectively, as shown diagrammatically in Fig. 6.4. These vertex functions, projected onto the physical subspace $Q = 1$ and analytically continued to real frequencies, obey the following Bethe–Salpeter equations,

$$T_{a\sigma}(\omega, \Omega) = \Gamma \int \frac{d\epsilon}{\pi} f(\epsilon - \Omega) A_{c-\sigma}^0(\epsilon - \Omega) G_{f-\sigma}(\epsilon) G_a(\epsilon + \omega - \Omega) + \Gamma \int \frac{d\epsilon}{\pi} f(\epsilon - \Omega) A_{c-\sigma}^0(\epsilon - \Omega) G_{f-\sigma}(\epsilon) G_a(\epsilon + \omega - \Omega) T_{a-\sigma}(\epsilon, \Omega) \quad (\text{G.1})$$

$$T_{b\sigma}(\omega, \Omega) = \Gamma \int \frac{d\epsilon}{\pi} f(\epsilon - \Omega) A_{c\sigma}^0(\Omega - \epsilon) G_{f-\sigma}(\epsilon) G_b(\epsilon + \omega - \Omega) + \Gamma \int \frac{d\epsilon}{\pi} f(\epsilon - \Omega) A_{c\sigma}^0(\Omega - \epsilon) G_{f-\sigma}(\epsilon) G_b(\epsilon + \omega - \Omega) T_{b-\sigma}(\epsilon, \Omega), \quad (\text{G.2})$$

where $f(\epsilon)$ is the Fermi function, $A_{c\sigma}^0(\epsilon) = \frac{1}{\pi} \text{Im} G_{c\sigma}^0(\epsilon) / \mathcal{N}(0)$ the bare conduction electron density of states per spin, normalized to the density of states at the Fermi level and, for concreteness, all propagators are to be understood as the retarded ones. The auxiliary particle self-energies (Fig. 6.3) are then given by,

$$\begin{aligned}
 \Sigma_{f\sigma}(\omega) = & \Gamma \int \frac{d\epsilon}{\pi} f(\epsilon - \omega) A_{c\sigma}^0(\omega - \epsilon) G_b(\epsilon) [1 + T_{a\sigma}(\omega, \epsilon)]^2 + \\
 & \Gamma \int \frac{d\epsilon}{\pi} f(\epsilon - \omega) A_{c-\sigma}^0(\epsilon - \omega) G_a(\epsilon) [1 + T_{b\sigma}(\omega, \epsilon)]^2 - \\
 & 2\Gamma^2 \int \frac{d\epsilon}{\pi} f(\epsilon - \omega) A_{c\sigma}^0(\omega - \epsilon) G_b(\epsilon) \times \\
 & \int \frac{d\epsilon'}{\pi} f(\epsilon' - \epsilon) A_{c-\sigma}^0(\epsilon' - \epsilon) G_{f-\sigma}(\epsilon') G_a(\epsilon' + \omega - \epsilon) \quad (\text{G.3})
 \end{aligned}$$

$$\begin{aligned}
 \Sigma_b(\omega) = & \Gamma \sum_{\sigma} \int \frac{d\epsilon}{\pi} f(\epsilon - \omega) A_{c\sigma}^0(\epsilon - \omega) G_{f\sigma}(\epsilon) [1 + T_{a\sigma}(\epsilon, \omega)] + \\
 & \Gamma^2 \sum_{\sigma} \int \frac{d\epsilon}{\pi} f(\epsilon - \omega) A_{c\sigma}^0(\epsilon - \omega) G_{f\sigma}(\epsilon) \times \\
 & \int \frac{d\epsilon'}{\pi} f(\epsilon' - \omega) A_{c-\sigma}^0(\epsilon' - \omega) G_{f-\sigma}(\epsilon') G_a(\epsilon' + \epsilon - \omega) \times \\
 & \{ [1 + T_{b\sigma}(\epsilon, \epsilon' + \epsilon - \omega)] [1 + T_{b-\sigma}(\epsilon', \epsilon' + \epsilon - \omega)] - 1 \} \quad (\text{G.4})
 \end{aligned}$$

$$\begin{aligned}
 \Sigma_a(\omega) = & \Gamma \sum_{\sigma} \int \frac{d\epsilon}{\pi} f(\epsilon - \omega) A_{c-\sigma}^0(\omega - \epsilon) G_{f\sigma}(\epsilon) [1 + T_{b\sigma}(\epsilon, \omega)] + \\
 & \Gamma^2 \sum_{\sigma} \int \frac{d\epsilon}{\pi} f(\epsilon - \omega) A_{c-\sigma}^0(\omega - \epsilon) G_{f\sigma}(\epsilon) \times \\
 & \int \frac{d\epsilon'}{\pi} f(\epsilon' - \omega) A_{c\sigma}^0(\omega - \epsilon') G_{f-\sigma}(\epsilon') G_b(\epsilon' + \epsilon - \omega) \\
 & \{ [1 + T_{a\sigma}(\epsilon, \epsilon' + \epsilon - \omega)] [1 + T_{a-\sigma}(\epsilon', \epsilon' + \epsilon - \omega)] - 1 \} \quad (\text{G.5})
 \end{aligned}$$

In order to calculate the physical impurity electron spectral function $A_{d\sigma}$ from the selfconsistently determined G_a , G_b , G_f , it is convenient to define modified vertex functions as

$$S_{a\sigma}^R(\omega, \Omega) = 1 + \Gamma \int \frac{d\epsilon}{\pi} f(\epsilon - \Omega) A_{c\sigma}^0(\epsilon - \Omega) \text{Re}\{G_{f\sigma}(\epsilon) [1 + T_{a\sigma}(\epsilon, \Omega)]\} G_a(\epsilon + \omega) \quad (\text{G.6})$$

$$S_{a\sigma}^I(\omega, \Omega) = 1 + \Gamma \int \frac{d\epsilon}{\pi} f(\epsilon - \Omega) A_{c\sigma}^0(\epsilon - \Omega) \text{Im}\{G_{f\sigma}(\epsilon) [1 + T_{a\sigma}(\epsilon, \Omega)]\} G_a(\epsilon + \omega) \quad (\text{G.7})$$

$$S_{b\sigma}^R(\omega, \Omega) = 1 + \Gamma \int \frac{d\epsilon}{\pi} f(\epsilon - \Omega) A_{c-\sigma}^0(\Omega - \epsilon) \text{Re}\{G_{f\sigma}(\epsilon) [1 + T_{b\sigma}(\epsilon, \Omega)]\} G_b(\epsilon - \omega) \quad (\text{G.8})$$

$$S_{b\sigma}^I(\omega, \Omega) = 1 + \Gamma \int \frac{d\epsilon}{\pi} f(\epsilon - \Omega) A_{c-\sigma}^0(\Omega - \epsilon) \text{Im}\{G_{f\sigma}(\epsilon) [1 + T_{b\sigma}(\epsilon, \Omega)]\} G_b(\epsilon - \omega) \quad (\text{G.9})$$

The impurity spectral function then reads

$$\begin{aligned}
A_{d\sigma}(\omega) = & -\frac{1}{\pi} \text{Im} \int \frac{d\Omega}{\pi} \frac{e^{-\beta\Omega}}{f(-\omega)} G_{f\sigma}(\Omega + \omega) \left\{ \text{Im}[G_b(\Omega)] [S_{a-\sigma}^R(\omega, \Omega)^2 - S_{a-\sigma}^I(\omega, \Omega)^2] + \right. \\
& \left. 2\text{Re}[G_b(\Omega)] S_{a-\sigma}^R(\omega, \Omega) S_{a-\sigma}^I(\omega, \Omega) \right\} \\
& -\frac{1}{\pi} \text{Im} \int \frac{d\Omega}{\pi} \frac{e^{-\beta\Omega}}{f(\omega)} G_{f-\sigma}(\Omega - \omega) \left\{ \text{Im}[G_a(\Omega)] [S_{b\sigma}^R(\omega, \Omega)^2 - S_{b\sigma}^I(\omega, \Omega)^2] + \right. \\
& \left. 2\text{Re}[G_a(\Omega)] S_{b\sigma}^R(\omega, \Omega) S_{b\sigma}^I(\omega, \Omega) \right\} \\
& + 2\frac{\Gamma}{\pi} \int \frac{d\Omega}{\pi} \frac{e^{-\beta\Omega}}{f(\omega)} \int \frac{d\epsilon}{\pi} f(\epsilon - \Omega) A_{c-\sigma}^0(\epsilon - \Omega) \text{Im}[G_b(\Omega) G_{f-\sigma}(\epsilon)] \times \\
& \text{Im}[G_{f\sigma}(\Omega + \omega) G_a(\epsilon + \omega)] . \quad (1.10)
\end{aligned}$$

Note that the exponential divergencies of the statistical factors appearing in Eq. (G.10) are compensated by the threshold behavior of the corresponding auxiliary particle spectral functions $A_\mu(\omega) = \frac{1}{\pi} \text{Im} G_\mu(\omega)$, $\mu = a, b, f$ in the integrands. For the numerical treatment, these divergencies can be explicitly absorbed by formulating the self-consistency equations (A1)–(A10) in terms of the functions $\tilde{A}_\mu(\omega)$ which are defined via

$$A_\mu(\omega) = f(-\omega) \tilde{A}_\mu(\omega) \quad (\text{G.10})$$

and, hence, have no exponential divergence. We thus have, e.g., $\exp(-\beta\omega) A_\mu(\omega) = f(\omega) \tilde{A}_\mu(\omega)$. Details of this representation are described in Ref. [91].

APPENDIX G. SUNCA EQUATIONS

Bibliography

- [1] J.G. Bednorz and K.A. Müller. *Z. Phys. B* **64**, 189 (1986).
- [2] D.M. Newns and N. Read. *Adv. Phys.* **36**, 799 (1987).
- [3] G. Kotliar. *Correlated Electron Systems*. World Scientific, Singapore, (1993).
- [4] W. Metzner and D. Vollhardt. *Phys. Rev. Lett.* **62**, 324 (1989).
- [5] A. Georges, G. Kotliar, W. Krauth, and M.J. Rozenberg. *Rev. Mod. Phys.* **68**, 13 (1996).
- [6] Q. Si and J.L. Smith. *Phys. Rev. Lett.* **77**, 3391 (1996).
- [7] J.L. Smith and Q. Si. *Phys. Rev. B* **61**, 5184 (2000).
- [8] H. Kajuter. *Pd.D. Thesis, Rutgers University*. (1996).
- [9] J. Jaklič and P. Prelovšek. *Adv. Phys.* **49**, 1 (2000).
- [10] C.M. Varma, P.B. Littlewood, S. Schmitt-Rink, E. Abrahams, and A.E. Ruckenstein. *Phys. Rev. Lett.* **63**, 1996 (1989).
- [11] M.H. Hettler, A.N. Tahvildar-Zadeh, M. Jarrel, T. Pruschke, and H.R. Krishnamurthy. *Phys. Rev. B* **58**, 7475 (1998).
- [12] G. Kotliar, S.Y. Savrasov, G. Palsson, and G. Biroli. *Phys. Rev. Lett.* **87**, 186401 (2001).
- [13] E.H. Lieb and F.Y. Wu. *Phys. Rev. Lett.* **20**, 1445 (1968).
- [14] B. Sutherland. *An Introduction to the Bethe Ansatz in Exactly Solvable Problems in Condensed Matter and Relativistic Field Theory*. ed. S. Shastry, S.S. Jha, V. Singh, (1985).
- [15] J. Hubbard. *Proc. Roy. Soc. A* **276**, 238 (1963).

BIBLIOGRAPHY

- [16] J. Hubbard. *Proc. Roy. Soc. A* **277**, 237 (1964).
- [17] J. Hubbard. *Proc. Roy. Soc. A* **281**, 401 (1964).
- [18] F.J. Ohkawa. *J. Phys. Soc. Jpn* **60**, 3218 (1991).
- [19] F.J. Ohkawa. *Prog. Theor. Phys. (Suppl.)* **106**, 95 (1991).
- [20] A. Georges and G. Kotliar. *Phys. Rev. B* **45**, 6479 (1992).
- [21] *see for example*: J.W. Negele and H. Orland. *Quantum Many-Particle Systems*. Addison-Wesley, (1988).
- [22] R. Chitra and G. Kotliar. *Phys. Rev. Lett.* **84**, 3678 (2000).
- [23] R. Strack and D. Vollhardt. *Phys. Rev. B* **46**, 13852 (1992).
- [24] T. Obermeier, T. Pruschke, and J. Keller. *Ann. Physik* **5**, 137 (1996).
- [25] G. Baym and L.P. Kadanoff. *Phys. Rev.* **124**, 287 (1961).
- [26] P. Coleman. *Phys. Rev. B* **29**, 3035 (1984).
- [27] A.A. Abrikosov. *Physics* **2**, 21 (1965).
- [28] T. Pruschke, D.L. Cox, and M. Jarell. *Phys. Rev. B* **47**, 3553 (1993).
- [29] K. Haule, J. Bonča, and P. Prelovšek. *Phys. Rev. B* **61**, 2482 (2000).
- [30] T. Moriya and A. Kawabata. *J. Phys. Soc. Jpn.* **34**, 639 (1973).
- [31] T. Moriya and A. Kawabata. *J. Phys. Soc. Jpn.* **35**, 669 (1973).
- [32] S.G. Mishra and T.V. Ramakrishnan. *Phys. Rev. B* **18**, 2308 (1978).
- [33] M.A. Continento. *Phys. Rep.* **239**, 179 (1994).
- [34] B.I. Halperin and P.C. Hohenberg. *Rev. Mod. Phys.* **49**, 435 (1977).
- [35] S.K. Ma. *Modern theory of critical phenomena*. Benjamin, Cummings, Reading, (1976).
- [36] S. Sachdev. *Quantum Phase Transitions*. Cambridge University Press, (1999).
- [37] C.M. Varma, Z. Nussinov, and Wim van Saarloos. *Physics Reports* **360(5-6)**, 353 (April 2002).

-
- [38] C.M. Varma. *Int. J. Mod. Phys. B* **3**, 2083 (1989).
- [39] M. Imada, A. Fujimori, and Y. Tokura. *Rev. Mod. Phys.* **70**, 1039 (1998).
- [40] A. Ramšak, P. Prelovšek, and I. Sega. *Phys. Rev. B* **61**, 4389 (2000).
- [41] A. Ramšak, P. Prelovšek, and I. Sega. *Nato ARW Proceedings: Open Problems in Strongly Correlated Electron Systems*. Kluwer Academic Publisher, 33 (2000).
- [42] A. Fujimori, A. Ino, T. Yoshida, T. Mizokawa, Z.-X. Shen, C. Kim, T. Kakeshita, H. Eisaki, and S. Uchida. *Nato ARW Proceedings: Open Problems in Strongly Correlated Electron Systems*. Kluwer Academic Publisher, 119 (2000).
- [43] A. Ino, T. Mizokawa, K. Kobayashi, A. Fujimori, T. Sasagawa, T. Kimura, K. Kishio, K. Tamasaku, H. Eisaki, and S. Uchida. *Phys. Rev. Lett.* **81**, 2124 (1998).
- [44] Y. Nagaoka. *Phys. Rev.* **147**, 392 (1966).
- [45] F. Becca and S. Sorella. *cond-mat/0102249*, 2001.
- [46] J.M. Luttinger. *Phys. Rev.* **119**, 1153 (1960).
- [47] P. Nozières. *Interacting Fermi Systems*. Benjamin, New York, 1963.
- [48] A.A. Abrikosov, L.P. Gorkov, and I.E. Dzialoshinski. *Methods of Quantum Field Theory in Statistical Physics*. Pergamon, Elmsford, New York, 1965.
- [49] M. Oshikawa. *Phys. Rev. Lett.* **84**, 3370 (2000).
- [50] K.B. Blagoev and K.S. Bedell. *Phys. Rev. Lett.* **79**, 1106 (1997).
- [51] M. Yamanaka, M. Ochikawa, and I. Affleck. *Phys. Rev. Lett.* **79**, 1110 (1997).
- [52] C. Gröber, R. Eder, and W. Hanke. *Phys. Rev. B* **62**, 4336 (2000).
- [53] W. Stephan and P. Horsch. *Phys. Rev. Lett.* **666**, 2482 (2000).
- [54] W.O. Putikka, M.U. Luchini, and R.R.P. Singh. *Phys. Rev. Lett.* **81**, 2966 (1998).

BIBLIOGRAPHY

- [55] Th.A. Maier, Th. Pruschke, and M. Jarrell. *cond-mat/0111368*.
- [56] R. Eder, C. Gröber, M.G. Zacher, and W. Hanke. *Nato ARW Proceedings: Open Problems in Strongly Correlated Electron Systems*. Kluwer Academic Publisher, 23 (2000).
- [57] C. Gröber, M.G. Zacher, and R. Eder. *cond-mat/9902015*.
- [58] A. Sherman and M. Schreiber. *cond-mat/9808087*.
- [59] M. Langer, J. Schmalian, S. Grabowski, and K.H. Bennemann. *cond-mat/9505063*.
- [60] J. Schmalian, M. Langer, , S. Grabowski, and K.H. Bennemann. *Phys. Rev. B* **54**, 4336 (1996).
- [61] A.V. Chubukov, D.K. Morr, and K.A. Shakhnovich. *cond-mat/9511138*.
- [62] B.L. Altshuler, A.V. Chubukov, A. Dashevskii, and A.M. Finkelstein D.K. Morr. *cond-mat/9703120*.
- [63] R. Preuss, W. Hanke, and W. von der Linden. *Phys. Rev. Lett.* **75**, 1344 (1995).
- [64] A. Ino, C. Kim, T. Mizokawa, Z.-X. Shen, A. Fujimori, M. Takaba, K. Tamasuku, H. Eisaki, and S. Uchida. *J. Phys. Soc. Jpn.* **68**, 1496 (1999).
- [65] U. Brandt and C. Mielsch. *Z. Phys.* **82**, 37 (1991).
- [66] R. Chitra and G. Kotliar. *Phys. Rev. B* **63**, 115110 (2001).
- [67] J.W. Loram, K.A. Mirza, J.R. Cooper, N.A. Athanassopoulou, and W.Y. Liang. *Proc. of 10th Anniversary HTS Workshop, Houston*. World Scientific, 341 (1996).
- [68] E. Manousakis. *Rev. Mod. Phys.* **63**, 1 (1991).
- [69] T. Pruschke, M. Jarrell, and J. Freericks. *Adv. Phys.* **44**, 187 (1995).
- [70] P. Majumdar and H.R. Krishnamurthy. *cond-mat/9512151*, (unpublished).
- [71] E. Lange and G. Kotliar. *Phys. Rev. B* **59**, 1800 (1999).

- [72] E. Müller-Hartmann. *Z. Phys. B* **74**, 507 (1989).
- [73] A. Khurana. *Phys. Rev. Lett.* **64**, 1990 (1990).
- [74] J.C. Ward. *Phys. Rev.* **78**, 182 (1950).
- [75] H. Kohno and K. Yamada. *Prog. Theor. Fiz.* **80**, 623 (1988).
- [76] P. Voruganti, A. Golubetsev, and S. John. *Phys. Rev. B* **45**, 13945 (1992).
- [77] E. Lange and G. Kotliar. *Phys. Rev. Lett.* **82**, 1317 (1999).
- [78] P. Prelovšek. *Phys. Rev. B* **55**, 9219 (1997).
- [79] T. Nishikawa, J. Takeda, and M. Sato. *J. Phys. Soc. Jpn.* **63**, 1441 (1994).
- [80] A.C. Hewson. *The Kondo Problem to Heavy Fermions*. Cambridge University Press, 1993.
- [81] D.L. Cox and A. Zawadowski. *Adv. Phys.* **47**, 599 (1998).
- [82] T. K. Ng and P. A. Lee. *Phys. Rev. Lett.* **61**, 1768 (1988).
- [83] L. I. Glazman and M. E. Raikh. *Pis'ma Zh. Eksp. Teor. Fiz.* **47**, 378 (1999).
- [84] L. I. Glazman and M. E. Raikh. *JETP Lett.* **47**, 452 (1988).
- [85] N. Andrei and C. Destri. *Phys. Rev. Lett.* **52**, 364 (1984).
- [86] S.E. Barnes. *J. Phys. F* **6**, 1375 (1976); **7**, 2637 (1977).
- [87] P. Coleman. *Phys. Rev. B* **29**, 3035 (1984).
- [88] H. Keiter and J.C. Kimball. *J. Appl. Phys.* **42**, 1460 (1971).
- [89] N. Grewe and H. Keiter. *Phys. Rev. B* **24**, 4420 (1981).
- [90] Y. Kuramoto. *Z. Phys. B* **53**, 37 (1983).
- [91] T. A. Costi, J. Kroha, and P. Wölfle. *Phys. Rev. B* **53**, 1850 (1996).
- [92] J. Kroha, P. Wölfle, and T. A. Costi. *Phys. Rev. Lett.* **79**, 261 (1997).
- [93] D. L. Cox and A. E. Ruckenstein. *Phys. Rev. Lett.* **71**, 1613 (1993).

BIBLIOGRAPHY

- [94] Th. Pruschke and N. Grewe. *Z. Phys. B* **74**, 439 (1989).
- [95] K. Haule, S. Kirchner, H. Kroha, and P. Wölfle. *Phys. Rev. B* **64**, 155111 (2001).
- [96] J. Kroha and P. Wölfle. *Proceedings of the International Conference on “Mathematical Methods in Physics”*. Montreal 2000, D. Senechal, ed., (Springer, in press).
- [97] J. Kroha and P. Wölfle. *Acta Phys. Pol. B* **29**, 3781 (1998).
- [98] I. Holm and K. Schönhammer. *Solid State Comm.* **69**, 969 (1989).
- [99] T. A. Costi, P. Schmitteckert, J. Kroha, and P. Wölfle. *Phys. Rev. Lett.* **73**, 11275 (1994).
- [100] T. A. Costi, P. Schmitteckert, J. Kroha, and P. Wölfle. *Physica C* **235-240**, 2287 (1994).
- [101] T. Schauerte, J. Kroha, and P. Wölfle. *Phys. Rev. B* **62**, 4394 (2000).
- [102] P. Nozierès and C. T. DeDominicis. *Phys. Rev.* **178**, 1073 (1996); **178** 1084 (1996); **178** 1097 (1969).
- [103] B. Menge and E. Müller-Hartmann. *Z. Phys. B* **73**, 225 (1988).
- [104] J. Friedel. *Phil. Mag.* **43**, 153 (1952).
- [105] J.S. Langer and V. Ambreagaokar. *Phys. Rev.* **121**, 1090 (1961).
- [106] J.M. Luttinger and J.C. Ward. *Phys. Rev.* **118**, 1417 (1960).